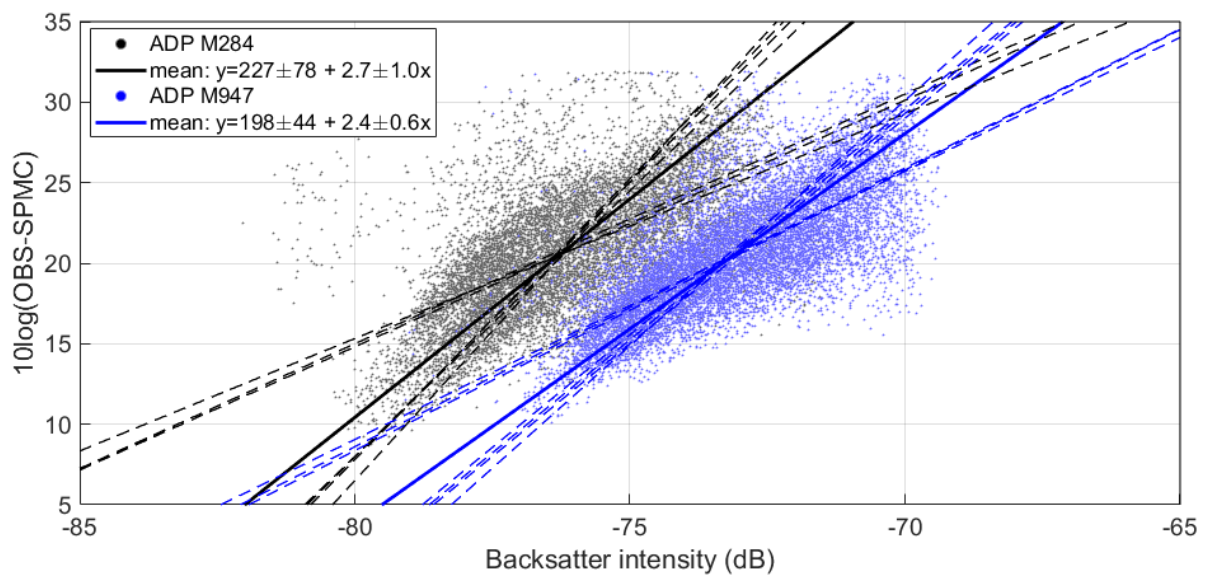


MONitoring en MOdellering van het cohesieve sedimenttransport en evaluatie van de effecten op het mariene ecosysteem ten gevolge van bagger- en stortoperatie (MOMO)



Activiteitsrapport (1 januari 2018 – 30 juni 2018)

Michael Fettweis, Matthias Baeye, Frederic Francken, Dries Van den Eynde

MOMO/8/MF/201807/NL/AR/3

Inhoudstafel

1.	Inleiding	3
2.1.	<i>Voorwerp van deze opdracht</i>	3
2.2.	<i>Algemene doelstellingen</i>	3
2.3.	<i>Onderzoek Januari 2017 – December 2018</i>	4
2.4.	<i>Gerapporteerde en/of uitgevoerde taken</i>	9
2.5.	<i>Publicaties (januari 2017 – december 2018)</i>	10
2.	Onzekerheden verbonden aan in situ hoogfrequente en langdurige metingen van SPM concentratie met behulp van optische en akoestische sensoren	12
2.1.	<i>Methods for long-term in situ SPMC measurements</i>	13
2.1.1.	<i>Terminology</i>	13
2.1.2.	<i>Inherent properties of the SPM</i>	14
2.1.3.	<i>Sensors used to obtain long-term SPMC time series</i>	16
2.1.4.	<i>Existing international guidelines and standards</i>	19
2.2.	<i>Sources of uncertainties</i>	21
2.2.1.	<i>Sensor related uncertainties</i>	21
2.2.2.	<i>Environmental related uncertainties</i>	24
2.2.3.	<i>Sample related uncertainties</i>	27
2.2.4.	<i>Relating sensor output to sample SPMC</i>	29
2.2.5.	<i>Additional uncertainties</i>	39
2.3.	<i>Towards best practice</i>	41
2.3.1.	<i>Best practice workflow</i>	41
2.3.2.	<i>Discussion and ranking of the uncertainties</i>	43
2.3.3.	<i>Turbidity as a surrogate for SPMC?</i>	47
2.4.	<i>Conclusions and outlook</i>	49
3.	Referenties	51
Appendix 1:	Bijdrage 50 th Liège Colloquium on Ocean Dynamics, 18 May – 1 June, Liège (Belgium).	
Appendix 2:	Adriaens R, Zeelmaekers E, Fettweis M, Vanlierde E, Vanlede J, Stassen P, Elsen J, Śröder J, Vandenberghe N. 2018. Quantitative clay mineralogy as provenance indicator for recent muds in the southern North Sea. <i>Marine Geology</i> , 398, 48-58. doi:10.1016/j.margeo.2017.12.011	

Het startsein voor het werk voorgesteld in dit rapport was een workshop georganiseerd door het KBIN in February 2016. Als uitkomst werden een aantal aanbevelingen geformuleerd die de basis hebben gevormd van dit rapport. De hoofdauteurs zijn M Fettweis (KBIN, Brussel), R Riethmüller (HZG, Hamburg), R Verney (IFREMER, Brest) en M Becker (MARUM, Bremen). Verder hebben meegewerkt J Backers, W Vanhaverbeke (KBIN, Oostende); M Baeye M, B Nechad (KBIN, Brussel); M Chapalain (IFREMER, Brest); S Claeys, H Vereecken (Flanders Hydraulics, Borgerhout); J Claus, D Depreiter (IMDC, Antwerpen); T Cox (Universiteit Antwerpen); J Deloffre, F Druine, R Lafite (Universiteit Rouen); G Flöser, R Röttgers (HZG, Hamburg); S Grünler (BAW, Hamburg); F Jourdin (SHOM, Brest); J Nauw (NIOZ, Texel) en A Sotollichio (Universiteit Bordeaux).

1. Inleiding

2.1. Voorwerp van deze opdracht

Het MOMO-project (monitoring en modellering van het cohesieve sedimenttransport en de evaluatie van de effecten op het mariene ecosysteem ten gevolge van bagger- en stortoperatie) maakt deel uit van de algemene en permanente verplichtingen van monitoring en evaluatie van de effecten van alle menselijke activiteiten op het mariene ecosysteem waaraan België gebonden is in overeenstemming met het verdrag betreffende de bescherming van het mariene milieu van de noordoostelijke Atlantische Oceaan (1992, OSPAR-Verdrag). De OSPAR Commissie heeft de objectieven van haar Joint Assessment and Monitoring Programme (JAMP) gedefinieerd tot 2021 met de publicatie van een holistisch “quality status report” van de Noordzee en waarvoor de federale overheid en de gewesten technische en wetenschappelijke bijdragen moeten afleveren ten laste van hun eigen middelen.

De menselijke activiteit die hier in het bijzonder wordt beoogd, is het storten in zee van baggerspecie waarvoor OSPAR een uitzondering heeft gemaakt op de algemene regel “alle stortingen in zee zijn verboden” (zie OSPAR-Verdrag, Bijlage II over de voorkoming en uitschakeling van verontreiniging door storting of verbranding). Het algemene doel van de opdracht is het bestuderen van de cohesieve sedimenten op het Belgisch Continentaal Plat (BCP) en dit met behulp van zowel numerieke modellen als het uitvoeren van metingen. De combinatie van monitoring en modellering zal gegevens kunnen aanleveren over de transportprocessen van deze fijne fractie en is daarom fundamenteel bij het beantwoorden van vragen over de samenstelling, de oorsprong en het verblijf ervan op het BCP, de veranderingen in de karakteristieken van dit sediment ten gevolge van de bagger- en stortoperaties, de effecten van de natuurlijke variabiliteit, de impact op het mariene ecosysteem in het bijzonder door de wijziging van habitatten, de schatting van de netto input van gevaarlijke stoffen op het mariene milieu en de mogelijkheden om deze laatste twee te beperken.

Een samenvatting van de resultaten uit de voorbije vergunningsperiode kan gevonden worden in het Syntheserapporten over de effecten op het mariene milieu van baggerspeciestortingen (Lauwaert et al. 2016) dat gepubliceerd werd conform art. 10 van het K.B. van 12 maart 2000 ter definiëring van de procedure voor machtiging van het storten in de Noordzee van bepaalde stoffen en materialen.

2.2. Algemene doelstellingen

Het onderzoek heeft als doel om de effecten van baggerspeciestortingen op het mariene ecosysteem (fysische aspecten) te onderzoeken en kadert in de algemene doelstellingen om de baggerwerken op het BCP en in de kusthavens te verminderen en om een gedetailleerd inzicht te verwerven van de fysische processen die plaatsvinden in het mariene kader waarbinnen deze baggerwerken worden uitgevoerd. Dit impliceert enerzijds beleidsondersteunend onderzoek naar de vermindering van de sedimentatie op de baggerplaatsen en het evalueren van alternatieve stortmethoden. Anderzijds is vernieuwend onderzoek vereist om een beter inzicht te bereiken over de fysische processen van slibtransport en het inschatten van de effecten van het storten van baggerspecie. Dit is specifiek gericht op het dynamische gedrag van slib in de waterkolom en op de bodem en zal uitgevoerd worden met behulp van modellen, in situ metingen en remote sensing data.

1) In situ en remote sensing metingen en data analyse

De monitoring van effecten van baggerspeciestortingen gebeurt met behulp van een vast meetstation in de nabijheid van MOW1, en met meetcampagnes met de RV Belgica (een 4

tal meetcampagnes voor het verzamelen van traject informatie, profielen en de calibratie van sensoren; en een 10 tal campagnes voor het onderhoud van het meetstation te MOW1). De geplande monitoring is gericht op het begrijpen van processen, zodoende dat de waargenomen variabiliteit en de effecten van baggerspeciéstortingen in een correct kader geplaatst kunnen worden. Een belangrijk deel is daarom gericht op zowel het uitvoeren van de in situ metingen, het garanderen van kwalitatief hoogwaardige data en het archiveren, rapporteren en interpreteren ervan. Remote sensing data afkomstig van onder andere satellieten worden gebruikt om een ruimtelijk beeld te bekomen.

2) Uitbouw en optimalisatie van het modelinstrumentarium

Het tijdens de voorbije jaren verbeterde en aangepaste slibtransportmodel zal verder worden ontwikkeld. Dit zal parallel gebeuren met de nieuwe inzichten die voortvloeien uit de metingen en de proces gerichte interpretatie van de metingen.

3) Ondersteunend wetenschappelijke onderzoek

Monitoring gebaseerd op wetenschappelijke kennis is essentieel om de effecten van menselijke activiteiten (hier het storten van baggerspecie) te kunnen schatten en beheren. Om te kunnen voldoen aan de door OSPAR opgelegde verplichtingen van monitoring en evaluatie van de effecten van menselijke activiteiten is het ontwikkelen van nieuwe monitorings- en modelleeractiviteiten nodig. Dit houdt in dat onderzoek dat de actuele stand van de wetenschappelijke kennis weerspiegelt wordt uitgevoerd en dat de hieruit voortvloeiende nieuwe ontwikkelingen geïntegreerd zullen worden in zowel de verbetering van het modelinstrumentarium als voor het beter begrijpen van het fysisch milieu.

2.3. Onderzoek Januari 2017 – December 2018

In het bijzonder is bij het opstellen van de hieronder vermelde taken rekening gehouden met de aanbevelingen voor de minister ter ondersteuning van de ontwikkeling van een versterkt milieubeleid zoals geformuleerd in het “Syntheserapport over de effecten op het mariene milieu van baggerspeciéstortingen (2011)” dat uitgevoerd werd conform art. 10 van het K.B. van 12 maart 2000 ter definiëring van de procedure voor machtiging van het storten in de Noordzee van bepaalde stoffen en materialen. De specifieke acties in de periode 2017-2018 zullen uitgevoerd worden om de algemene doelstellingen in te vullen zijn de volgende:

Streven naar een efficiënter stortbeleid door:

- Optimalisatie van de stortlocaties. Bijkomende simulaties worden uitgevoerd voor het opzetten van een MER voor een alternatieve stortplaats (zie taak 2.2). Verder zullen de effecten van een efficiënter verplaatsen van het gebaggerde materiaal te Nieuwpoort en Blankenberge naar de stortzones (lozen i.p.v. storten) geëvalueerd worden (zie Taak 3.4);
- Onderzoek naar de mogelijkheden voor het opzetten van een operationeel stortmodel in overleg met aMT (Taak 2.3). Dit model zal geïntegreerd worden in de binnen BMM-OD Natuur beschikbare operationele modellen. Het model zal gebruikt worden om in functie van de voorspelde fysische (wind, stroming, golven, sedimenttransport, recirculatie), economische (afstand, grootte baggerschip) en ecologische aspecten op korte termijn een keuze te kunnen maken tussen de beschikbare stortlocaties. Hiervoor zal binnen de huidige periode het slibtransportmodel gevalideerd worden op de geografische variabiliteit van de turbiditeitszones en de flocculatie van het slib.

Continue monitoring van het fysisch-sedimentologische milieu waarbinnen de baggerwerken worden uitgevoerd (Taak 1) en aanpassing van de monitoring aan de nog op te stellen targets voor het bereiken van de goede milieutoestand (GES), zoals gedefinieerd

binnen MSFD;

Uitbouw en optimalisatie van het numerieke modelinstrumentarium, ter ondersteuning en verfijning van het onderzoek (Taak 2.1).

Taak 1: In situ en remote sensing metingen en data analyse

Taak 1.1 Langdurige metingen

Sinds eind 2009 worden er continue metingen uitgevoerd te MOW1 met behulp van een meetframe (tripode). Met dit frame worden stromingen, slibconcentratie, korrelgrootteverdeling van het suspensiemateriaal, saliniteit, temperatuur, waterdiepte en zeebodem altimetrie gemeten. Om een continue tijdreeks te hebben, wordt gebruik gemaakt van 2 tripodes. Na ongeveer 1 maand wordt de verankerde tripode voor onderhoud aan wal gebracht en wordt de tweede op de meetlocatie verankerd. Op de meetdata wordt een kwaliteitsanalyse uitgevoerd, zodat de goede data onderscheiden kunnen worden van slechte of niet betrouwbare data.

In 2013-2016 werden enkele langdurige metingen uitgevoerd met behulp van een OBS-5 sensor vastgemaakt aan de AW boei; deze metingen zullen verdergezet worden. De data geven informatie over de SPM concentratie aan het oppervlak en zijn aldus complementair aan de bodem nabije metingen met de tripode. De data zijn ook van belang voor het calibreren en valideren van de oppervlakte SPM concentraties uit satellietbeelden.

Taak 1.2 Calibratie van sensoren tijdens in situ metingen

Tijdens 4 meetcampagnes per jaar met de R/V Belgica zullen een voldoende aantal 13-uursmetingen uitgevoerd worden met als hoofddoel het calibreren van optische of akoestische sensoren en het verzamelen van verticale profielen. De metingen zullen plaatsvinden in het kustgebied van het BCP. De optische metingen (transmissometer, Optical Backscatter Sensor) zullen gecalibreerd worden met de opgemeten hoeveelheid materie in suspensie (gravimetrische bepalingen na filtratie) om te komen tot massa concentraties. Naast de totale hoeveelheid aan suspensiemateriaal (SPM) wordt ook de concentratie aan POC/PON, TEP, chlorofyl (Chl-a, Chl-b) en phaeofytine (a, b) bepaald. Stalen van suspensiemateriaal zullen genomen worden met de centrifuge om de samenstelling ervan te bepalen.

Taak 1.3 Kwaliteitscontrole van de data

In situ metingen zijn steeds onderhevig aan onzekerheden ten gevolge van random meetfouten (gebrek aan precisie), systematische fouten (onnauwkeurigheid), menselijke fouten, en de statistische variabiliteit van de parameter. De fouten hebben hun oorsprong in de onnauwkeurigheid en het gebrek aan precisie van het meetinstrument of de procedures (bv. waterstaalname en filtratie). Doel is om de fout op de verschillende onderdelen van de metingen (filtratie, calibratie, langdurige trends...) te schatten. Een procedure die de best practice beschrijft zal worden opgesteld.

Een belangrijk aandachtspunt bij deze langdurige datareeksen is het garanderen van een gelijke kwaliteit in de tijd van de verzamelde data. De vraag die zich bij onze SPM concentratiemetingen stelt is niet zozeer het opmeten van hogere of lagere waarden, mogelijks veroorzaakt door het toepassen van een andere stortstrategie, maar het garanderen dat deze waarden inderdaad veroorzaakt worden door menselijke activiteiten (bv. storten) en niet het effect zijn van natuurlijke fluctuaties. Om kwaliteitsvolle data te kunnen leveren over een lange periode, die gebruikt kunnen worden om langdurige trends te identificeren, is het nodig om een rigoureuze kwaliteitscontrole uit te voeren. OBS alsook akoestische sensoren zijn gevoelig aan de samenstelling en korrelgrootte van het gesuspendeerde materiaal. Dit kan variëren in functie van de boven vermelde frequenties, maar hierom-

trent is er nog geen afdoende duidelijkheid wat de metingen te MOW1 betreft. De wetenschappelijke vragen die daarom moeten worden, hebben betrekking tot in situ en in lab calibratie van de OBS sensoren en van akoestische backscatter sensoren en de meetfouten.

Taak 1.4: Verwerking en interpretatie van de data

De metingen vergaard tijdens de 13-uursmetingen aan boord van de Belgica en met de tripod worden verwerkt en geïnterpreteerd. Hiervoor werden in het verleden al heel wat procedures (software) toegepast of ontwikkeld, zoals de berekening van de bodemschuifspanning uit turbulentiemetingen, entropieanalyse op partikelgrootteverdelingen, de opsplitsing van multimodale partikelgrootteverdeling in een som van lognormale verdelingen, het groeperen van de data volgens getij, meteorologie, klimatologie en seizoenen. Deze methodes zijn opgenomen in de standaardverwerking van de data. De aldus verwerkte data dienen als basis voor het verder gebruik binnenin wetenschappelijke vragen.

Taak 1.5: Sedimentologie van zeebodem

De sedimentologie van stortplaatsen en referentiezones zal, in samenwerking met het ILVO, worden bestudeerd met alternatieve meettechnieken, zoals de Sediment Profile Imaging (SPI).

Taak 1.6: TBT analyses

TBT analyses op stalen aangeleverd door het ILVO zullen door het chemisch labo van het KBIN (Ecochem) worden uitgevoerd. Het betreft de analyse van 6 stalen (2 replica's).

Taak 2: Uitbouw en optimalisatie van het modelinstrumentarium

Taak 2.1: Verdere ontwikkelingen en validatie van een slibtransportmodel voor het BCP gebaseerd op Coherens V2

Het tijdens de voorbije jaren verbeterde en aangepaste slibtransportmodel zal worden gevalideerd met behulp van de langdurige meetreeksen en de satellietbeelden. Hierbij zal dezelfde methode als in Baeye et al. (2011) en zoals in taak 1.4 worden gebruikt om de modelresultaten te groeperen en te klasseren volgens windrichting, weertype en getij. Het voordeel van deze werkwijze is dat niet zozeer gekeken wordt of de correlatie tussen meting en modelresultaat in één of meerder punt goed is, maar dat globaal nagegaan wordt of het model de SPM dynamica op het BCP goed kan reproduceren.

Verdere ontwikkelingen aan het model parallel met nieuwe inzichten die voorvloeien uit de metingen en de proces gerichte interpretatie van de metingen zullen worden geïmplementeerd in het model.

Taak 2.2: Ondersteuning bij de MER studie van een alternatieve stortlocatie

Op dit moment worden op het BCP vijf stortplaatsen gebruikt voor het gebaggerd materiaal afkomstig uit de vaargeulen op zee en de zeehavens: Zeebrugge Oost, S1, S2, B&W Oostende en Nieuwpoort. Door OD Natuur- BMM werd in het kader van het MOMO project onderzoek gedaan naar de efficiëntie van de stortplaatsen. Daaruit blijkt dat de recirculatie naar de baggerplaatsen het grootste is vanuit de stortplaats Zeebrugge Oost. Met behulp van numerieke modellen werden een aantal alternatieve locaties voor de stortplaats Zeebrugge Oost bestudeerd. In 2012-2013 werd een terreinproef uitgevoerd om de resultaten van de numerieke modellering op het terrein te valideren. Uit de resultaten van de terreinproef bleek dat er aanwijzingen zijn die de resultaten van de numerieke modellering bevestigen.

OD Natuur-BMM zal in deze studie instaan voor het uitvoeren van de nodige numerieke modelleringen in de eerste helft van 2017. Hiervoor zal gebruik gemaakt worden van het geüpdatete 3D stromingsmodel dat beschikbaar is bij OD Natuur-BMM. Het model is opgebouwd in Coherens V2, inclusief sedimenttransportmodule en flocculatiemodel. Meer

specifiek zal de OD Natuur-BMM betrokken zijn bij:

Fase 1 (long list van mogelijke locaties en exploitatiescenario's opgemaakt worden): berekening van de recirculatie voor maximaal 10 mogelijke locaties en/of stortscenario's. Voor iedere berekening zullen voor een aantal combinaties van hydro-meteo randvoorwaarden simulaties uitgevoerd worden. Deze randvoorwaarden zijn zo gekozen dat ze optimale aansluiting verzekeren met de al eerder uitgevoerde simulaties.

Fase 2 (opmaak Milieu Effect Rapport): Bij de opmaak van het MER zelf is geen specifieke modellering nodig voor de inschatting van de effecten. Indien uit overleg met de vergunningverlenende instanties blijkt dat simulaties moeten uitgevoerd worden ter onderbouwing van de gemaakte keuzes (recirculatie bij een bepaalde locatie/stortstrategie) kan dit uitgevoerd worden.

Taak 2.3: Operationeel stortmodel (vanaf 2018)

Overleg met aMT over het opstellen van een operationeel stortmodel om de noden en de mogelijkheden te definiëren. Het model zal later (vanaf 2018) kunnen opgesteld worden en kan dan geïntegreerd worden in de binnen BMM-OD Natuur beschikbare operationele modellen. Het model zal kunnen gebruikt worden om in functie van de voorspelde fysische (wind, stroming, golven, sedimenttransport, recirculatie), economische (afstand, grootte baggerschip) en ecologische aspecten op korte termijn een keuze te kunnen maken tussen de beschikbare stortlocaties.

Taak 3: Ondersteunend wetenschappelijk onderzoek

Monitoring gebaseerd op wetenschappelijke kennis is essentieel om de effecten van menselijke activiteiten (hier het storten van baggerspecie) te kunnen schatten en beheren. Om te kunnen voldoen aan de door OSPAR opgelegde verplichtingen van monitoring en evaluatie van de effecten van menselijke activiteiten is een verdere implementatie van huidige en het ontwikkelen van nieuwe monitoringsactiviteiten nodig. Meer specifiek gericht op de activiteit 'storten van baggerspecie' worden hier – wat het fysische milieu betreft - turbiditeit, samenstelling van de zeebodem, bathymetrie en hydrografische condities beoogd. Deze taak speelt hierop in door de ontwikkeling van nieuwe tools die de actuele stand van de wetenschappelijke kennis weerspiegelen teneinde de mathematische modellen te optimaliseren en verfijnen.

Taak 3.1: Sedimentuitwisseling tussen de zee en de haven van Zeebrugge

Slib stroomt de haven van Zeebrugge binnen rond HW, wanneer de stroming maximaal is. Gezien de grote turbulentie op dit moment op zee bestaat het SPM uit voornamelijk kleine vlokken met een lage valsnelheid. Eens het suspensiemateriaal de haven binnenkomt, neemt de turbulentie plots af, ontstaan er grotere vlokken en treed er een snelle bezinking op. Het verloop van de SPM concentratie in de haven zelf is goed gekend (zie onder andere de SPM concentratie metingen in de haven tijdens de terreinproef en de metingen van de topsliblaag), maar aan de havenmond zijn minder data beschikbaar om de sedimentuitwisseling in kaart te brengen en dit tijdens verschillende getij- en meteocondities. In deze taak zal de sedimentdynamica bestudeerd worden gebruikmakend van ADCP transects gemeten met de RV Belgica, van verticale profielen van SPM concentratie en vloggrootte in en uit de haven, en van remote sensing beelden.

Taak 3.2: Microbiologische activiteit en de wisselwerking met sedimentdynamica

Een sleutelement in het functioneren van kustnabije ecosystemen is de aanwezigheid van biotische en abiotische partikels. Verticale en dus ook horizontale fluxen van SPM worden bepaald door hun valsnelheid, die afhangt van de capaciteit van de deeltjes om te flocculeren. Flocculatie beïnvloedt de grootte van de gesuspendeerde deeltjes en bepaald daardoor de depositie van het slib. Op zijn beurt wordt flocculatie gestuurd door turbulen-

tie, de SPM concentratie, en de oppervlakte eigenschappen van de deeltjes, die van elektrochemische of biologische oorsprong kunnen zijn. Wat dit laatste betreft heeft dit een wederzijdse invloed tot gevolg tussen het SPM en de primaire productie doordat stoffen zoals TEPs (transparent exopolymeric particles), die vrijkomen door het fytoplankton en de bacteriën, de vlok grootte en dus ook de valsnelheid van het SPM beïnvloeden. Het belang van deze processen voor de slibdynamica in onze kustzone en dus ook voor de aanslibbing van havens en vaargeulen wordt gegeven door de uitzonderlijk hoge primaire productie in de Belgische kustzone ten gevolge van eutrofiëring (algenbloei). Dat er een effect is werd al aangetoond door de metingen te MOW1 die lieten zien dat het SPM zich anders gedraagt in de winter dan in de biologisch actieve zomerperiode. In de winter is het SPM beter gemengd in de waterkolom dan in de zomer en treden er dus hogere concentraties op in de waterkolom. In de zomer bevindt zich meer suspensiemateriaal dicht tegen de bodem en daalt de SPM concentratie in de waterkolom. Dit roept volgende vragen op, in het bijzonder 1) Hoe moet het modelinstrumentarium (flocculatiemodule) worden aangepast om deze seizoensaliteit te kunnen modelleren? 2) Wordt de seizoensaliteit in SPM concentratie en biologische activiteit veroorzaakt doordat de algen TEP produceren, dat aanleiding geeft tot de vorming van grotere vlokken en dus een hogere bezinking van het SPM als gevolg heeft, of daalt eerst de SPM concentratie ten gevolge van fysische processen (afname van de stormfrequentie in de lente) en start de algenbloei nadat het water minder troebel is geworden?) De troebelheid in de waterkolom is in de Belgische kustzone altijd hoog en de lichtindringing is ook in de zomer beperkt. Speelt troebelheid (en dus ook SPM concentratie) een belangrijke rol bij start van de algenbloei bepaald of is dit eerder een secundair proces?

Het onderzoek zal gericht zijn op het verzamelen van in situ meetdata van TEP, SPM en Chl concentratie te MOW1 en op andere plaatsen; het analyseren van de data in functie van boven aangehaalde vragen; het incorporeren van de biologische activiteit in een flocculatiemodel en het uitvoeren van modelberekeningen.

Taak 3.3: Overgang kustzone – offshore: Waarom is het turbiditeitsgebied beperkt tot de kustzone?

Turbulentie samen met de SPM concentratie bepalen de lichthoeveelheid in het water. De cross-shore stroming in vele kustgebieden is gekenmerkt door landinwaarts gerichte stroming dicht tegen de bodem en een zeewaarts gerichte aan het wateroppervlak (estuariene circulatie). Het is op dit moment niet duidelijk hoe het Schelde estuarium deze circulatie beïnvloed. Hierdoor wordt het SPM (en het fytoplankton) naar de kust getransporteerd in de bodemlaag nadat het eerst naar offshore werd getransporteerd in de oppervlaktelaag. Dit mechanisme is mogelijks verantwoordelijk voor de scherpe gradiënt in SPM concentratie langsheen onder andere de Belgische kust en de Westerscheldmond. Ook turbulentie is gekenmerkt door een gradiënt: hoog dicht tegen de kust en afnemend naar offshore toe. Dit komt overeen met een toename in waterdiepte naar offshore toe. Bij geringere waterdieptes is de turbulentie hoger, de verticale menging dus sneller en dus de tijd met lage SPM concentratie korter. Naar offshore toe zal de lichthoeveelheid in de waterkolom dus toenemen in de oppervlaktelaag omdat de diepte toeneemt. Vanaf een bepaalde diepte bereikt het SPM niet meer de oppervlakte tijdens verticale menging. De afname in SPM concentratie is dus mogelijks een afspiegeling van de gradiënten in diepte en turbulentie. Dit proces werd aangetoond in andere delen van de Noordzee (Duitse Bocht), maar nog niet in de Belgische kustzone.

Het onderzoek zal gericht zijn op het verzamelen van in situ meetdata van TEP, SPM en Chl concentratie op een drietal locaties gelegen op verschillende afstanden van de kust; het varen van ADCP transects dwars op de kust; en het analyseren van de data. TEP en Chl

zijn een onderdeel van het SPM, die een significante invloed heeft op de seizoenaliteit van de SPM dynamica.

Taak 3.4: Alternatieve Stortstrategie Nieuwpoort

Er zal ondersteuning gegeven worden aan afdeling kust in verband met het opzetten van een wetenschappelijke terreinproef om de impact van het verpompen van baggerspecie uit de haven van Nieuwpoort op een stortzone te evalueren. Details hiervan zullen op een vergadering van de technische werkgroep besproken worden.

2.4. Gerapporteerde en/of uitgevoerde taken

Periode Januari 2017 – Juni 2017

Taak 1.1: De meetreeks te MOW1 werd verdergezet.

Taak 1.2: Calibratie van sensoren werd uitgevoerd tijdens campagne 2017/20 (21-23/06/2017).

Taak 2.1 De bodemschuifspanning gemodelleerd met het hydrodynamisch model werd gevalideerd met in situ data te MOW1. Dit is een eerste stap bij de validatie van een slibtransportmodel voor het BCP gebaseerd op Coherens V2, zie Appendix 2 van activiteitenrapport MOMO/8/MF/201707/NL/AR/1.

Taak 2.2 Simulaties met de nieuwe versie van het COHERENS V3 model voor de Belgische kustzone werden uitgevoerd ter ondersteuning van de MER studie voor een alternatieve stortlocatie, zie Hoofdstuk 2 in activiteitenrapport MOMO/8/MF/201707/NL/AR/1

Taak 3.2 Waterstalen voor de bepaling van TEP concentratie werden 1-2 wekelijks genomen te Oostende.

Een 1 klasse flocculatiemodel werd aangepast om biologisch flocculatie te simuleren. De resultaten werden gevalideerd met metingen te MOW1, zie Hoofdstuk 3 in activiteitenrapport MOMO/8/MF/201707/NL/AR/1.

Periode Juli 2017 – December 2017

Taak 1.1 De meetreeks te MOW1 werd verdergezet. Het factual data rapport voor 2016 werd opgesteld.

Taak 1.2 Calibratie van sensoren werd uitgevoerd tijdens campagne 2017/24 (16-18/08/2017), 2017/34 (21-22/11/2017), 2017/38 (18-21/12/2017).

Taak 1.3 Een uitgebreide onzekerheidsanalyse van de optische en akoestische sensoren gebruikt bij langdurige metingen is in uitvoering. Resultaten werden op de INTERCOH conferentie getoond, zie Appendix 1 van activiteitenrapport MOMO/8/MF/201801/NL/AR/2

Taak 3.2 Waterstalen voor de bepaling van TEP concentratie werden 1-2 wekelijks genomen te Oostende. TEP werd tijdens de 13 uursmeting als standaard parameter opgenomen.

Taak 3.3 De stalen en data genomen tijdens 13 uursmetingen (vanaf 2003 t.e.m. nu) in de kustzone en offshore werden geanalyseerd om de geografische verschillen in SPM eigenschappen tussen het kustgebonden turbiditeitsmaximum en het offshore gebied met lage turbiditeit te beschrijven, zie Hoofdstuk 2 in activiteitenrapport MOMO/8/MF/201801/NL/AR/2.

Periode Januari 2018 – Juni 2018

Taak 1.1 De meetreeks te MOW1 werd verdergezet. Het factual data rapport voor 2017 werd opgesteld.

Taak 1.2 Calibratie van sensoren werd uitgevoerd tijdens campagne 2018/01 (23-26/01/2018), 2018/08 (27-30/03/2018), 2018/13 (15-16/05/2018).

Taak 1.3 De uitgebreide onzekerheidsanalyse van de optische en akoestische sensoren

gebruikt bij langdurige metingen werd afgewerkt en is gerapporteerd in activiteitsrapport MOMO/8/MF/201807/NL/AR/3. De bevindingen werden op het Liège Colloquium voorgesteld, zie Appendix 1 van activiteitsrapport MOMO/8/MF/201807/NL/AR/3

- Taak 3.2 Waterstalen voor de bepaling van TEP concentratie werden 1-2 wekelijks genomen te Oostende. TEP werd tijdens de 13 uursmeting als standaard parameter opgenomen.
- Taak 3.3 13 uursmetingen worden uitgebreid naar de kustzone (MOW1) en offshore (monitoring punt W05 en W08) om de geografische verschillen in SPM eigenschappen tussen het kustgebonden turbiditeitsmaximum en het offshore gebied met lage turbiditeit te beschrijven.

2.5. Publicaties (januari 2017 – december 2018)

Hieronder wordt een overzicht gegeven van publicatie met directe betrokkenheid van het KBIN waar resultaten en data uit het MOMO project in werden gebruikt.

Activiteits-, Meet- en Syntheserapporten

- Fettweis M, Baeye M, Francken F, Van den Eynde D. 2018. MOMO activiteitsrapport (1 januari – 30 juni 2018). BMM-rapport MOMO/8/MF/201808/NL/AR/3, 61pp + app.
- Backers J, Hindryckx K, Vanhaverbeke W. 2018. Rapport van de RV Belgica Meetcampagnes en Verankering van Meetsystemen MOMO - 2017. BMM rapport ODNatuur-MDO/2018-03/MOMO/2017, 164pp + CD.
- Fettweis M, Baeye M, Francken F, Van den Eynde D, Lee BJ. 2018. MOMO activiteitsrapport (1 juli – 31 december 2017). BMM-rapport MOMO/8/MF/201801/NL/AR/2, 27pp + app.
- Backers J, Hindryckx K, Vanhaverbeke W. 2017. Rapport van de RV Belgica Meetcampagnes en Verankering van Meetsystemen MOMO - 2016. BMM rapport ODNatuur-MDO/2017-04/MOMO/2016, 103pp + CD.
- Fettweis M, Baeye M, Francken F, Van den Eynde D, Chen P, Yu J. 2017. MOMO activiteitsrapport (1 januari – 30 juni 2017). BMM-rapport MOMO/8/MF/201707/NL/AR/1, 32pp + app.

Conferenties/Workshops

- Fettweis M, Riethmüller R, Verney R, Becker M. 2018. Uncertainties associated with long-term observations of suspended particulate matter concentration using optical and acoustic sensors. 50th International Liege Colloquium on Ocean Dynamics, 28 May-1 June, Liège (Belgium).
- Fettweis M. 2018. Long-term and continuous measurements of SPM dynamics in the Belgian nearshore area. Lifewatch Data Analysis Workshop, 22-23 February, VLIZ, (Belgium).
- Fettweis M. 2018. Dynamics of SPM on regional scales: Challenges and research opportunities. Workshop on Algae-Silt Interactions, 31 January, Delft (The Netherlands).
- Adriaens R, Zeelmakers E, Fettweis M, Vanlierde E, Vanlede J, Stassen P, Elsen J, Środoń J, Vandenberghe N. 2017. Quantitative clay mineralogy as provenance indicator for the recent muds located in the southern North Sea. INTERCOH, 13-17 November, Montevideo (Uruguay). Poster
- Fettweis M, Riethmüller R, Verney R, Becker M, Backers J, Baeye M, Chapalain M, Claeys S, Claus J, Cox T, Deloffre J, Depreiter D, Druine F, Flöser G, Grünler S, Jourdin F, Lafite R, Nauw J, Nechad B, Röttgers R, Sotollichio A, Vanhaverbeke W, Van Hoestenbergh T, Vereecken H. On best practice for in situ high-frequency long-term observations of suspended particulate matter concentration using optical and acoustic systems. IN-

- TERCOH, 13-17 November, Montevideo (Uruguay).
- Shen X, Toorman E, Fettweis M. 2017. A tri-modal flocculation model coupled with TELEMAC for suspended cohesive sediments in the Belgian coastal zone. INTERCOH, 13-17 November, Montevideo (Uruguay).
- Vanlede J, Dujardin A, Fettweis M. 2017. Mud dynamics in the harbor of Zeebrugge. INTERCOH, 13-17 November, Montevideo (Uruguay).
- Adriaens R, Zeelmakers E, Fettweis M, Vanlierde E, Vanlede J, Stassen P, Elsen J, Środoń J, Vandenberghe N. 2017. Quantitative clay mineralogy as provenance indicator for the recent muds located at the marine limit of influence of the Scheldt estuary. Schelde-Ems workshop, 16-17 February, Antwerp (Belgium). Poster

Publicaties (tijdschriften, hoofdstuk in boeken)

- Adriaens R, Zeelmaekers E, Fettweis M, Vanlierde E, Vanlede J, Stassen P, Elsen J, Środoń J, Vandenberghe N. 2018. Quantitative clay mineralogy as provenance indicator for recent muds in the southern North Sea. *Marine Geology*, 398, 48-58. doi:10.1016/j.margeo.2017.12.011.
- Chen P, Yu JCS, Fettweis M. 2018. Modelling storm-influenced SPM flocculation using a tide-wave-combined biomineral model. *Water Environment Research*, 90. doi:10.2175/106143017X15131012152799
- Fettweis M, Lee BJ. 2017. Spatial and seasonal variation of biomineral suspended particulate matter properties in high-turbid nearshore and low-turbid offshore zones. *Water*, 9, 694. doi:10.3390/w9090694.

2. Onzekerheden verbonden aan in situ hoogfrequente en langdurige metingen van SPM concentratie met behulp van optische en akoestische sensoren

Water clarity is an important parameter to understand marine ecosystems and is mainly controlled by suspended particulate matter concentration (SPMC). Data on water clarity collected during the last century, indicate significant local and global environmental changes due to human activities and climate change (Capuzzo et al., 2015; van Maren et al., 2016). The conclusions from these studies are, however, hampered by the often poor quality of the historical data and the very low time resolution of the measurements with regard to the high dynamic nature of the systems in which the data have been collected. In view of documenting current and future trends, high quality measurements spanning long time, large geographical scales and high time resolutions, became a matter of growing importance (Henson, 2014). To detect variabilities in SPMC, networks of observations platforms have been installed worldwide using optical and acoustical sensors as well as sensors that give additional information on shape and size of the SPM, and as the ground truth reference, gravimetric measurements of filtered water samples (e.g. Butman et al., 1979; Grabemann and Krause, 1989; Fettweis et al., 1998; Guézennec et al., 1999; Ganju and Schoelhamer, 2006; Krivtsov et al., 2008; Badewien et al., 2009; Cartwright et al., 2009; Gray and Gartner, 2009; Palinkas et al., 2010; Garel and Ferreira, 2011; Nauw et al., 2014; Anastasiou et al., 2015; Fettweis and Baeye, 2015; Jalón-Rojas et al., 2015; van der Hout et al., 2015; Baschek et al., 2017; Druine et al., 2018). The infrastructure on which the sensors are attached includes fixed (piles, benthic landers, tripods) and moving platforms (vessels, gliders, AUV, ROV) or a combination of both, and the SPMC may cover the whole range from oligotrophic to hyperturbid conditions.

Long-term and high frequent data series of SPMC are typically collected indirectly with unsupervised sensors that measure either the optical beam attenuation as a percentage of light transmission (Moody et al., 1987; Spinrad et al., 1989; Agrawal and Pottsmith, 2000), the back- or sidescatter intensity of light in volt or the backscatter of sound in dB (Thorne and Hanes, 2002; Downing, 2006; Rai and Kumar, 2015). The combination of different sensors measuring in environments with high temporal and spatial variations implicitly demands adapted pre- and post-measurement procedures in order to obtain homogenous data sets. Conversion of the sensor output to physical units (e.g. mass or volume concentration of particles) results from laboratory and field calibrations, and data post processing procedures. The whole procedure requires direct measurements in the laboratory using calibration against standard turbidity solutions and in the field using SPM mass concentrations determined through filtration of water samples. The way the sensor output is transformed to SPMC (in g/l) depends further on the modelling techniques used to relate sensor output to SPMC and is further complicated by the significant variability of the inherent optical and acoustical properties of the SPM. To guarantee the repeatability, not only the laboratory procedures, but also the measuring process, from the planning to the measurements itself and the post processing of the data, needs to be documented (Lane et al., 2000; Waldmann et al., 2010; Bolanos et al., 2011; Gil et al., 2016).

Direct or indirect measurements of SPMC are inherently associated with a number of uncertainties along the whole operational chain from planning over laboratory work, to system problems during mostly unsupervised deployment and to converting the observed continuous proxy values of optical and acoustic signals to SPMC. Little is found in documented guidelines or standards that can be applied to long term observation programs of SPMC in marine and estuarine environments. Recent literature highlights only part of un-

certainties or problems related with the use of optical and acoustical sensors (Rai and Kumar, 2015; Rymaszewicz et al., 2017). The aim of this study is goes further as it discusses potentials, limitations and problems of present practices related with the use of optical and acoustical sensors in long-term deployments and formulates recommendations that may form a basis to acquire best quality-assured SPMC data sets. Other uncertainties or biases in the observation, which are e.g. related to the representativeness of the measuring location within the regional context, the interactions of the measuring infrastructure with the environment, are not part of this study.

2.1. Methods for long-term in situ SPMC measurements

Long-term in-situ measurements of SPMC in coastal seas and estuaries involve in general one or several optical and acoustical sensors of similar or different technical specifications and, as the ground truth reference, gravimetric measurements of filtered water samples. The combination of indirect and reference measurements require two main calibration steps (sensor and model parameter calibration) at different moments during the workflow in order to extract reliable and homogeneous SPMC. These calibration steps are essential to be able to relate possible changes in calibration constants (sensor and model parameter) to sensor degradation or to natural variability in SPM inherent properties.

2.1.1. Terminology

The terminology related to calibration, turbidity or sensors is not unambiguously used, e.g. distinction between the two calibration steps is not mentioned explicitly and turbidity units are wrongly used. A well-defined terminology is important to obtain consistent and uniform sensor SPMC in long term (and other) measurements, where multiple sensors are used together (in parallel and in succession).

Sensor calibration refers to the comparison of the output signal of an optical or acoustical sensor against a standard in the laboratory (e.g. Thorne et al., 1991; Downing, 2006). For turbidity this is usually Formazin[®] or an alternative standard (AMCO clear[®], StablCal[®]), while for acoustical backscatter intensity a solution of standard spheres with a given size distribution, concentration and at a given distance from the transducer is used. Acoustic sensor calibration is not commonly applied for long-term measurements due to practical difficulties in setting up a laboratory device. Sensor calibration results in converting the sensor output to various turbidity units (see below) or decibels (dB). During long-term field operations the sensor calibration constants against a standard may alter, due to e.g. changes in battery supply, (bio-)fouling, degradation of the measuring window or of the sensor. Any of these changes in the sensor calibration constants are inherent to the sensors and not to the environment and must if possible be corrected.

Model parameter calibration is the result of a regression of inverse optimization with sensor signals, ideally from the undisturbed environment, as input and corresponding to the real SPMC as output. This type of calibration is well distinguished from sensor calibration as it relies on natural particles (in contrast with Formazin[®] or an alternative standard that consist of artificial polymeric particles, see Downing, 2005) and has to be carried out regularly or each time when the SPM inherent properties change significantly. If the sensors have been well-calibrated then any changes in model calibration constants are caused by changes in SPM inherent properties. Variabilities in these properties affect the relation between real SPMC and sensor signal.

Sample SPMC is the SPMC obtained from filtration and gravimetric measurements of water samples. As the real SPMC cannot be measured by any direct method we will use the sample SPMC as our reference SPMC, as it is by a lesser degree influenced by the inherent particle properties of the SPM (Neukermans et al., 2012a; Röttgers et al., 2014).

Sensor SPMC is a surrogate obtained by an acoustical or optical backscatter sensors or other type of sensors. Depending on the methods different surrogates of SPMC are obtained. In case of long-term measurements different sensor SPMCs are often obtained that represents surrogates or proxies that are not necessarily the same (e.g. Rai and Kumar, 2015; Rymaszewicz et al., 2017).

Turbidity refers to the optical water cloudiness caused by suspended particles and dissolved substances, which scatter and absorb light (Downing, 2005; Ziegler, 2003; Gray and Gartner, 2009). Turbidity has not a SI unit, is not uniquely defined and differs according to the applied protocols. It is thus an arbitrary unit that is incomparable to measurements taken at other times and places or with different turbidity meters, which diminishes the comparability of turbidity data for scientific purposes (Downing, 2006). The ISO Method 7027 (ISO, 1999) and the American EPA Method 180.1 (EPA, 1993) estimate turbidity in Formazin Nephelometric Units (FNU) or Nephelometric Turbidity Units (NTU), respectively. The optical sensor to be used is a nephelometer and must measure side-scattered light, i.e. at 90°, with a difference between the two norms regarding the source light wavelength: 860 nm is prescribed for ISO, 400 to 600 nm for EPA. Both refer to a Formazin®-equivalent turbidity value. In case an alternative standard is used, then it should be explicitly stated that turbidity refers to the alternative standard-equivalent NU or TU. The unit of the Formazin® (or of another) standard is generally –for historical reasons - given in NTU although the solution is established following the ISO or EPA protocol. In an ISO-compliant Formazin solution of 1000 "NTU" an ISO-compliant side-scattering sensor will measure 1000 FNU, whereas an EPA-compliant side-scattering sensor will measure another value in NTU. The difference between FNU and NTU is mainly due to the spectral range of lights that are emitted by the instruments.

Optical Backscatter Sensors (OBS) measure the particle backscattering of light at different angles of detection (120°-165°, or even including side and forward scattering depending on the type of sensor); although highly correlated, the turbidity measured by an OBS and a Nephelometer is not necessarily the same; e.g. Nechad et al. (2016) report a large variability in the relationship between in situ side- and back-scattering coefficients in the lower turbidity range (<20 FNU) and a drastic decrease with increasing turbidity. Turbidity from backscatter devices should be expressed in **Formazin Backscatter Units** (FBU) for the near IR (830-890nm) light (ISO Method 7027) and **Backscatter Turbidity Units** (BTU) for the EPA Method 180.1 (Dogliotto et al., 2016; Nechad et. al, 2016). Often FTU (Formazin Turbidity Unit) or NTU are used as unit without specifying how the instrument measures the sample (side, back or forward scattering) or which protocol it follows (ISO or EPA). By adapting the correct units the confusion on protocol or scattering angle can be avoided.

2.1.2. Inherent properties of the SPM

SPM consists of a mixture of clay to sand sized particles in suspension that comprise with varying amounts minerals from physico-chemical (e.g. clay minerals, quartz, feldspar) and biogenic origin (e.g. calcite, aragonite, opal), and living (bacteria, phyto- and zooplankton) and non-living organic matter (fecal and pseudo-fecal pellets, detritus and its decomposed products from microbial activity such as mucus, exopolymers), see Table 2.1 and Figure 2.1. SPMC measurements are only meaningful if they can be measured with sufficient accuracy using samples and sensors, a condition that is often attained in coastal seas and estuaries. Particles are considered in suspension as long as they do not form an interconnected matrix of bonds that prevents mobility; this corresponds to a concentration that is below the gelling point (McAnally et al., 2007). The lower limit in concentration corresponds to the detection limit of the instrumentation or sampling; the upper limit is theoretically just below the gelling point when the particles are so close together that settling is

substantially hindered and a two-layer stratified flow with a distinct density interface remains (Ross and Mehta, 1989; Winterwerp and van Kesteren, 2004), practically the upper limit depends on the sensor specifications and on the difficulties to measure in the very near-bed layer where these high concentrated layers are found. For many sensors, the upper limit is O(10g/l), far below the gelling point concentration O(50g/l).

Table 2.1: Bulk mineralogical composition (in %) of the SPM in the English Channel and southern North Sea sampled with a centrifuge during transect or anchoring of the vessel. Offshore Somme mouth, Dover Strait, Calais, Zeebrugge and north of the Rhine mouth. Qtz=Quartz; Kspar =K-feldspar; Plag=Plagioclase; Carb=Sum of Calcite, Mg-rich Calcite, Dolomite, Aragonite; Am=Amorphous fraction (organic matter and biogenic opal); Hal=Halite; NClays=Sum of non-clay minerals; Kaol=Kaolinite; Chl=Chlorite; 2:1=Sum of 2:1 clays and micas; Clays= Sum of Kaol+chl+2:1. The samples have been collected with a centrifuge (water intake about 4 m below surface) during transects or anchoring of the RV Belgica and analysed with XRD (data from Adriaens et al., 2018).

	Qtz	Kspar	Plag	Carb	Am	Hal	NClays	Kaol	Chl	2:1	Clays
Somme	29	2	3	30	15	5	86	<1	<1	10	10
Dover Strait	22	3	2	21	18	7	84	2	4	20	26
Calais	10	1	<1	29	22	3	66	<1	2	31	33
Zeebrugge	20	1	5	24	10	2	61	2	4	33	39
Rhine offshore	29	4	1	21	12	3	70	1	2	27	30
Rhine nearshore	17	4	2	21	16	1	61	2	1	35	38

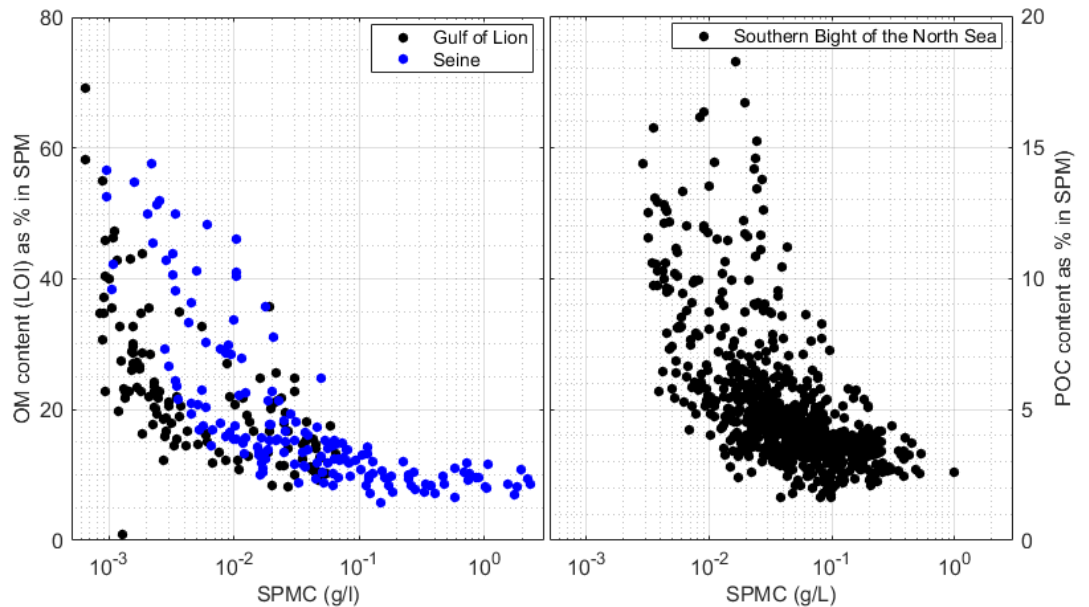


Figure 2.1: Organic matter (OM) content in the SPM from the Seine estuary and the Gulf of Lions (left) determined through Loss-on-Ignition (LOI) and Particulate Organic Carbon content from the Southern Bight of the North Sea (right) determined through element analysis. The OM data are about four times larger than the POC data (Grove and Bilotta, 2014). Both data set show that largest variation in organic matter content occurs at low SPMC.

Depending on the seafloor composition (cohesive and non-cohesive sediments), the vicinity of sediment sources, the hydrodynamics, the measuring height above the bed and

biological activity, the composition of the SPM may change with time. Sand grains are generally limited to the near-bed layer (bed-load), while fine-grained sediments can be found all over the water column. The fine particles, such as clay minerals, other charged particles and polymers in suspension may become attached to each other (flocculation) to form fragile structures or flocs with compositions, sizes, densities, and structural complexities that vary as a function of turbulence, chemical environment (salinity) and biochemical composition (e.g. Eisma, 1986; Dyer and Manning, 1999; Droppo et al., 2005; Fettweis and Lee, 2017). While the size of the building particles of flocs is of the order of a few μm , fully developed flocs may grow up to a few hundreds of μm or more; larger flocs have generally higher water content, higher organic content and lower density.

Changes in the concentration and the composition of the SPM influence the optical and acoustical properties and if not calibrated for these conditions also the sensor SPMC. Further to changes in composition the SPMC is generally higher in the estuarine and nearshore areas (10 mg/l up to O(1-10 g/l)), due to resuspension and erosion of bed material, river inputs, coastal erosion, and estuarine circulation, than in more offshore deeper areas of the continental shelf (<10 mg/l). As a consequence, SPM properties and concentration fluctuate on a broad range of temporal and spatial scales with different magnitudes and exhibit substantial gradients along estuaries and with distance from the coast (Fettweis et al., 2006; Becker et al., 2013; Maerz et al., 2016).

2.1.3. Sensors used to obtain long-term SPMC time series

2.1.3.1 Sensitivity of optical sensors to inherent particle properties

Various measurements of inherent optical properties (IOPs), which do not change with changing light field in water, are used as surrogate to SPMC. Optical sensors rely on propensity of SPM to interact with light (at a given wavelength λ) through absorption $a(\lambda)$ and scattering $b(\lambda)$. For long-term measurements, the attenuation or the scattering at a given angle are mainly used to obtain the SPMC surrogates. The attenuation coefficient, c [m^{-1}], at a given wavelength, λ , is the ratio of the radiant flux, I , lost from a beam of infinitesimal width, to the incident flux E , per unit distance is

$$c(\lambda) = \frac{I(\lambda)}{E(\lambda)} \quad (1)$$

The volume scattering function (VSF) denoted by $\beta(\lambda, \theta)$ [$\text{m}^{-1} \text{sr}^{-1}$], which describes the amount of radiant intensity $I(\lambda)$ [W sr^{-1}] scattered in a given direction θ , by an infinitesimal volume ∂v , relative to the direction of the incident irradiance $E(\lambda)$ [W m^{-2}] (i.e. radiant flux coming from all directions, at wavelength λ) is

$$\beta(\lambda, \theta) = \frac{\partial I(\lambda, \theta)}{E(\lambda) \partial v} \quad (2)$$

The spectral absorption and scattering coefficients, $a(\lambda)$ (m^{-1}) and $b(\lambda)$ (m^{-1}) verify $c(\lambda) = a(\lambda) + b(\lambda)$. The scattering defined as the integral of $\beta(\lambda, \theta)$ over all directions is

$$b(\lambda) = 2\pi \int_0^\pi \beta(\lambda, \theta) \sin(\theta) d\theta \quad (3)$$

The spectral side-scattering coefficient $b_s(\lambda)$ [m^{-1}] is equal to $\beta(\lambda, 90^\circ)$. The spectral backscattering coefficient $b_b(\lambda)$ [m^{-1}] is the integral of $\beta(\theta)$ over the backward directions:

$$b_b(\lambda) = 2\pi \int_{\frac{\pi}{2}}^\pi \beta(\lambda, \theta) \sin(\theta) d\theta \quad (4)$$

Available sensors can differ in wavelength and backscattering angle. Particles backscattering of light, $b_b(\lambda)$, is theoretically calculated as the integration of VSF covering all backward directions. Boss and Pegau (2001) and Berthon et al. (2007) showed that b_b is highly correlated to β at angles between 120° - 140° . A good approximation for $b_b(\lambda)$ is to be estimated from $b_b(\lambda, 140^\circ)$, while Chami et al. (2006) found that the increase of β at

$\theta > 150^\circ$ can significantly impact the backscattering. The backscattering of particles at large wavelengths ($\lambda > 700\text{nm}$) gives the best estimations for SPMC (Downing, 2006; Boss et al., 2009). The effects of absorptions by particles and colored dissolved organic matter is high at shorter wavelengths (Yentsch, 1962) and can impact (back)scattering or turbidity estimation by sensors that use light source emitting at short wavelengths, as was highlighted by Sutherland et al. (2000) and Downing (2005). In more turbid waters, high particles absorption impacts more the estimation of backscattering coefficient even at longer wavelengths and should be properly corrected for (Doxaran et al., 2016). As mentioned above, ISO Method 7027 (ISO, 1999) and EPA Method 180.1 (EPA, 1993) estimate turbidity T in Formazin Nephelometric Units (FNU) or Nephelometric Turbidity units (NTU), respectively, such as $T = \frac{\beta^{(90^\circ)}}{\beta^F(90^\circ)}$ where $\beta^F(90^\circ)$ [m^{-1}] is the volume scattering function at 90° of a unit of Formazin, at prescribed wavelength. However, other types of optical sensors, such as backscatter sensors, are widely used to measure turbidity and hence to estimate SPMC. In terms of sensor calibration, i.e. based on successive dilution of a standard solution, this does not cause problems as the sensor output will be compared, and then associated, to the standard solution that can be expressed in a turbidity unit. This calibration must then be used for quality control to ensure the stability of the intrinsic sensor performance, and possible drifts induced by electronic failure or damages on optical windows that may induce maintenance and repair. The main issue comes when these instruments measure turbidity in situ or from natural water samples as IOPs (i.e. scattering efficiency K) and hence the VSF are dependent on particles shape (Slade et al., 2013), particles size and density, refractive index (Mishchenko et al., 2002; Boss et al., 2004), and color (Sutherland et al., 2000; Hatcher et al., 2000).

Generally, $b(\lambda) = K(\lambda, r)N(r)\pi r^2$, where K is the scattering efficiency factor for non-absorbing particles, N the number density of particles, and r the particle radius. For spherical particles $SPMC = \frac{4}{3}N\rho\pi r^3$, where ρ is the dry density (i.e. particle mass divided by the particle volume), resulting in a ratio of turbidity to SPMC that is inversely proportional to the particle radius and density (Sutherland et al., 2000):

$$b = \frac{3}{2} k(\lambda, r) \frac{SPMC}{\rho r} \quad (5)$$

The SPM dry density (proportional to the excess density) can, depending on the particle composition, be anywhere in between the range of well below 100 kg m^{-3} for the organic flocs and up to 2650 kg m^{-3} or more for the individual mineral particles. In case the SPM consists of flocs the variations in density and size can be very large, with the densest flocs having the smallest size and vice versa. With this consideration, the dependence of b on ρr is weaker than $1/r$ (Bowers et al., 2009) but can still be significant (Gibbs, 1985; Babin et al., 2003; Baker and Lavalley, 1984). This demonstrates that a change in the composition of particles and/or their shape, size and density affects the turbidity measured by a backscatter sensor (e.g. Binding et al., 2005; Neukermans et al., 20012b; Zhang et al., 2014; Druine et al., 2018), but also indicates that the model parameter calibration of optical backscatter instruments using a single optical property (backscattering coefficient or beam attenuation) against sample SPMC is often successful over a wide range of particle sizes (Boss et al., 2009b; Bowers et al., 2017).

2.1.3.2 Sensitivity of acoustical sensors to inherent particle properties

Acoustics devices commonly used in coastal areas, i.e. ADVs or ADCPs are primarily designed for current velocity measurement. Similarly to optical devices, the emitted acoustic wave, at a given frequency, interacts with particles in suspension while propagating in the medium and are backscattered to the receivers (Thorne and Hanes, 2002). The recorded

volume backscattering strength (S_v , in dB) is a proxy of the SPM concentration, but is also strongly modulated by SPM features such as size, density and shape, depending on the acoustic wavelength. Originally used in sandy environments (Sheng and Hay, 1988; Thorne and Hanes, 2002), these devices are now routinely deployed in fine sediments environments (e.g. Gartner, 2004; Hoitink and Hoekstra, 2005; Tessier et al., 2008; Sahin et al., 2013). The sonar equation (Urlick, 1975) is commonly used to relate S_v (in dB) and SPMC concentration, including acoustic signal correction for geometry compensation, spherical spreading, and water and particle attenuation:

$$\frac{S}{N} = SL - 20 \log_{10}(\psi R^2) - 2 \int_0^R (\alpha_w(r) + \alpha_s(r)) dr + BI + 10 \log_{10} \left(\varphi R^2 \frac{ws}{2} \right) \quad (6)$$

and

$$BI = 10 \log_{10} \left(\frac{SPMC \bar{\sigma}}{\rho_s \bar{v}_s} \right) \quad (7)$$

where S/N is the signal to noise ratio (dB) received by the device. After Gostiaux and Van Haren (2010), Mullison (2017) specifies the values of S/N in function of the raw echo readings (in counts) of the ADCP devices. SL is the source level (dB); R is the along-beam distance from transducers, α_w and α_s respectively the water and sediment attenuation, φ the angular aperture; ws the cell size and ψ the near field correction. $\bar{\sigma}$, ρ_s and \bar{v}_s are particle features: backscattering cross section, particle dry density and volume respectively.

Similarly than optical devices, the relationship between the acoustic backscatter and SPMC strongly depends on the nature, size, density and shape of the particles, either flocs or grains, both for the estimation of the particle attenuation and for the calculation of the backscattering cross section (Ha et al., 2009; Salehi and Strom, 2011; Rouhnia et al., 2014), achieved using theoretical acoustic models (Thorne and Hanes, 2002; Stanton, 1998). However, contrary to optical devices, the sensor calibration is not routinely (often never) operated due to the difficulty to access requested laboratory facilities. Hence this step is often skipped and quality check is based on comparison with other in situ sensors or SPMC samples.

2.1.3.3 Conversion of optical and acoustical sensor output to SPMC

The relationship between OBS or nephelometer signal and SPMC is almost linear as long as the sensor is not deployed in highly concentrated waters (Downing, 2006), and the simplest model is a linear regression model. The same holds for single point acoustical sensors (ADV) or for the first bin of a profiling acoustical sensor, where the target volume is very close to the sensors. As far as SPMC are lower than several g/l, a direct empirical relationship can be built such as $\log_{10}(SPMC) \sim S_v$, where S_v can be related to the signal/noise ratio (Fugate and Friederichs, 2002; Voulgaris and Meyers, 2004; Verney et al., 2007; Ha et al., 2009; Salehi and Strom, 2011).

For profiling acoustic sensors the sonar equation should be considered to correct for the signal loss along the acoustic path. The conversion factor from counts to dB, as commonly used in acoustics, is typically provided by the manufacturer. Close to the transducer, the acoustic signal has to be corrected for near-field effects (Downing et al., 1994) and for ringing effects that may affect the first bins, in particular when blank distance is set too small by in the configuration parameters. Corresponding data cannot be corrected and should be discarded (Muste et al., 2006). A formulation for the water absorption coefficient was proposed by e.g. François and Garrison (1982a, 1982b) and later simplified by Ainslie and McColm (1998), who showed that their result did not differ from the original equation more than the accuracy error. The sonar equation yields the so-called water-corrected backscatter, which is a property of the suspension at all locations along the acoustic path. Subsequent processing depends on the SPMC. In case of moderately turbid

environment, i.e. lower than 100mg/l, sound attenuation by SPM is usually neglected as it is one or two orders of magnitude lower than the water absorption coefficient (Ha et al., 2011). SPMC is then either determined by applying an appropriate calibration, similar to single point optical sensors, or by a theoretical acoustic model. In the latter case, physical properties of the transducer and of the SPM must be exactly known, which are rarely available. If SPMC exceeds 100mg/l, sediment absorption should be considered. While the calibration is performed to calculate SPMC profiles, these are in turn required correcting backscatter for sediment attenuation. This is solved by iterative methods (Thorne et al., 1994; Holdaway et al., 1999). A critical point is that the sediment absorption coefficient is assumed to be known a-priori, which is somewhat contradicting. The actual calibration is correcting for unknown backscattering properties of particles in suspension, while these are implicitly assumed to be known calculating the sediment absorption coefficient (Becker et al., 2013). This technique is efficient but requires assumption or knowledge about SPM characteristics (size, density) and is based on the choice of an acoustic model adapted to the observed SPM, and may in some specific case exponentially propagate uncertainties and fail to estimate SPMC.

When sediment attenuation must be accounted for, theoretical acoustic model must be built, simulating the physical interactions between particles and the acoustic signal (Sheng and Hay, 1988, Medwin and Clay, 1998). These models were originally designed for sand particles and hence considering particles in suspension as rigid spheres (Thorne and Hanes, 2002). They fail to represent low density aggregated SPM, and a first model derived from works by Stanton (1998) could be applied. Recent developments achieved to adapt a hybrid acoustic model for flocs, through a transition between quasi-rigid primary particles and floc-like fluid-elastic spheres (McDonald et al., 2013, Thorne et al., 2014). Differences between models mainly appear in the methodology to calculate the total scattering and backscattering cross section as well as the compressibility of flocs and their ability to interact with sound. For more details, see Thorne et al. (2014). This hybrid model was successfully applied by Sahin et al. (2017) to an estuarine environment with SPMC larger than 1g/l.

2.1.4. Existing international guidelines and standards

In the European context the only guidelines exist for OSPAR's Joint Assessment and Monitoring Programme (JAMP), see JAMP (2012). They refer to the ICES TIMES report by Yeats and Brüggmann (1990) that deals with the collection methods of water samples. The Trilateral Monitoring and Assessment Program for the Wadden Sea (TMAP) mentions suspended matter concentration as a supporting, not mandatory parameter in their handbook on nutrients, see TMAP (2009). The handbook explicitly refers to the corresponding guidelines of JAMP. HELCOM (2015) also treats SPMC as a co-factor in water analysis and again keeps its determination by filtration according to ISO (1997) and includes as an indirect measure for SPMC, the Secchi depth. ICES itself stipulates only guidelines for data formats.

In a global framework, the IOC-EU-BSH-NOAA-(WDC-A) International Workshop on Oceanographic Biological and Chemical Data Management dealt with a number of biogeochemical bulk parameters, but does not contain SPMC in the variable list. GOOS so far does not present best practice manuals. For the ARGO program QC manuals for bio-Argo particle backscattering measurements are yet in development (Schmechtig et al., 2015), the main purpose of these measurements is the use of the backscattering coefficient as proxy for POC concentration (IOCCG, 2011); which will possibly limit the usefulness of such QC systems to coastal seas and estuaries. NOAA is responsible for numerous monitoring programs along the US coasts, but does not provide standards for SPMC measurements in official documents. In some technical reports, however, the methods to obtain SPMC are

described, always using gravimetric analyses of water samples (e.g. Pait et al., 2015)

For the large-scale integrated ocean and coastal ocean observatories, such as IOOS (<https://www.ioos.us/>) and IMOS (<http://www.imos.org.au/>), no guidelines for best practice of SPMC measurements are put forward. SPMC is not part of operational real-time observation, but at least in the case of IMOS, SPMC data sets based on water samples are regularly created at reference stations (e.g. Lynch et al., 2008).

Table 2.2: List of additional state parameter needed to interpret the results of long-term SPMC measurements with more accuracy and completeness.

State parameter	Method	Type
Particle size in situ	Laser diffractometer, holography, optical camera systems	sensor
Particle size in lab	Grain size analysis (primary particle size)	water, centrifuge sample
Particle composition	LOI: Organic matter Element analysis: POC, PON XRD: Mineral composition Pigment analysis: Chlorophyll Colorimetric analysis: TEP concentration Electron microscopy	water, centrifuge sample
Particle composition	Fluorimeter: Fluorescence Primary production: Fast Repetition Rate Fluorimeter	sensor
Particle shape	Holography, floc camera Electron microscopy	sensor water sample
Turbulence	High frequency Acoustic Doppler Sensor	sensor
Currents	Acoustical Doppler Sensor	sensor
Waves	Acoustic Doppler Profiler, Wave rider, floater	sensor or station
Density	Conductivity, Temperature	sensor
Water level	Pressure sensor; tide gauge	sensor, station
Distance to bed	Acoustic altimeter	sensor
Meteo	from relevant meteo stations	station

The U.S. Geological Survey provides a number of documents comprising guidelines for the sampling (Edwards and Glysson, 1999), for the lab analysis of the samples (Matthes et al., 1992; Shreve and Downs, 2005), for the proper layout and operation of field stations and sensors to meet accuracy and precision requirements (Wagner et al., 2006), and how to compute time series of SPMC and their related loads using proper statistical regression models between turbidity and sample SPMC and evaluating their outcomes (Rasmussen et al., 2009). The latter was expanded for acoustical backscatter measurements (Topping and Wright, 2016). These guidelines were developed for measurements in rivers, but many of them can be transferred to estuaries and coastal seas in a straight forward way, except that ones need to take into account that the conditions in estuarine and coastal ocean waters differ in two major aspects. Firstly, the field stations are generally more remotely located from the landside and much harder to access and to maintain. Secondly, the SPM exhibit much higher variability on texture and composition. Fluvial SPM consists predominantly of mineral matter with generally minor changes in particle size and composition, except during high river runoff, when particle size may significantly change. Estuarine and marine SPM on the other hand exhibits significant inherent variability in composition, cohesiveness and size, which increases the occurrence of uncontrolled uncertainties, the need for additional instrumentation (see Table 2.2) and the number of model parameter calibrations to perform.

2.2. Sources of uncertainties

Uncertainties, as described in Ramsey and Ellison (2007) and ISO (2008; 2017), hamper data quality and may arise from mal-functioning of sensors (2.2.1), the environment influencing the sensors without changes in SPMC (2.2.2), SPMC sample collection and analysis (2.2.3), modelling of sensor output to sample SPMC (2.2.4), the variability of the model that relates sample and sensor (2.2.5), and additional uncertainties arising from human error and uncontrolled environmental boundary conditions (2.2.6).

2.2.1. *Sensor related uncertainties*

Sensor related uncertainties occur if the sensor output changes over time unrelated to changes in inherent particle properties or SPMC. Concerning optical backscatter sensors this is caused by variations in voltage supply, changes in the transmittance of the window that is the interface between the sensor and the water or other degradations. Concerning acoustical backscatter sensors the main sensor related uncertainty is related to battery power. The reason that no other sensor related uncertainties are documented is due to the limited availability of facilities to test acoustic sensors in a lab, and that in contrast to optical sensor, no standards and norms exists so far to test and calibrate acoustical backscatter sensors. Other uncertainties may arise from the drift of the internal clock of the sensor or the data logger in particular in case of long term monitoring.

2.2.1.1 *Drift of a sensor with time*

Optical sensors are subject to gradual decreasing transmittance of the sensor window during deployment due to damages caused by the collision of particles. Therefore the factory calibration parameters should be used with care and be checked regularly. After intense and occasional usage during several years the slope between factory calibration and Formazin recalibration of 11 Seapoints agreed on the average within 1% but showed standard deviation of 15%. Figure 2.2 shows a comparison between an OBS3+ factory calibration and a sensor calibration obtained after 329 and 421 days highly turbid (SPMC > 1g/l) sea water. Using the factory calibration constants without recalibration would indicate an apparent increase of the turbidity. Any of these changes in the calibration constants are inherent to the sensors itself and the need of recalibration has to be specified by the user based on the required precision.

Variations in voltage supply result in a drift, which is unrelated to variations in SPMC or inherent particle properties. In clear water the output of e.g. an OBS3+ will be a minimum voltage, increasing to a maximum voltage at the maximum turbidity range. The sensor needs to be fed by a constant minimum voltage in order to give good data. Lower voltage supply results in an apparent decrease in turbidity. Figure 2.3a shows an OBS3+ in low (0-2000 BU) and high (0-4000 BU) range that has been fed with different input voltages while measuring in a standard of 2000 Amco-Clear®-equivalent BU. For an input voltage of more than 6 V the low range registers a constant value of 5.1 V (saturation), while the high range registers about half of it (2.5 V). If the supplied voltage decreases, the signal registered by the OBS3+ decreases as well. An example of a time series collected with a corrupted and a well-functioning sensor is illustrated in Figure 2.3b. Due to an insufficient voltage supply the recorded SPMC signal was on average about 90% lower than it should

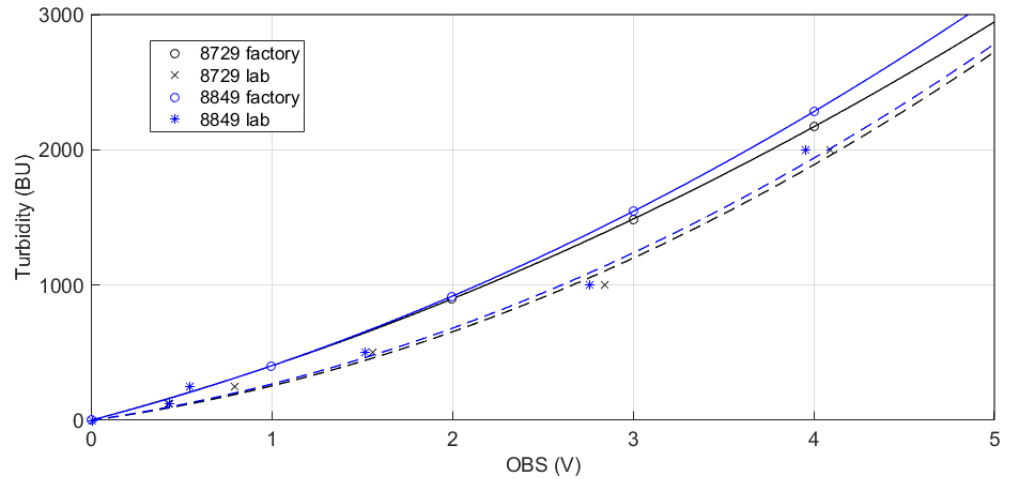


Figure 2.2: Factory and in lab sensor calibration of two OBS3+. The laboratory calibration was done after 421 (8729) and 329 (8849) days of measurements in high turbid (SPMC > 1g/l) sea water during 2014-2016. The solid lines are the 2nd order polynomial fittings provided by the factory, the dashed lines are the 2nd order fittings after recalibration.

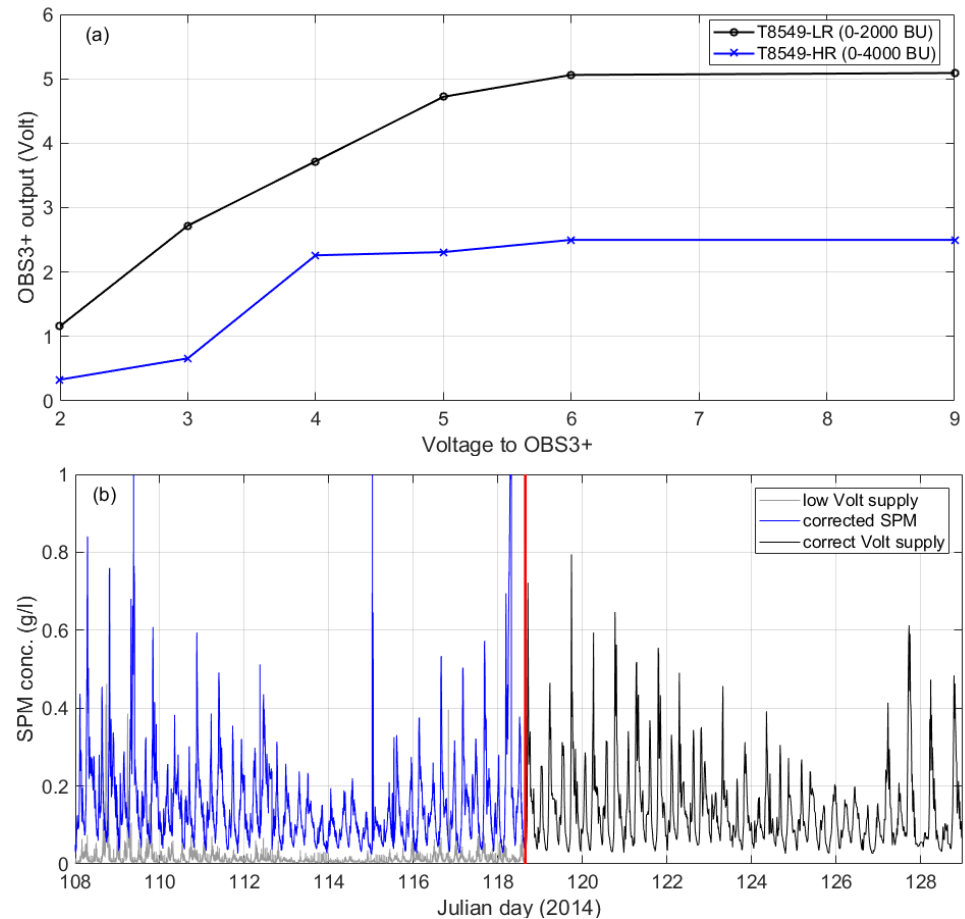


Figure 2.3: (a) Power provided by an external source to a OBS3+ measuring in a solution of 2000 AmcoClear® equivalent BU. When the voltage drops below 6 V, the sensor registers low voltage output values. (b) SPMC time series measured with a OBS3+ that was attached to a SonTek Hydra for storage and battery supply. The system was replaced on day 118.7 by a similar system. The first system was not providing the minimum of 6V to the OBS. The second system worked correctly. In blue is shown the corrected time series.

be. After sensor calibration with lower voltage supply the data could be corrected. Battery

power affects also acoustical backscatter sensors (Tessier et al., 2008). From the registered battery voltage during the deployment the emitted power can be converted into the correction factor P_{dbw} calculated as $P_{dbw}=10\log(P^2)/R$, with R the electrical resistance. If only one of the transducers of profiling acoustical sensors supplies more or less power than the others, then this can be corrected using the other transducers (Tessier, 2006).

2.2.1.2 Sensitivity of sensors

Some optical backscatter sensors, such as an OBS3+, are dual range sensors having both a low- and a high-range output. The two measuring ranges increase the resolution of the measurements, but each output is more accurate when its designed turbidity range matches its calibrated range. The RMS error between high and low range output depends on the turbidity, e.g. for an averaged turbidity around 20 the low range (500 BU) recordings during a tidal cycles differed by about 2% with the high range ones (2000 BU). When increasing the ranges (low: 1000 BU, high 4000 BU) then the relative difference increased to 24%. The optimal range is to be chosen according to the expected range of turbidity values in the field.

2.2.1.3 Inter-sensor variability

The aim of multi-sensor calibration is to generate a reliable model parameter calibration to estimate SPMC at long-term monitoring stations by repeated field surveys and to record variabilities caused by the use of similar types of sensors. Figure 2.4 shows the result of a simultaneous calibration of three OBS3+ sensors during a tidal cycle. The RMSE between the three OBS3+ sensors, which have been calibrated against the same sample SPMC, was 2.6% for 1 Hz sampling and 2% for an averaging over 60s. The difference between sensor outputs is changing during the course of the measurements. This points to small scale variations in the SPMC (sensor are located about 50 cm from each other) and to different sensitivities of the individual sensors. These examples presented strengthen the necessity of sensor calibration (difficult to achieve for profiling acoustic sensors) and model calibration for each sensor separately.

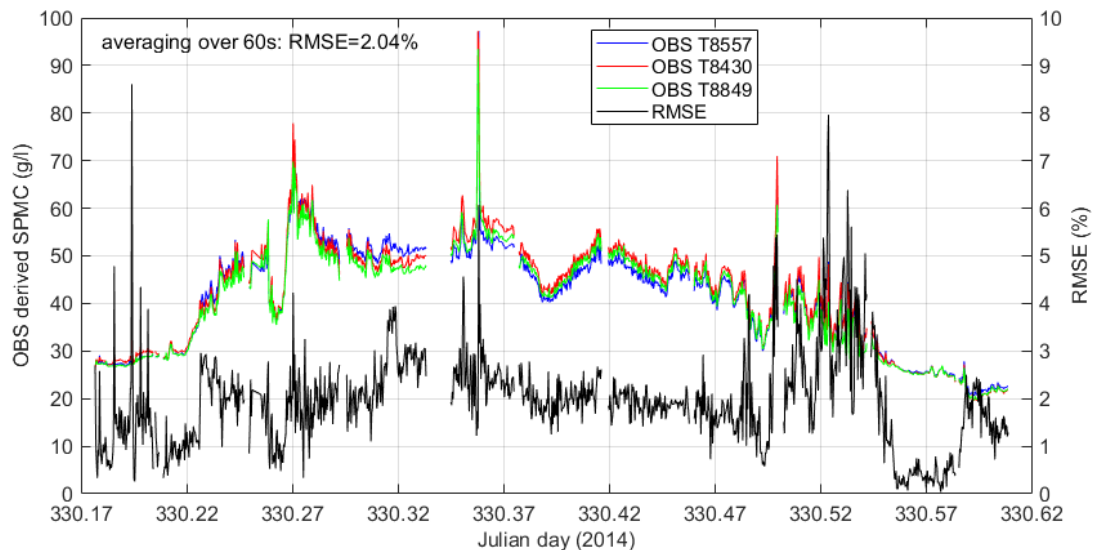


Figure 2.4: Inter-sensor variability between three OBS3+ sensors measuring at about 50 cm from each other during a tidal cycle (Belgian nearshore area). The sensors have been calibrated using the same sample SPMC. The differences between the OBS's change during the course of the tide. This points possibly to variations in the SPMC (sensor are located about 50 cm from each other) or to different sensitivities of the individual sensors.

2.2.2. Environmental related uncertainties

Environmental related uncertainties occur when the acoustic or optical backscatter sensor output changes over time unrelated to changes in inherent particle properties or SPMC or when the sensor measures outside its designated range. The former occurs when the signal is attenuated by biofouling or the occurrence of air bubbles. The latter occurs, e.g. in case of an OBS, when the emitted light beam is strongly attenuated and backscattered light decreases with increasing sediment concentration, resulting in an ambiguous interpretation of the signal (Downing, 2006; Sottolichio et al., 2011).

2.2.2.1 Biofouling

Biofouling or other type of fouling can limit the accuracy and quality of long-term SPMC measurements within a week, depending on the season and the environment. Biofouling occurs in four phases starting with the development of an organic film, followed by primary and secondary micro colonizers and finally tertiary colonizers attach to the microfouling film (Abarzua and Jakubowski, 1995). The impact of the different phases on the recorded signal remains difficult to estimate and can result in a temporary or permanent increase of the backscattered signal due to additional reflection or a decrease due to attenuation (Kerr et al., 1998; Delauney et al., 2010). Increase of the backscattered signal can also be caused by plant or artificial (e.g. fishnet) filaments trapped by the measuring infrastructure and constantly or ephemerally influencing the detection volume. There are several methods and reasons to protect the sensors against biofouling (Ridd and Larcombe, 1994; Manov et al., 2004; Whelan and Regan, 2006). The most obvious reason is to obtain good quality data. Another one is that the fouling development on the whole measuring infrastructure can disturb the properties of the study site. For example, the growth of epi-fauna on the infrastructure may influence the measurements as they trap, accumulate and temporarily release SPM (Baeye and Fettweis, 2015). Effectively biofouling results in a gradual and continuous drift of the signal over time together with an apparent decrease in sensitivity (Dolphin et al., 2000; Downing, 2006; Jourdin et al., 2014). Permanent biofouling events will gradually change the backscatter intensity and can only be corrected if a non affected reference sensor is at hand. The reference sensor can be single beam acoustic or optical backscatter sensor or a not-affected beam of an acoustic profiler. The onset of a change in the SPMC signal due to biofouling is difficult to identify and therefore should be based on the hypothesis that the observed changes cannot anymore be explained by known physical behavior of SPMC variations.

Figure 2.5 is an example of epi-fauna (barnacles) growing on an OBS that resulted in an increase of backscatter intensity until saturation and thus an overestimation of the SPMC. The timing of biofouling was estimated at the point where the ratio of the affected sensor to a non affected one started to increase monotonically. Acoustical sensors are less sensitive to biofouling than optical sensors. Nevertheless biofouling has been observed on moored up-ward looking ADCPs. A straightforward identification of these events is possible by computing the maximum backscatter ratio (Jourdin et al., 2014). In absence of biofouling the ratio will have values close to the sensor noise (typically 1 dB). A drop of up to 10 dB has been observed in ADCP moorings deployed off the French coast (Jourdin et al., 2014), while in an ADCP mooring off the Belgian coast a gradual drop of more than 20 dB in backscatter strength have been recorded. A value of 10 dB leads to under-estimation of the suspended sediment concentration by one order of magnitude, over the entire acoustic profile. If only one beam of an ADCP is affected by biofouling, this can be corrected by applying the median function to all beams as explained in Jourdin et al. (2014). Figures 2.6 is an example of permanent biofouling resulting in a gradually decrease of the backscatter

strength during the mooring, while in Figure 2.7 shows episodic biofouling events.

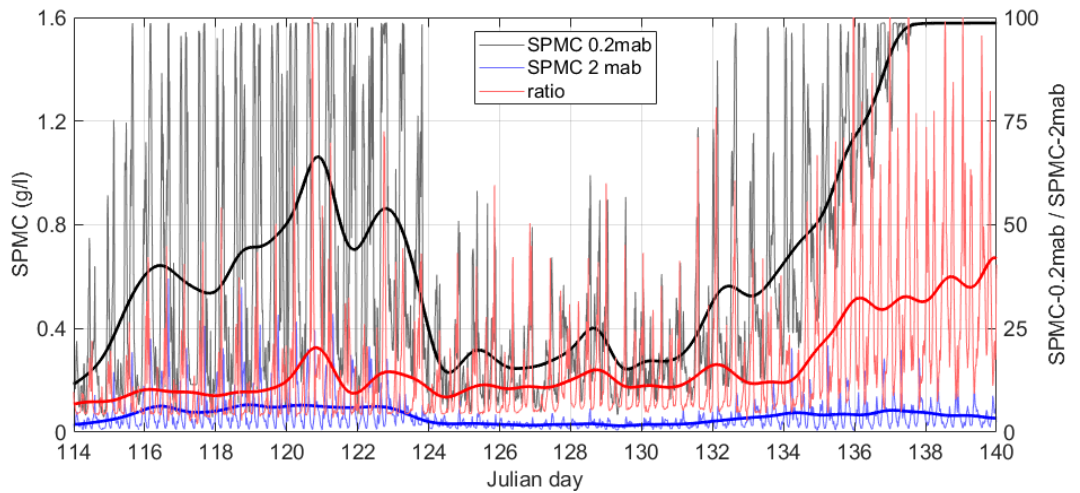


Figure 2.5: The time series collected in the Belgian nearshore area show the OBS derived SPMC at 0.2 and 2 mab (left axis) and the ratio between SPMC at 0.2 and at 2mab (right axis). The thick lines are the low-pass filtered data. The OBS at 0.2 mab was covered by barnacles, while the one at 2 mab was not affected by biofouling. The low-pass filtered ratio indicates that biofouling started to affect the OBS at 0.2 mab from about day 134 onward. The OBS at 0.2 mab saturated during the measuring period when the SPMC exceeded about 1.6 g/l.

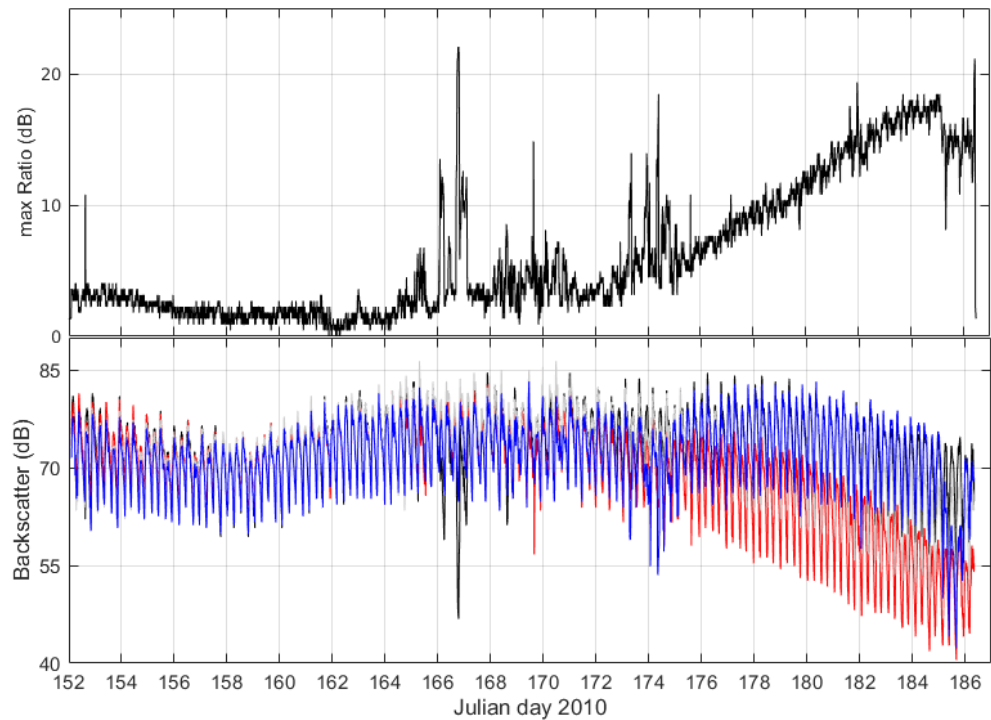


Figure 2.6: 35-day time series of maximum backscatter ratio (up) and the backscatter strength (down) recorded by an upward-looking 1.2 MHz RDI ADCP (5th bin at about 1.5 m above the ADCP is shown) moored offshore the Belgian coast. Changes in the maximum backscatter ratio occurred from day 165 onward. Superposed are quarter-diurnal variations in R_v of the order of 2-3 dB that result from the deposition of fine sediments during slack water and the subsequent erosion during increasing currents. The recovered ADCP was massively fouled by barnacles, tube building worms and hydrozoa.

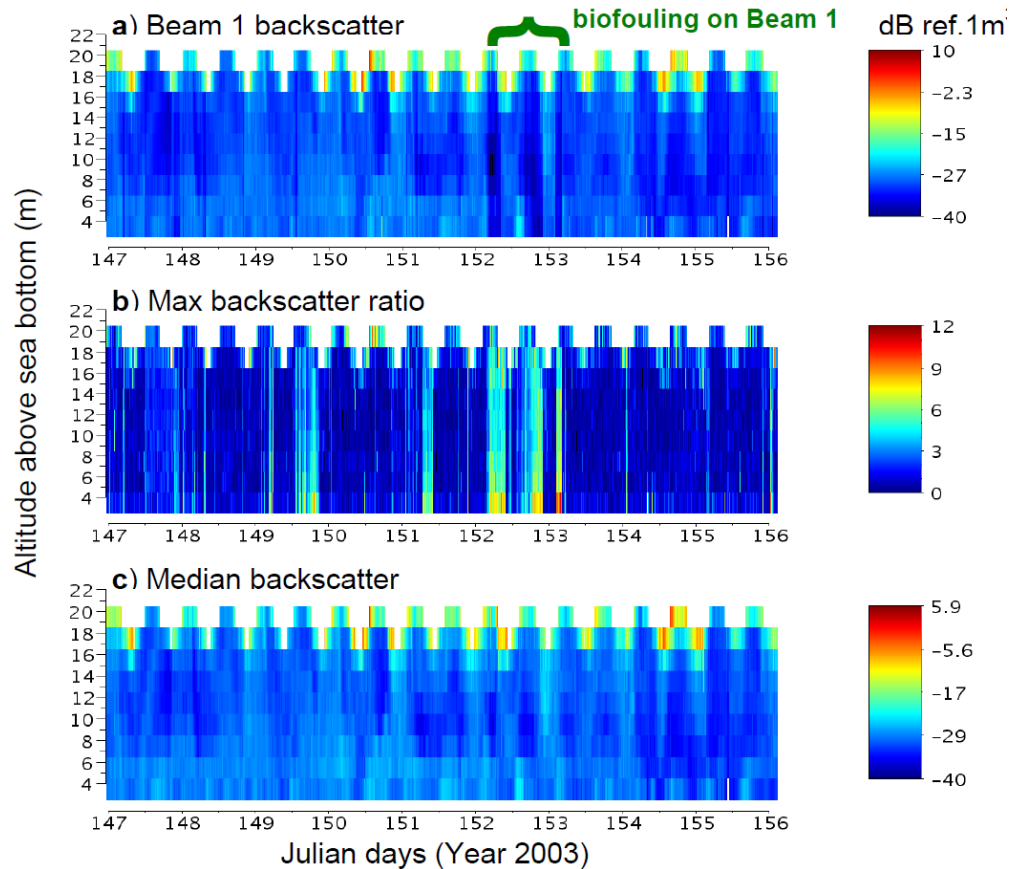


Figure 2.7: 9-day time series of the backscattering strength vertical profile recorded by an upward-looking 500 kHz ADCP (Nortek ADP) moored on the sea bottom at 20 m depth in the Bay of Vilaine, South of Brittany (France). The surface oscillation corresponds to the tidal elevation. a) Volume backscatter strength measured by the transducer 1. At day 152 a biofouling event caused a sudden drop in all backscatter values of the profile, by nearly 10 dB. Following, backscatter values rise again and drop again until day 153. b) Maximum backscatter ratio R_v . Biofouling events on other transducers are identified at days 149 and 151. c) Median backscatter strength. The median allows a computation of a backscattering strength without perturbations by the biofouling.

2.2.2.2 Saturation and ambiguity problems

SPMC in the field may vary from several mg/l to a few g/l. At these ranges, the OBS output increases with SPMC, and the gain setting is adjusted by the manufacturer for an optimized sensitivity at the expected concentrations in the field. However for very high SPMC values, saturation occur and the OBS output will show a plateau as long as SPMC remains above the saturation range as illustrated in Figure 2.5. The individual setting of certain probes can be adjusted (see §2.2.1.2) to broaden the range of SPMC before saturation, but this operation is limited for water where concentration exceeds several g/l.

For many OBS probes, beyond the saturation range, the output signal decreases with increasing concentration as was first observed in the field by Kineke and Stenberg (1992). They attributed this trend to the partial blockage of the emitted beam by highly concentrated suspensions, the reduction of the scattering volume relative to the area of detection. Figure 2.8 shows typical bell-shaped backscatters curve, meaning that a given OBS output can correspond to two possible SPMC values. The two values that can be obtained (i.e. the up and over response) depend on the sensitivity of the individual sensor. This bell-

shaped response can be particularly useful when measuring very high concentrations (Sottolichio et al., 2011). Because of this ambiguity, the determination of SPMC in highly concentrated waters (>4 g/l) is not always possible. A correction is possible in case of vertical profiles, where SPMC is continuously increasing downward (Kineke and Sternberg, 1992). However, this does not help in case of time series, obtained by one probe at fixed height above the bed. The use of a second probe above the other helps to solve the ambiguity of one of the two probes. Acoustic backscattering shows the same type of response than optical probes, and the ambiguity issue apply thus also to acoustic devices, such as single point ADV sensors (Ha et al., 2009; Sottolichio et al., 2011).

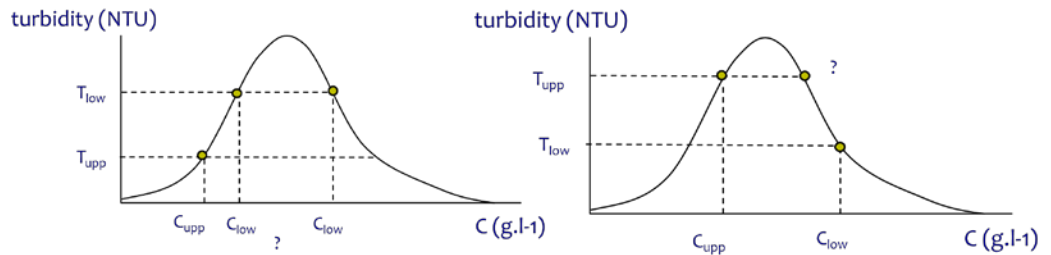


Figure 2.8: Typical bell-shaped backscatters curve of an OBS (Sottolichio et al., 2011), meaning that a given OBS output can correspond to two SPMC values. The figure shows how this ambiguity can be solved by using two superimposed sensors. Left: when the upper probe records lower turbidity than the lower probe, upper concentration is solved, but the lower remains unsolved. Right: when the upper probe records higher turbidity than the lower one, lower concentration is solved, but the higher remains ambiguous and unsolved.

2.2.2.3 Effects of air/gas bubbles

Due to the high acoustic impedance or the very different refractive indices between gas and water, the volumetric backscattering strength measured by acoustical sensors or the scattering efficiency measured by an optical sensor is sensitive to the presence of air or gas microbubbles (1 to 500 μm in radius) in water. These bubbles are mainly generated at the sea surface by wave breaking or white-capping (e.g. Schwendeman and Thomson, 2015) and as a consequence the backscattering strength also depends on the sea state in addition to SPMC (e.g. Klein, 2003; Downing, 2006; Puleo et al., 2006). The finest bubble population of typical size less than 50 μm in radius penetrates deeper within the water column where it can remain in near-equilibrium suspension (e.g. Randolph et al., 2014). Outside the surf zone, bubbles can be carried down in form of plumes or patches by convergent fronts or wind-induced down-welling to depths up to 30 m (Wang et al., 2016). The vertical distribution of wave bubbles decays exponentially with depth resulting in a similar decrease of the backscattering strength at lengths scales of 0.5 to 5 m (Wang et al., 2016). Expressed in decibels the backscattering intensity displays a linear decrease with depth (e.g. Wang et al., 2011) and this property together with measurements of the wind speed (U_{10}) and wave height in parallel can be used to discard parts of profiles affected by wave bubbles, see the example in Jourdin et al. (2014).

2.2.3. Sample related uncertainties

Sample related uncertainties occur during collection and analysis of the sample SPMC, i.e. the filtering and weighing. A diversity of methods and equipment are used to collect water samples, such as Niskin bottles, Go-Flow bottles and stand-alone or on-board sea water pump or suction systems. The bottles attached on a CTD system (vertical), Rosette (vertical) or other profiling frame (horizontal), or the intake for the pump system should be in

the vicinity of the sensors, which are deployed for model calibration. To our knowledge no conclusive investigations have been published so far on sampling devices for fine-grained (cohesive) SPM in turbulent coastal and estuarine waters.

Standard protocols for dry mass SPMC determination (Strickland and Parsons, 1968; Pearlman et al. 1995) and additional procedures to partition SPMC into its organic and inorganic content (e.g. loss on ignition, element analysis) are straightforward: They include filtering a specific volume through a pre-weighed filters, washing of sample filters to remove salt, drying, and weighing of the filter to determine the dry mass of the SPMC. In early years, paper filters were used; later membrane filters (Banse et al., 1963) have been in use, while nowadays often glass-fiber filters (type GF/F or GF/C) are used. A critical step in the determination of SPMC is the removal of the salt in filters from seawater samples (Banse et al., 1963). Additional uncertainties are related to the determination of the dry mass and filter volume and the amount of structural water in minerals (Barillé-Boyer et al., 2003), see Stavn et al. (2009) for an overview. Most uncertainties are related to a constant mass offset (salt, weight and volumetric determination) and are, hence, relatively small when enough mass of particulates (several milligram) is collected on the filter. The collection of a sufficient mass is easy to achieve in turbid nearshore or estuarine waters dominated by mineral material, but more difficult in low turbid organic-rich waters or e.g. during a *Phaeocystis* bloom. In the latter case the gelatinous algal colonies may clog the filter before enough material is collected and prevent the removal of the salt. In cases where the sample mass on the filter is not very high, errors due to salt are significant (Banse et al., 1963; Stavn et al., 2009; Röttgers et al., 2014). In cases where the sample is turbid (>100 mg/l), the main uncertainty is often caused by the difficulty to homogenize the sample prior to subsampling and filtration (Fettweis 2008). Methodological improvements include the optimization of the filtration volume and cleaning of the filter margin after the funnel is removed (Neukermans et al., 2012a); the correction of the salt mass bias using procedural control filters (Stavn et al., 2009), the filling of the filter margin with salt-free water before filtration and the determination of a SPMC free of the salt-bias using a set of different sample volumes (Röttgers et al., 2014).

The uncertainty in sample SPMC decreases with increasing SPMC as shown for a data set of about 2500 sample SPMC from the Belgian nearshore obtained with the method of triplicates with the same volume using GF/C filters. The uncertainty (expressed as the RMSE of the triplicates divided by the mean value) is highest (8.5%) for sample SPMC lower than 5 mg/l and decreases with increasing SPMC to 6.7% (<10 mg/l), 3.5% (10-50 mg/l) and 2.1% (>100 mg/l). This error corresponds to the uncertainty introduced if only one replica was used instead of three replicas. In case of triplicates the error is limited by excluding sample SPMC with a RMSE exceeding a threshold value. The need of subsamples with different volumes versus subsamples with the same volume has been checked from samples collected in three stations with different turbidity in the southern North Sea. The estimated slope, i.e. the SPMC, has an uncertainty that can be higher than 1 mg/l (>30%) for clearer waters (SPMC about 3 mg/l) and then it drops to about 0.3 mg/l for SPMC of about 11 mg/l (3%) or 25 mg/l (1%). Using the method with the same volume, the uncertainty is about 0.3 mg/l (10%) for the clearest sample, about 0.4 mg/l (4%) for SPMC around 11 mg/l and about 0.8 mg/l (3%) for SPMC of around 25 mg/l. The relative difference between the estimated SPMC using this method and the different volume method (applied three times, and averaged) is about 11% for clear waters, 6% and 4% for higher levels of turbidity. One should consider that the uncertainty (standard deviation) of the SPMC through averaging of triplicates with the same volume is not the same uncertainty as obtained via the slope determination in the different volume method. The latter in-

cludes a measurement and a systematic error due to the offset by salt, while the same volume method provides only a measurement error. The systematic error is ignored in the same volume method, which explains the apparent lower uncertainty of this method, especially at low SPMC as compared to the different volume method. The method with different volumes is more accurate, the latter holds especially in low turbid waters, where the effect of salt is important (Röttgers et al., 2014).

2.2.4. Relating sensor output to sample SPMC

Modelling techniques establish a statistical relationship between turbidity or acoustical backscatter intensities and reference SPMC data. This relationship is applied to convert the time-series of turbidity or acoustical backscattered signal into SPMC. The reference SPMC should preferably be the sample SPMC (ISO, 2014), however, for acoustic devices such as an ADCP a calibration against in situ water samples is challenging, as samples are often difficult to collect next to the profiling sensor and as the property of the SPM may change over the water column. For these cases the SPMC derived from optical sensors is often used as reference. This procedure will add additional uncertainty to the model.

The first part of this section (§2.2.4.1 and §2.2.4.2) deals with a purely technical aspect, i.e. the biases involved with the choice of the linear regression model. The second part addresses uncertainties that are caused by systematic changes of the particle IOPs or IAPs that will result in varying proportional factors between the detected signal and SPMC that are not detected during the generally short calibration periods (§ 3.4.3). Very often, these cover only a tidal cycle in the pre- or post-measurement phases using, e.g. a rosette with Niskin bottles or a water pump. A general bias in the model parameter calibration relation may be caused by the spatio-temporal mismatch between the sample and the sensor, by local changes in the turbulence and floc size caused by the sampling device or by the calibration period that is not necessarily representative for the whole unsupervised time series. The latter may result from changes of the particle properties within the same area, due to variable meteorological and hydrodynamic conditions that lead to the resuspension of particles of different size, composition, shape and dynamic modification of the particle characteristics due to flocculation processes. The third part (§2.2.4.4) deals with the inconsistencies between parallel optical and acoustical data that are caused by the uncorrelated and random variations in the IOPs and IAPs.

2.2.4.1 Modelling techniques for optical and acoustical sensors

The relationship between optical sensor output to SPMC or the acoustic backscatter to the $10\log_{10}(\text{SPMC})$ can be modelled using a linear model (see §2.2.3). The model can be applied to the linear domain or the log-log transformed domain (the latter only for turbidity data). Mostly, after quality checks of the data, linear regression finds optimal regression parameters by minimization of the squared differences between the values of the dependent variable and the regression line (χ^2 method, further called LSQ). In general, however, different options for the linear regression method can be considered that lead to different values in the regression parameters for the same data set and different levels of predictability of SPMC from optical turbidity or acoustic backscatter intensity.

The first option is the choice of the independent (explanatory) and dependent (response) variable. As one finally wants SPMC as a function of turbidity, mostly SPMC is used as dependent variable. On the other hand, as turbidity depends on SPMC and not vice versa, causality requires turbidity as dependent variable to compute SPMC from turbidity using the inverse of the regression. As another option, one may regard both SPMC and turbidity as only statistically, but not causal dependent on each other. This situation may be

adequate for cases where water sampling locations and turbidity detection volumes differ by typically more than the coherence lengths of the SPMC in the observation area. Then the minimization of the difference between data and regression line should take place perpendicularly to the regression line solving an Eigenvalue problem. This method leads to symmetric results no matter whether SPMC or turbidity is the dependent or independent variable.

In most real data sets, the assumptions for linear regressions, i.e. the residuals are normally distributed, linear along the zero line, and of constant variance across the range of the dependent variable (homoscedastic), are not met (e.g. Gilbert, 1987). Often, the data sets may contain outliers, i.e. data that do not follow the pattern of the other observations beyond the tails of normal distributions. Ordinary least-squares fitting then can have undesired sensitivities both in best model parameter or confidence interval estimations. In this study, two examples of robust fitting are contrasted with ordinary least-squares. The Theil-Sen estimator is a non-parametric method that determines model slope m by the median of the slopes through all data pairs of data points and then computes the intercept from the median of all data pair residuals $y_i - mx_i$ (Wilcox, 2001). The second method is the “iteratively reweighted least squares” (further called Robust) in which the weighted sum of the absolute differences between the regression line and the dependent data is minimized with the weight being the inverse of the differences in the former iteration step (Press et al., 1989).

To overcome the problems with data heteroscedasticity, \log_{10} - transformations of the variables can be applied, a decision that should be based on the examination of the model residuals (Helsel and Hirsch, 2002). This transformation has also the advantage that the distribution of data along the independent variable is more homogeneous as there is very often a bias in the coastal water sample data sets towards lower concentrations. The re-transformation of the regression line into the original units introduces a bias that arises as the regression estimates are computed from means in log units unequal to the mean in original units. Helsel and Hirsch (2002) recommend the usage of the non-parametric “smearing” estimator

$$BCF = \frac{\sum_{i=1}^n 10^{e_i}}{n} \quad (8)$$

introduced by Duan (1983) as bias correction factor (BCF) with n the number of samples, and e_i the residual of sample i in log-units. This BCF is not symmetric when using the Eigenvalue regression in the log space as SPMC and turbidity have different units.

An example of the different methods and the exchange of dependent and independent variables is shown in Figure 2.9 for the calibration of an OBS against sample SPMC. The next example shows the direct calibration of an ADCP (1 MHz Nortek AWAC) against sample SPMC in a moderately turbid environment (<100 mg/l) is shown in Figure 2.10. The direct calibration with sample SPMC was performed for the surface and bottom samples separately as they originate from different population of particles in suspension, i.e. surface plume and bottom resuspension. The data are from a coastal observatory located at the mouth of the Seine estuary and consists of a bottom station equipped with an ADCP and a Wetlabs NTUSB optical backscatter sensor (Wetlab OBS) and a surface buoy measuring turbidity with a similar Wetlab NTUSB sensor. Seasonal field campaigns are conducted each year to collect surface and bottom water samples and perform CTD and turbidity vertical profiles (OBS3+ sensor).

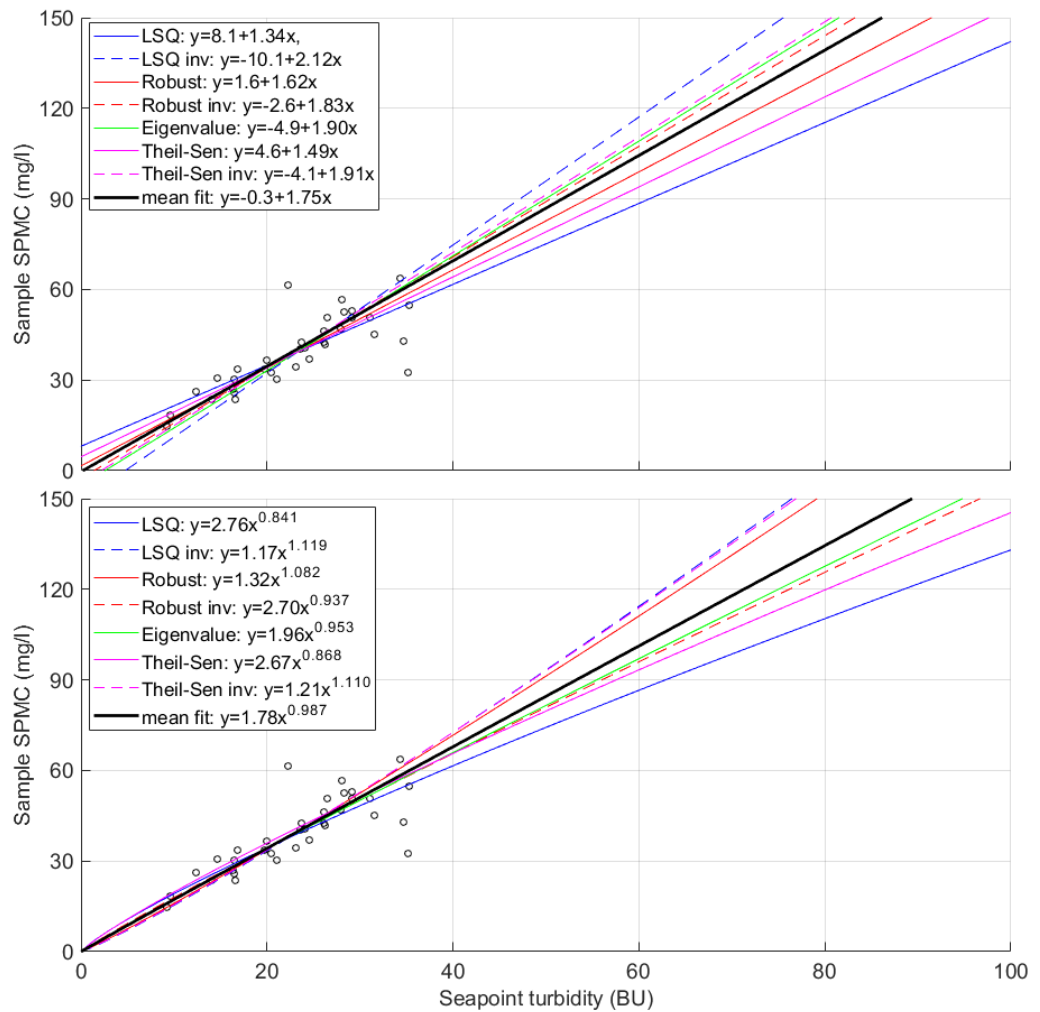


Figure 2.9: Relating sample SPMC to sensor output using different linear regression models for the actual and the log transformed data. The data have been collected in the Belgian nearshore area and consist of 26 sample SPMC and corresponding turbidity values from a Seapoint OBS. The solid lines correspond to the relationship $BU=f(\text{sample SPMC})$ and the dash lines to $\text{sample SPMC}=f(BU)$.

In Figure 2.11 the model calibration of two acoustic sensors (3 MHz Sontek ADP with series number M284 and M947) is shown using the OBS-derived SPMC as the reference SPMC. The data is from a one year time series in 2013 collected in the turbid Belgian nearshore area at about 2 m above the bed (Fettweis et al., 2016). Both acoustic sensors have measured about half of the period at a burst rate of 15 minutes and all the available OBS and ADP data pairs have been used for the model calibration (M284: 12280; M947: 14923). The OBS sensors have been calibrated twice during the period against sample SPMC. The model calibration (M284: $R^2=0.4$; M947: $R^2=0.6$) shows strong scatter in the data and thus a high uncertainty in the acoustic derived SPMC. Additional examples for calibration of long-term ADCP measurements are given by e.g. Fugate and Friedrichs (2002), Gartner (2004), Tessier et al. (2008) or Dufois et al. (2014).

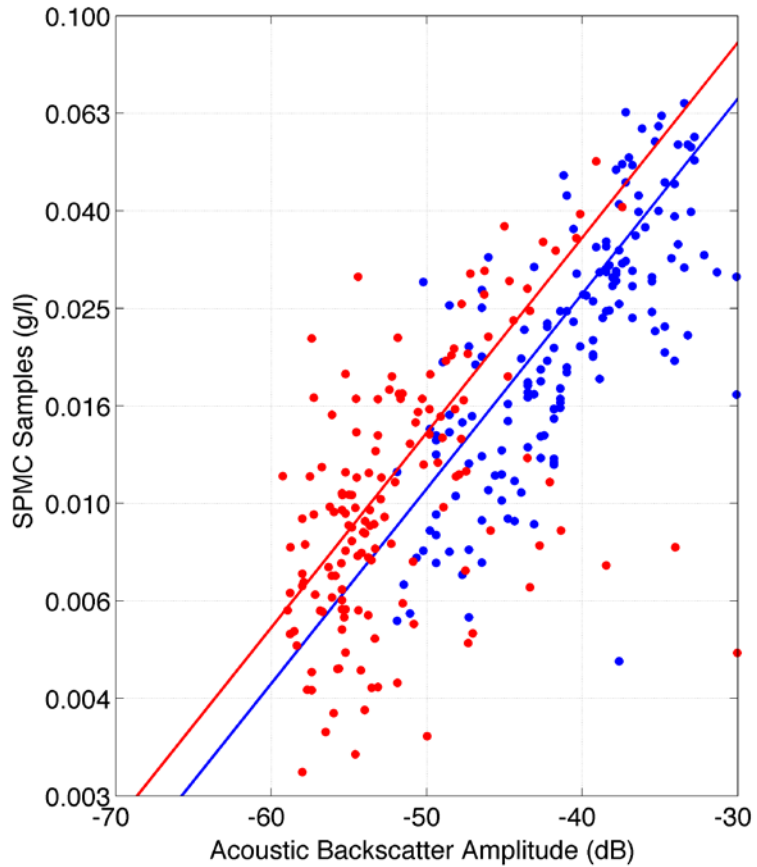


Figure 2.10: Direct calibration of an profiling acoustic sensor (Nortek AWAC) against sample SPMC in a moderately turbid environment (<100 mg/l) located at the mouth of the Seine estuary (red dots: surface samples, blue dots: bottom samples).

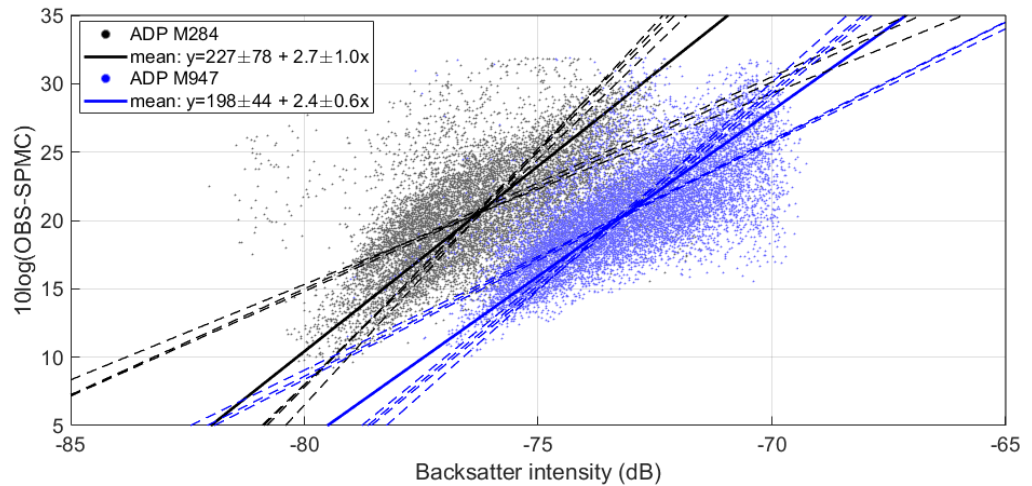


Figure 2.11: Relating OBS derived SPMC to the backscatter intensity of the first bin of two Sontek 3 MHz ADP profilers (M284, M947) using linear regression models. The data set consists of about 1 year data collected in 2013 in the Belgian nearshore area; every sensor measured about half of the period. The bold lines are the mean of 8 different regression models (Least square, Eigenvalue, Theil-Senn, Robust fit and each one with interchanging dependent and independent variables), the dashed lines are the regressions lines (M284: $R^2=0.4$; M947: $R^2=0.6$).

2.2.4.2 Uncertainty due to the choice of the linear regression model

To estimate the uncertainties introduced by the choice of a specific regression method, we applied fifteen different combinations of regression methods to eleven data sets using the three minimisation schemes plus the Theil-Sen estimator, exchanging turbidity and SPMC as independent variable and with and without \log_{10} -transformations of the data. The data sets consist of pairs of sample SPMC and turbidity collected at various location with Hach nephelometers (North Sea, English Channel, Mediterranean Sea, French Guiana coast, Gironde estuary, Rio de la Plata) and Seapoint sensors (Wadden Sea, North Sea, Oosterscheldt, Weser estuary). The variability of the resulting regressions increases considerably with decreasing R^2 of the data set. In Figure 2.12 the percentage range of slopes (maximum – minimum) of the regression functions as $SPMC=f(\text{Turbidity})$ is computed for the not-transformed (i.e. linear scale) and the \log_{10} -transformed data for different values of the normalized turbidities following

$$Turb_{Norm} = (Turb - \langle Turb \rangle) / std(Turb) \quad (9)$$

where $\langle \rangle$ is the average and std the standard deviation of the turbidities in each data set.

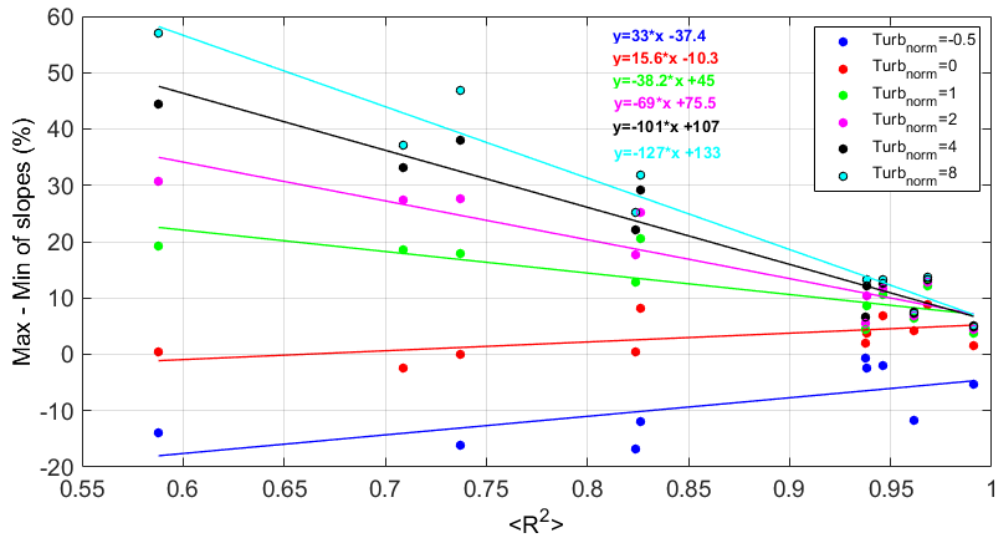


Figure 2.12: Mean spreading of the slopes of the regression lines (maximum – minimum) with respect to the normalized turbidity ($Turb_{norm}$) as a function of the mean R^2 over all regressions (mean regression over the 7 regression models in the linear domain). The slope of the curve for $Turb_{norm}=0$ is close to zero. For higher and lower $Turb_{norm}$ values the spreading and thus the uncertainty increases. The uncertainty of the model increases with decreasing R^2 .

The spreading of slopes increases significantly with decreasing R^2 from 0% for $R^2=1$, to 10% for $R^2=0.93$ and 30% for $R^2=0.60$ at $Turb_{Norm}=2$ (typically the 95% percentile of the turbidities). At the center of the turbidities ($Turb_{Norm}=0$) the spreading of slopes is close to zero, as expected. For cases, where the calibration data represent only a limited range of the totally observed turbidities in the time series, the spreading at higher values of turbidity should also be taken into account, e.g. at $Turb_{Norm}=8$ the percentage spreading of slopes amounts to more than 50%.

The slopes and intercepts of linear regression (Eigenvalue method) of the percentage slope spreading versus R^2 can be closely fitted by exponentials and yields the following formula for the percentage slope spreading ($S\%$) as a function of R^2 and $Turb_{Norm}$:

$$S\% = (140 e^{-0.35 \cdot Turb_{Norm}} - 135) \langle R^2 \rangle + 140 (1 - e^{-0.44 \cdot Turb_{Norm}}) - 5 \quad (10)$$

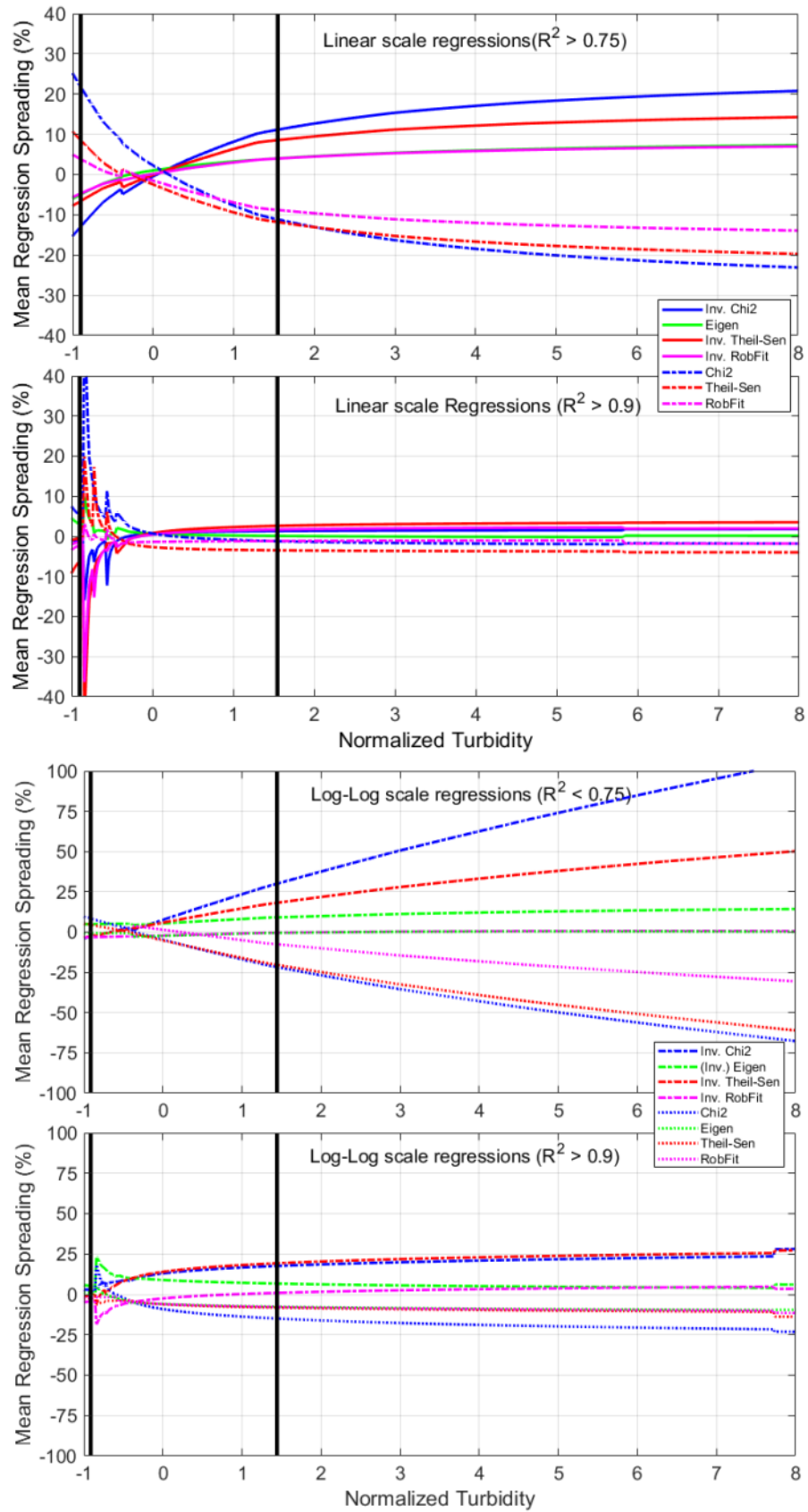


Figure 2.13: Mean spreading of the regression (maximum – minimum) for the different regression models as a function of the normalized turbidity for left the linear scale and right the \log_{10} – transformed data. The examples show the spreading for data sets with $R^2 < 0.75$ and for $R^2 > 0.90$. The black lines are the 10 and 90% percentiles of the data.

This formula predicts the percentage spreading within 5% for an R^2 of 0.91 and can be used to estimate the uncertainties involved with the choice of the regression method applied based only on R^2 and dependent on the value of $Turb_{Norm}$.

To investigate how the type of regression method relates to the mean of all (7) linear scaled data regressions, we averaged the percentage spreading of each regression method over all data sets as a function of $Turb_{Norm}$ and displayed it with respect to the mean of all regressions (Figure 2.13). The deviation of all methods from their mean are nearly zero at $Turb_{Norm}=0$, diverge sharply towards negative $Turb_{Norm}$ up to $\pm 50\%$ at $Turb_{Norm}=-1$ (average 10% percentile of the turbidities), and increase again towards higher $Turb_{Norm}$ to a plateau, that depends both of the R^2 of the data set and the regression method. For data sets with $R^2 > 0.90$, this plateau remains below ± 5 percent for all regression methods, but raises to nearly $\pm 20\%$ for data sets with $R^2 < 0.75$. Here, the regression methods differentiate distinctively from each other, see Figure 12. The LSQ method with turbidity as dependent variable and SPMC computed from the inverse of the regression, exceeds the mean regression by $+20\%$, whereas the Eigenvalue and inverse robust fit regression still remain close to $+5\%$. All inverse regressions have a positive bias with respect to the mean, whereas the regressions with SPMC as dependent variable have a negative bias of the same amount. Hence averaging the direct and the inverse regressions of one method equals the mean regression.

Within the range of the calibration data ($Turb_{norm}$ between 0 and 1) the percentage spreading remains below 10% with $R^2 > 0.6$. At the lower range end of the calibration data ($Turb_{norm} < 0.5$) the relative uncertainties rapidly diverge (Figure 2.13).

The situation is quite different for the regressions performed with \log_{10} -transformed data. The slope of the regression may deviate from 1, resulting in a non-linear power function after re-transformation. This may result in quite large percentage spreading's at high $Turb_{Norm}$, see Figure 2.13. For data sets with $R^2 < 0.75$, the spreading exceeds more than $\pm 50\%$ at $Turb_{Norm}=8$ with no signs to reach a plateau limit at higher $Turb_{Norm}$. For $R^2 > 0.9$, the percentage spreading is much lower with $\pm 20\%$ at most and reaching the plateau at $Turb_{Norm}=6$. This value still is four times higher than for the regressions with not transformed data. Within the calibration data range the uncertainties are still higher by a factor of 2 compared to the not transformed cases, but at the lower end of the turbidities they are more or less identical as all regressions are forced to cross the origin point.

Of course, the results shown here are valid for any data set independent of the meaning of the variables. This means that the uncertainties involved with the model calibration of acoustical backscatter data against an OBS derived SPMC are much larger as the examples in Figure 2.10 and 2.11 show, where the R^2 is 0.4 and 0.6 respectively. The situation is even aggravated by the fact that the linear relation is valid for the log of the SPMC. After raising the data to the power of 10, the uncertainties will increase accordingly and likely exceed 100 %.

2.2.4.3 *Natural variabilities in SPM inherent optical and acoustical properties*

Variabilities in IOPs may occur between different geographical areas or within a same measuring location. The former is illustrated in Figure 2.14, where the relation between sample SPMC and Seapoint turbidity is shown for different areas in the North Sea. The spreading in the data is caused by variabilities in inherent particle properties between the areas. Additional causes of the differences are inter-sensor variabilities and uncertainties due to the sampling and filtration protocols. The latter are thought to be of lesser importance as the differences in slope of the regression lines (German Bight: 1.05 and Ooster-

schelde estuary: 2.34) is larger than these additional uncertainties. Local variation in the IOPs have to be considered when turbidity data are compiled on regional scales as a basis for SPMC mappings, as in the e.g. for coastal observatories that deliver time series of optical turbidities at different locations.

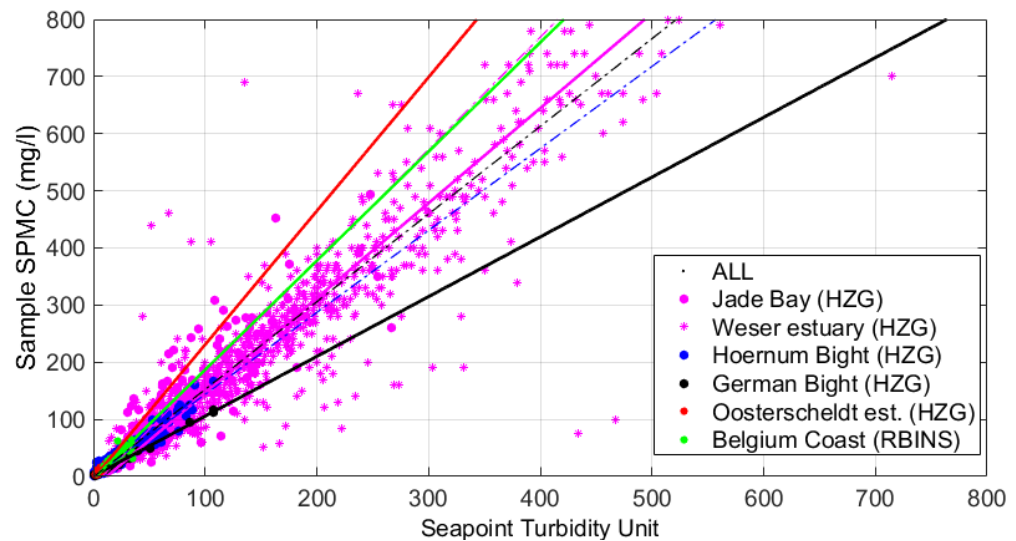


Figure 2.14: Sample SPMC as a function of Seapoint turbidity collected at various locations in the southern North Sea. The regression is calculated with the Eigenvalue model. The mean regressions are ($SPMC=ax+b$): all data ($R^2=0.88$; $a=1.53$, $b=-1$); Jade ($R^2=0.83$; $a=1.96$, $b=-16$), Weser ($R^2=0.83$; $a=1.66$, $b=-20$); Hoernum ($R^2=0.95$; $a=1.44$, $b=0$); German Bight ($R^2=0.99$, $a=1.05$, $b=1$); Oosterschelde ($R^2=0.74$; $a=2.34$, $b=-3$); Belgian coast ($R^2=0.60$, $a=1.91$, $b=-1$).

Intra-tidal variabilities in IOPs at a same location have been observed at various locations. Figure 2.15a shows that the specific backscatter ratio (i.e. turbidity divided by sample SPMC) is oscillating with the tides (Becherer et al., 2016). The magnitude and the tidal signal of the ratio nearly persisted after the storm even though sample SPMC at maximum currents increased threefold. With respect to the tidal mean this would result in a systematic over- and underestimation of the SPMC by 60 % over the tidal cycle. The data indicate that the product of particle density and radius is four times smaller at slack water than at maximum currents. This may be largely assigned to the organic content of the particles that increases with the specific backscatter ratio (Figure 2.15b). Variation in the specific backscatter ratio may also occur on seasonal time scales as observed in Liverpool Bay (Jafar-Sidik et al., 2017). These variations are caused by the seasonality of the primary production and turbulence regime and have changed the ratio by a factor 2.

Another example shows intra-tidal variations in acoustical and optical inherent particle properties due to occurrence of mixed particles (i.e. sand and mud) in suspension at a muddy and sandy bed site located in the main tidal channel of a brackish marsh in the Scheldt estuary (Schwarz et al., 2017). The optical sensor was calibrated with sample SPMC and the optical derived SPMC was subsequently used to calibrate the acoustic backscatter sensor. The muddy bed site shows a strong correlation in contrast with the sandy bed site between acoustical and optical backscatter during the two tidal cycles (Figure 2.16). These observations indicate constant particle properties during a tide at the muddy site and changing particle properties at the sandy site, indicating that the SPM at the muddy site consists mostly of muddy flocs resuspended from the bed, while at the sandy site sand grains with diameters comparable to those of flocs are eroded into suspension at high flow velocities. Their intermittent abundance will lead to changes in the IOP's of the SPM due to their higher specific density, i.e. the increase of rp will lower the

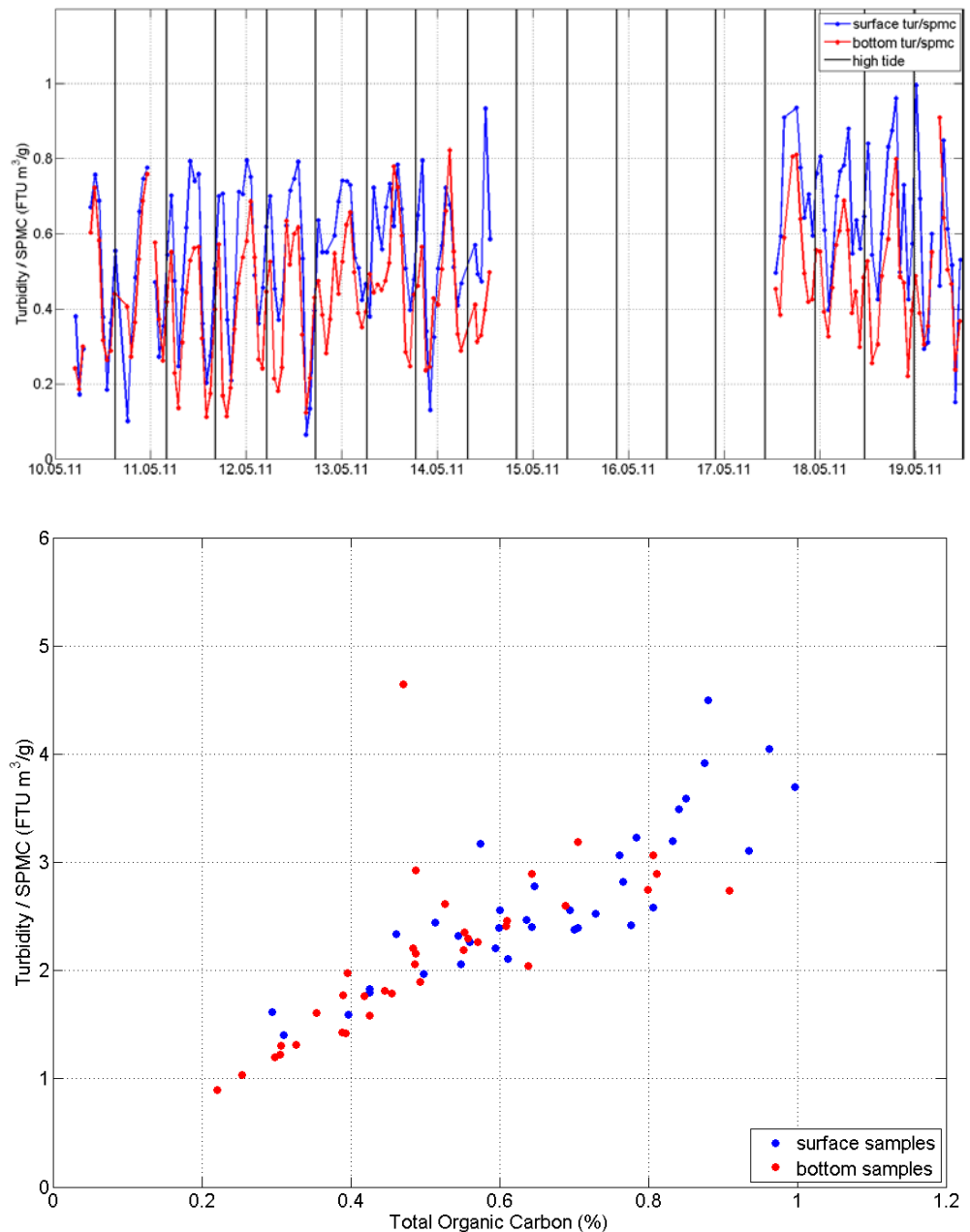


Figure 2.15: Sample SPMC and turbidity collected in the tidal inlet between two islands in the German Wadden Sea between 10 and 19 May 2011 (Becherer et al., 2016). Sample SPMC ranged between 7 mg/l and 500 mg/l, during the storm (14-17/05) no samples have been taken. (a) Time series of the ratio turbidity/sample SPMC and (b) dependence of the specific backscatter $b = \text{turbidity} / \text{sample SPMC}$ on total organic carbon. All samples shown are taken after the storm, from 17th through 19th May. Surface data are taken 1 m below water surface.

ratio of turbidity to sample SPMC (see §2.1.3.1, eq. 5). A storm event recorded at an observation pole in the Elbe (Baschek et al., 2017, Kappenberg et al., 2018), discloses a further example of significant changes in this ratio due to sand grains entrained into the water column. The ratio of optical turbidity to SPMC derived from water samples taken hourly over a period of 12 hours before, during and after the storm varied from 0.4 during the moderate wind phases to 0.12 just after the peak of the wind speed (Figure 2.17). Grain-size analysis of the samples revealed a significant increase of mainly sand around the 90 μm fraction. As a consequence, optical turbidity remained in the range of average tidal

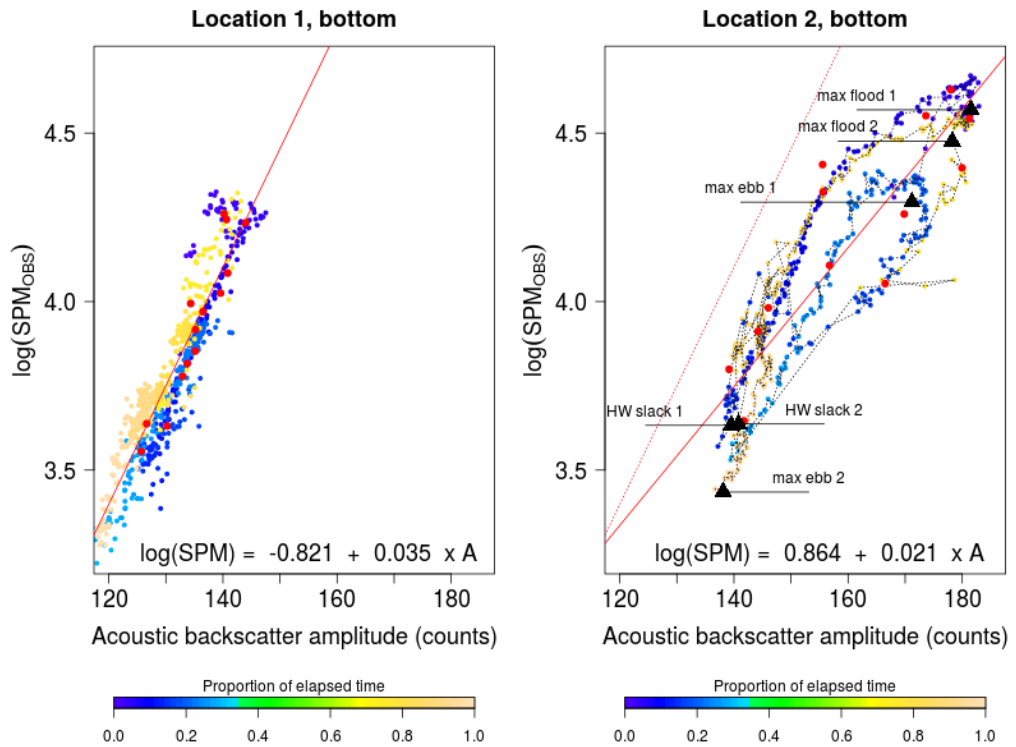


Figure 2.16: Relation between optical (YSI, type 6920 V2) and acoustical backscatter sensor (ADV (Nortek, 6MHz) at a muddy (location 1) and a sandy bed site (location 2) located 1200m apart in the main tidal channel of a brackish marsh located in the Scheldt estuary during 2 tidal cycles (Schwarz et al., 2017).

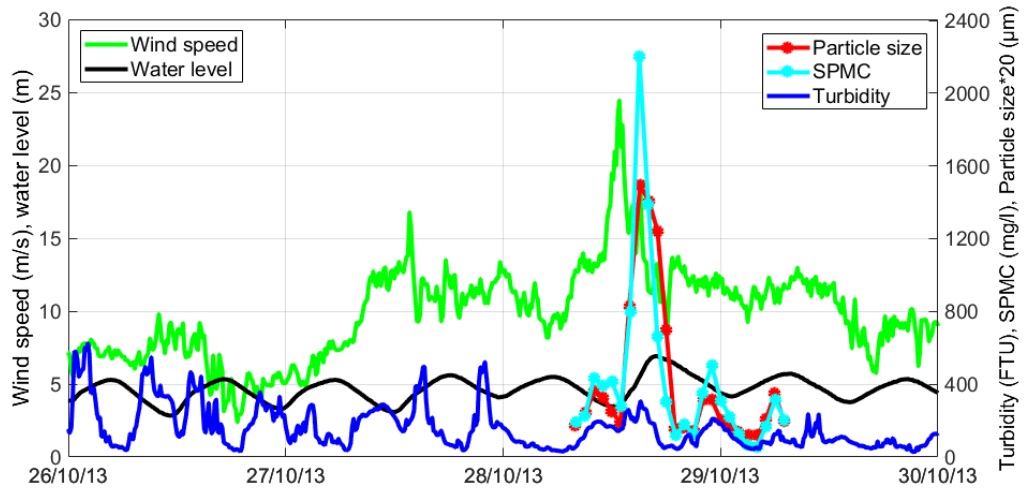


Figure 2.17: Changes in the ratio of turbidity to sample SPMC from 0.4 to 0.12 during a storm period in the Elbe estuary caused by the resuspension of sand grains.

variability during the storm, whereas sample SPMC exceeded this by a factor of five. Similar observations have been made at other locations where mixed sediments and/or strong changing current and wave conditions caused sandy material or particle with other erosion characteristics to be resuspended up to the detection volumes of the acoustic and optical sensors (see e.g. Fugate and Friedrichs, 2002; Fettweis et al., 2012).

The examples demonstrated that in-situ calibration with samples are necessary at all representative locations and phases of the local hydrodynamical and biogeochemical conditions to take the varying composition of the suspended particles into account.

2.2.4.3 *Uncertainties between optical and acoustical derived SPMC*

A comparison of the modelled SPMC was performed from different optical and acoustical sensors, based on the data from the mouth of the Seine estuary (§ 2.2.4.1 and Figure 2.10). The same sample SPMC was used to build models for a moored Wetlabs OBS, a profiling OBS3+ and a moored ADCP (1MHz Nortek AWAC) and the modelled optical derived SPMC was further used as reference SPMC to build a model for the moored ADCP in order to estimate and compare model performance and associated uncertainties (Figure 2.18). Results show that the optical sensors have highest accuracy against sample SPMC (OBS3+: 10%, Wetlab OBS: 40%) and that the acoustical derived SPMC compare well with the OBS3+ profiles for the period where both sensors have been calibrated against sample SPMC. In the same figure the acoustic derived SPMC is compared with the SPMC time series derived from the Wetlabs OBS's, thus for periods that are not covered by the field campaigns dedicated for calibration. The optical and acoustic derived SPMC values significantly differ, the ADCP underestimating large optical derived SPMC and overestimating the lower ones. The acoustic sensor has the larger uncertainty at lowest (400% for SPMC < 5 mg/l) and highest values; in the mid range the uncertainty is about 100% (5 mg/l < SPMC < 10mg/l) and below 50% (SPMC <75 mg/l). The results also show that the error of the reference SPMC propagates into the uncertainty of the acoustic derived SPMC, as can be seen when comparing the ADCP derived SPMC from Wetlabs OBS (20-150%) and OBS3+ (20-50%).

High uncertainties between acoustic and OBS derived SPMC have been observed in the data from the Belgian nearshore (§ 2.2.4.1 and Figure 2.11), see Figure 2.19. The normalized RMSE associated with the regression model varies between 100-500% (mean regression is 170%) for the M284 ADP and 90-140% (mean regression is 90%) for the M947 ADP. The uncertainty is lowest in the mid range SPMC (100-1000 mg/l), with normalized RMSE between 50-70% (M284) and 45-60% (M947) for the best regression models and higher for the lower and higher SPMC values.

Both examples indicate that the differences between acoustic and optic derived SPMC can be very large and that these uncertainties increase when long time series are used for calibration. These differences are probably caused by variabilities in inherent acoustical and optical properties of the SPM that occurred over time scales longer than the sampling surveys, by differences in built-in sensor technology or due to time-delay between sensor measurements and sample time. In order to improve the correlation, the inherent acoustic and optical properties of the particles should be incorporated into the model calibrations.

2.2.5. *Additional uncertainties*

So far aspects of human interference in the operation chain of long-term measurements and in the deployments have been neglected. These includes errors directly caused by the human variability that influence the outcome of the measurements or by the effects of human activities not related to the operational chain that have an impact on the SPMC.

2.2.6.1 *Human errors*

As everyone does also the people involved in the operation chain of long-term measurements make errors. These human errors may cover a broad range of failures related to human malfunction. Humans interfere during the maintenance, the sensor and model parameter calibration and the collection of sample SPMC. The errors are mistakes that may result in the not strictly following of the protocol, or simply by bumbling errors, such as mismeasures, miscalculations, mislabeling, malfunctioning of sensors or instruments.

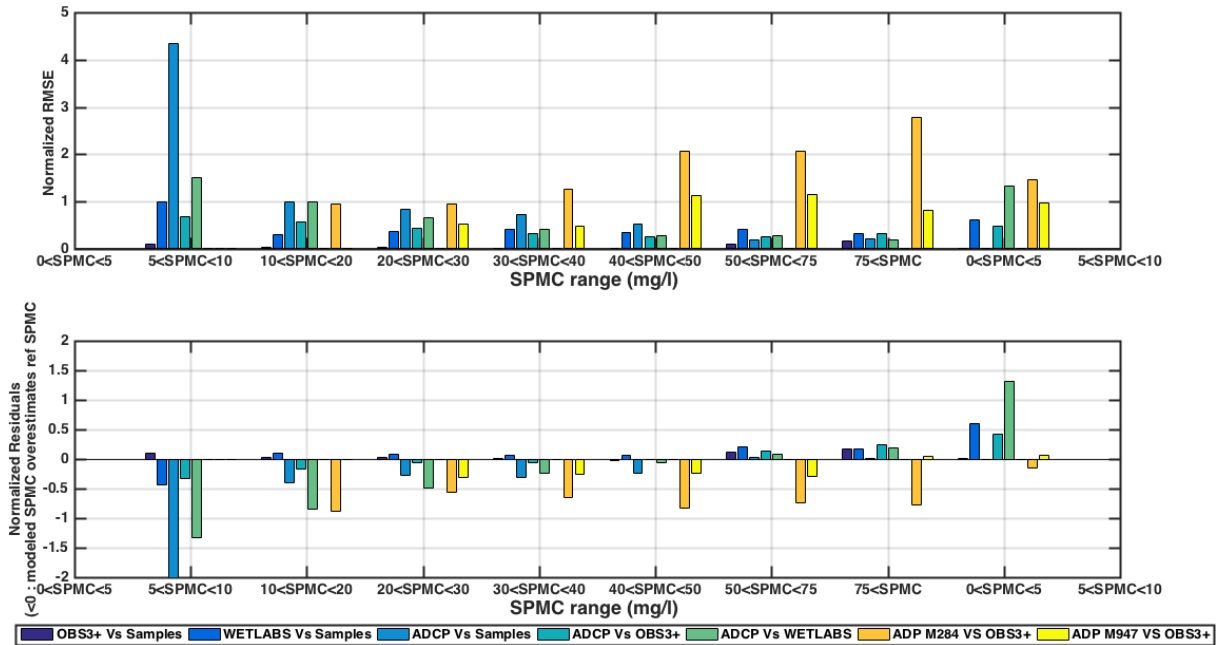


Figure 2.18: The model SPMC uncertainty (normalized RMSE and residuals) as a function of the reference SPMC (sample or sensor derived SPMC) and SPMC (see the dataset shown in Figure 10 and 11) for an acoustical and optical backscatter sensors. The reference SPMC is from sample or OBS3+ derived SPMC.

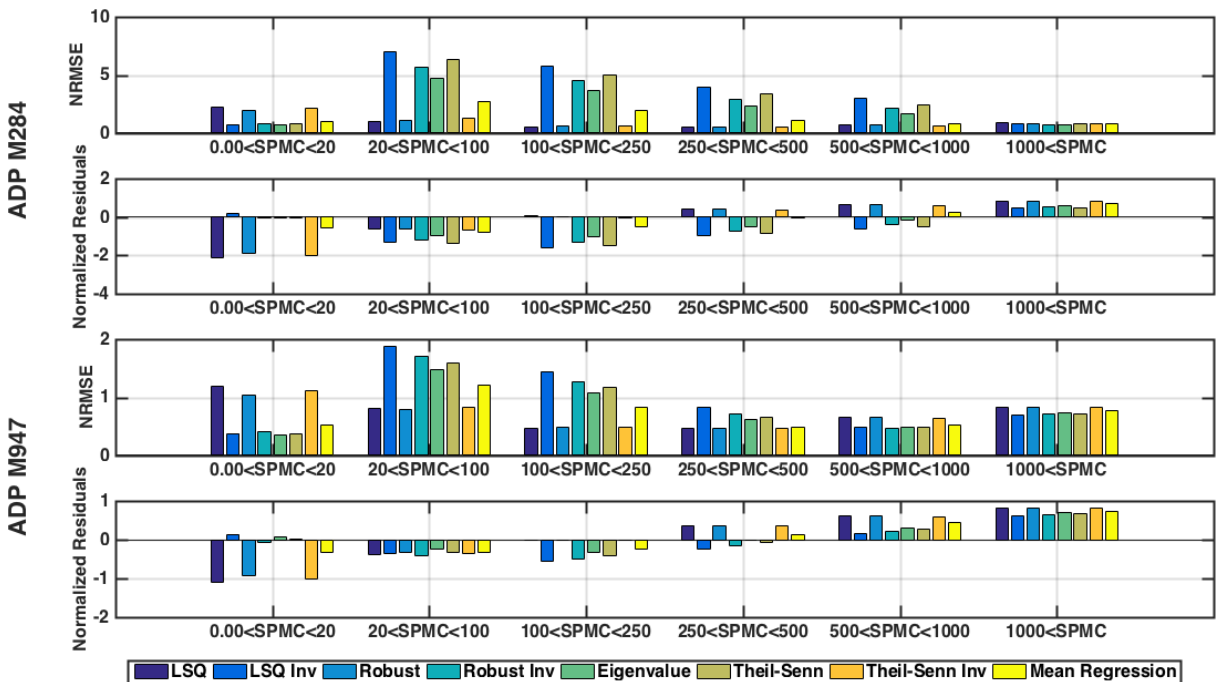


Figure 2.19: The model SPMC uncertainty for the ADP's of Figure 11 expressed as normalized RMSE and normalized residual for different regression models and as a function SPMC. Negative residuals have a higher ADP-derived SPMC than the OBS-derived one.

Maintenance, water sampling and filtering or sensor exchange often take place under tough sea state conditions and under time pressure that may result in stress, fatigue and reduced mental awareness. Under such conditions it is often difficult to strictly obey protocols and to identify and document, if any, possible deviations and mistakes in an appropriate way. Further many of the errors are often only detected after the measurements

and can therefore not be corrected but should be discarded (see e.g. the occurrence of outliers in the model parameter calibration that cannot be explained by natural processes).

2.2.6.2 *Uncertainties related to uncontrolled environmental boundary conditions*

The objective of all long-term measurements is to document trends or sudden changes of the monitored parameter. The uncertainties related to uncontrolled environmental boundary conditions are causing variation in the SPMC that may lead to wrong interpretation of the observations. Even if the protocols are strictly followed and the uncertainties described previously minimized, the measurements from the sensors may not reflect the broader situation as the measuring devices (pile, lander) or the nearby human activities have an influence on the measurements (Bolanos et al., 2011; Fettweis et al., 2016). Further piles, landers or other devices that are in contact with the sea floor may cause local scour and thus morphological, sedimentological and hydrodynamic changes that affect locally the concentration and the inherent properties of the SPM (e.g. Baeye et al., 2016).

2.3. Towards best practice

To come to best practice for long-term monitoring activities of SPMC an accurate documentation of the successive operations and of the accumulating effect of uncertainties is required. This means thus not only following a standard workflow, but also collecting meta-information about applied protocols, quality standards, error estimations, as well as of additional parameters that characterize e.g. human activities near the measuring site, climatological indicators, river runoff and oceanographic and atmospheric standard parameters.

2.3.1. *Best practice workflow*

A brief overview of the generic succession of operations required to run long-term or large-scale measurements of SPM concentrations is depicted in Figure 2.20. The activities can be divided into phases of pre-measurement, measurement and post-measurement and grouped into planning and resource allocation, accuracy and precision measures and post-processing of observation data and related ancillary information. In long-term observations the three phases and activities are not in strict sequence but interleave. Threats to accuracy and precision that are specific for long-term observations, define the type and timing of measures during the measurement phase to minimize or avoid them. They set the need to allocate steady and flexible operation resources and the set-up of a proper organizational framework linking laboratory and field work. (Near) real-time monitoring of the data is desirable to react promptly with remote or field operations on system failures or other threats to accuracy and precision. Processing of the data in the post-measurement phase comprises firstly quality safety measures. Finally all data from water samples, sensor output, sensor (inter-)calibration and interpretation parameters that reveal information about the optical and acoustical properties of the suspended particles and their changes are numerically assembled in the models that yield the final SPM concentrations and estimations of uncertainties.

2.3.1.1 *Pre-measurement phase*

The planning of the layout of the observational device is discussed in the following with respect to achieving the required precision and accuracy of the resulting SPMC. Planning covers the choice of required instrumentation, the resources needed to carry out repeated field operations and the sensor (inter-)calibration in the laboratory against standards before field usage. The first part deals with the sensitivities and ranges of the measuring

devices and with the need of adjoined measurements of state variables such as particle size, shape and composition, salinity, temperature, current velocity or turbulence, see Table 2.2. The second part covers the maintenance or exchange of instruments, the reaction on sudden system failure; the execution of regular or event-triggered ship surveys for in-situ sensor and model calibration, and the use of elaborate instrumentation to measure other state variables needed for a more accurate and complete interpretation of the data.

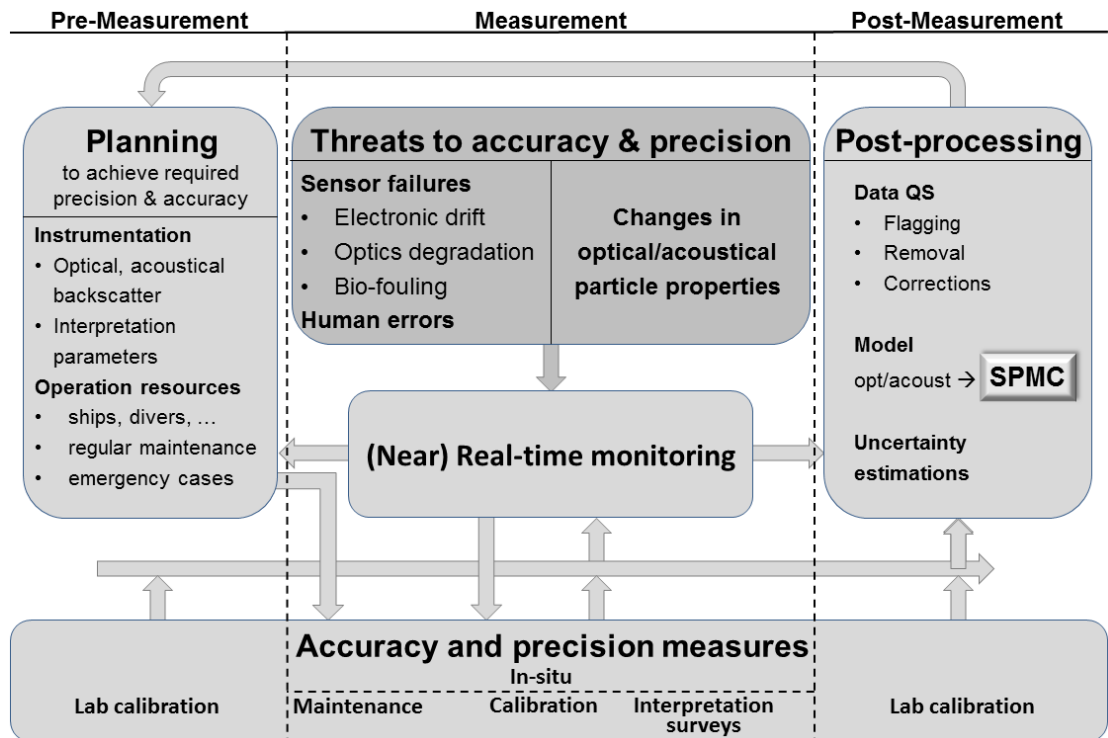


Figure 2.20: Workflow of activities and tasks to be performed in long-term SPMC measurements. The arrows indicate the flow information between the tasks and activities over the measurement phases. The measurement phases are plotted in serial order, but may overlap in the course of long-term installations.

2.3.1.2 Measurement phase

Once deployed in the field, the observing system remain unattended until the next maintenance service. Processes that disturb the sensor outputs with respect to the preceding sensor and model calibration have been presented in chapter 2.2. The functional understanding of the interrelation between inherent particle properties, system state conditions and sensor SPMC may benefit from additional surveys to estimate changes in the sensor SPMC between the in-situ calibration activities. Ongoing (near) real-time monitoring of sensor output in the land-based lab is very helpful to detect timely system failures and other needs for field operations. In this way it feeds back into ongoing planning and allocation of resources.

2.3.1.3 Post-measurement phase

Post-measurement starts with the downloading of the raw data and their conversion into data and archiving information that collate all so far undertaken calibration, accuracy and precision measures (Tzeng et al., 2016). After recovery from the field, optical and (if possible) acoustical sensors should be calibrated against the lab reference to quantify any changes in sensor response due to electronic drift or optical window damages. In post-

processing the data should first undergo an expert judgement to flag e.g. occurrences of spikes, stuck values or unreliable magnitudes. Further, any effects of sensor drift, between sensor differences with regard to lab or field standards, and bio-fouling effects should be identified and if possible corrected for. The resulting set of accepted and corrected data together with filter weights acts as input for the computation of the sensor SPMC. As these are in general variable in time, this step is not straightforward but may require some iterative optimization to find of statistically homogeneous sets. Finally, the errors due to all steps in the described work chain have to be figured out. These error estimates are only due to the measurement procedures themselves and yield only the errors at the observing point and for the calibration periods of the time series. Further uncertainties that relate to the representativeness of the measurements in time and space can be substantial for the interpretation of the data in terms of processes and trends.

2.3.2. Discussion and ranking of the uncertainties

All steps along the described chain of activities contribute to the overall error of the final SPMC data set estimated from the combination of sample SPMC and turbidity or acoustical backscatter signals. They comprise random errors that lead (1) to uncertainties of individual SPMC but approximate the accurate value with increasing amount of data; and (2) systematic errors (biases) that lead to an average over- or underestimation of all data. There exist two types of biases: one that is constant or independent of observing times and locations (e.g. from the choice of the regression method, as discussed in § 2.2.4.2) or changes with the time and location (§ 2.2.4.3). Some kinds of errors can be detected, and to some extent corrected, whereas, others are inherently associated with the applied technologies and its interference with the environment and remain spurious and difficult to quantify or to control. The first types of errors are related to the sensors, sampling and lab protocols or the modelling techniques used to establish a relation between the sensor output and the sample SPMC, while the latter are mainly related to systematic natural variabilities in SPM inherent properties that may occur during autonomous measurements. In table 2.3 we have listed the sources of uncertainties as described in chapter 3, and added the percentage error (1 standard deviation), being detectable and correctable and random or systematic (bias). For the levels of uncertainty we further distinguish cases with and without applied corrections. The listed numbers refer to our examples in chapter 3, and only some of them can be regarded as general. Rather they represent typical values that indicate their relative importance for the overall error. The following discussion continues along the vertical order of table 2.3, which reflects the structure of §2.2 and relates more or less directly to the major items of the workflow depicted in Figure 2.20.

2.3.2.1 Sensor related uncertainties

Most sensor related sources of uncertainty in the workflow can be deduced from the correct ratio of the sensor signal to a standard solution (e.g. formazine). Any deviation from the 1:1 ratio results in a bias that will pass through the whole workflow and needs to be detected and corrected for. As long-term and large-scale observation often employs more than one sensor the homogeneity of the data sets may be not preserved. This is also the case when just one sensor is used but its signal response changes with time. The example for the 11 Seapoint turbidity sensors described in §2.2.1.1 should be taken as a token to validate the factory calibration before its first field deployment, also to have trustable baseline to detect any sensor response drift over time. The shown examples of sensor drift were due to delivered power decrease (in case of battery depletion this can be up to 100%) or to the degradation of optical window surfaces that may become scratched or opaque by repeated impact of sharp-edged particles. Controlling such a sensor drift will

Table 2.3: Quantification and nature (random or bias) of uncertainties (in % based on normalized RMSE) from the examples described in § 2.2. Negative (positive) bias corresponds to an underestimation (overestimation) of the actual value.

Source of uncertainty	Detectable	Correctable	Uncertainty without correction		Uncertainty with correction		Comment
			random	bias	random	bias	
3.1 Sensor							
3.1.1 Factory calibration	yes	yes	-	± 15%	-	less than ± 2%	not fully conclusive, as sensors were checked after intense usage
3.1.1 Optical degradation	yes	yes	-	-20%	-	±5%	Figure 2
3.1.1 Voltage supply	yes	yes		-90%		±10%	Figure 3
3.1.2.Sensitivity of sensor	yes	no	<25%		no example	no example	depends on measuring range
3.1.3 Inter-sensor variability	yes	no	2%	no example provided	no example provided	no example provided	Figure 4 Comparing sensors of same type and applying the same set of sensor output to sample SPMC calibration constants for all sensors
3.2 Environment							
3.2.1 Biofouling	yes	no ¹ , yes ²	-	positive, large (up to >100%) ¹ negative ²	f(no of beams) ²	data loss ¹ partial data loss ²	¹ optical sensors ² acoustical sensors with >3 beams
3.2.2 Saturation	yes	no		Negative ¹	-	-	¹ numerically not specified
3.2.2 Ambiguity	yes	yes	not specified	-	-	-	
3.2.3 Air bubbles	yes	no	-	-	-	¹ data loss	¹ optical and acoustical sensors
3.3 Sample							
one filter	yes ¹		2%-10%		-		¹ only random uncertainty
triplicate filter	yes ¹	no	1%-6%	1%- 50% ³	-	not correctable	² random + bias
volume method	yes ²		3%		-	not correctable <5% ³	³ random bias per sample ; depends on SPMC (>50-<1 mg/l)
3.4 Model							
3.4.2 Regression model	yes	no	10%- 60% ¹	0->30% ^{1,2}			¹ depends on R ² and Turb _{norm} ² depends on regression model
3.4.3 Inherent particle properties	yes ¹	partly		± 50% ² 40%- 60% ³ 50%-200% ⁴			¹ only with sample SPMC ² geographical variation, Figure 14 ³ organic content, Figure 15 ⁴ sand in suspension, Figure 16+17
3.4.4 Optic vs. acoustic sensors	yes	no	50-100% ²	40% ¹ O(100%) ²			¹ acoustic sensor calibrated with sample SPMC, Figure 18 ² acoustic sensor calibrated with OBS, Figure 18, 19

require either the close follow up of the battery voltage and indirect field inter-calibration against a well calibrated reference sensor operated in parallel very close to the long-term observing location, or by regular re-calibration checks in the laboratory with formazine or other reference solutions after recovery of the sensor. This allows the intermittent adaptation of voltage to standard solution units and at least some correction for the sensor drift for the times between inter- or re-calibration.

Another type of uncertainty is the usage of sensors that are not adapted to the range of turbidity values of the site. As found in the example in §2.2.1.2, this may reduce the overall accuracy of the output in general by a bias of about 2% up to 24%. This error can in principle only be corrected for by intense calibration sampling but the limited resolution in turbidity may also increase the random variability in the ratio of sample SPMC to turbidity. Accuracy of the measurements can easily be increased by matching the in-situ turbidity with the designed range of the sensors and/or by using two or more sensors to cover a larger turbidity range.

Inter-sensor variability may result from uncertainties related to the so-far discussed items. The comparison of the SPMC derived from different OBS3+ sensors (§ 2.2.1.3) shows that inter-sensor variability for identical sensor types can be reduced to natural random fluctuations in the water bodies, if all sensors are calibrated separately against sample SPMC. If inter-comparing different types of sensors, it is not evident beforehand that even separate calibration leads to the same results for longer time series, as different sensors may react differently to changes in the IOPs of the SPM. This may result in time-dependent biases and has to be investigated case by case.

2.3.2.2 *Environmental related uncertainties*

Biofouling represents the largest challenge for accurate measurements of turbidity and in some cases of acoustical backscatter intensity in the field. If not detected and flagged, the bias (positive for turbidity; negative for acoustical backscatter) can easily reach many tens of percent. Especially optical sensor output is sensitive to increasing coverage of the sensors material disturbing the light pathways or scatter detection volume. Although technologies, such as wipers or irradiation with UV light (Bueley et al., 2014) exist to mitigate the impact of fouling, their applicability might be limited in many coastal waters during seasons with high biological productivity, so that regular cleansing of the sensors remains a necessity and needs to be properly considered when allocating ship and personal resources. Sensor cleansing needs to be accompanied by sensor inter-calibration against a reference device. Correction of the bio-fouled data has been shown for an acoustic profiler sensor (ADCP, ADP) in §2.2.2.1 and is described in literature for biofouled OBS data (e.g. Dolphin et al., 2000), however, the methods are case specific. As long as the effect of bio-fouling is limited corrections by means of independent not-affected devices is sometimes possible. In many cases, however, tagging and discarding bio-fouled data is the only option. Air bubbles enhance the turbidity and acoustical backscatter signals. As long as their presence can be detected they can be tagged and discarded.

Very high SPMC may produce backscatter intensities that saturate the sensor output. It is straightforward to tag these data. Discarding them will introduce a bias for the periods of very SPMC. Modelling the gaps by e.g. extending the power spectrum of the time series will lead to more realistic values, The degree of uncertainty cannot be provided numerically here as it is dependent on the specific situation and applied interpolation model. To mitigate this effect one simply has to use a type of sensor with higher output range. This case nicely demonstrates the need of adequate planning in the pre-measurement phase, the need of ongoing monitoring and the capabilities in allocating resources to exchange sen-

sors in due time.

2.3.2.3 Sample related uncertainty

The determination of sample SPMC is through three steps, sampling, filtering and subsequent weighing. The sampling involves systematic uncertainties that are related to the sampling technique, the sampling volume in relation to the temporal variability of the SPMC, and to the exact location of the sample versus the sensor. Weighting is considered a minor source of error. The main uncertainties involved are related to the filtering procedure at SPMC <3 mg/l, because the weights of the filter loadings are in the order of the sample specific filter offset. So far the only and most accurate protocol is the method with different filter volumes, where sample SPMC is determined by the linear regression of filter loading weight versus filtered volume, which cancels out the filter offset. At SPMC >25 mg/l the error without knowing the filter offset amounts to 3%, but raises to 50 % for SPMC <3 mg/l. Using the different volume method reduces the uncertainties to less than 10 % for SPMC <3 mg/l. For SPMC >25 mg/l the impact of the filter offset becomes negligible. Using only one filter in this range bears the risk that faulty sample SPMC cannot be identified and show up as outliers in the scatter plots that cannot be removed from the calibration data set. This can be avoided by working with e.g. triplicates and removing the sample that differs from the other two by more than a pre-defined value which reduces the random error by a factor of 2 down to the order of 5% and less.

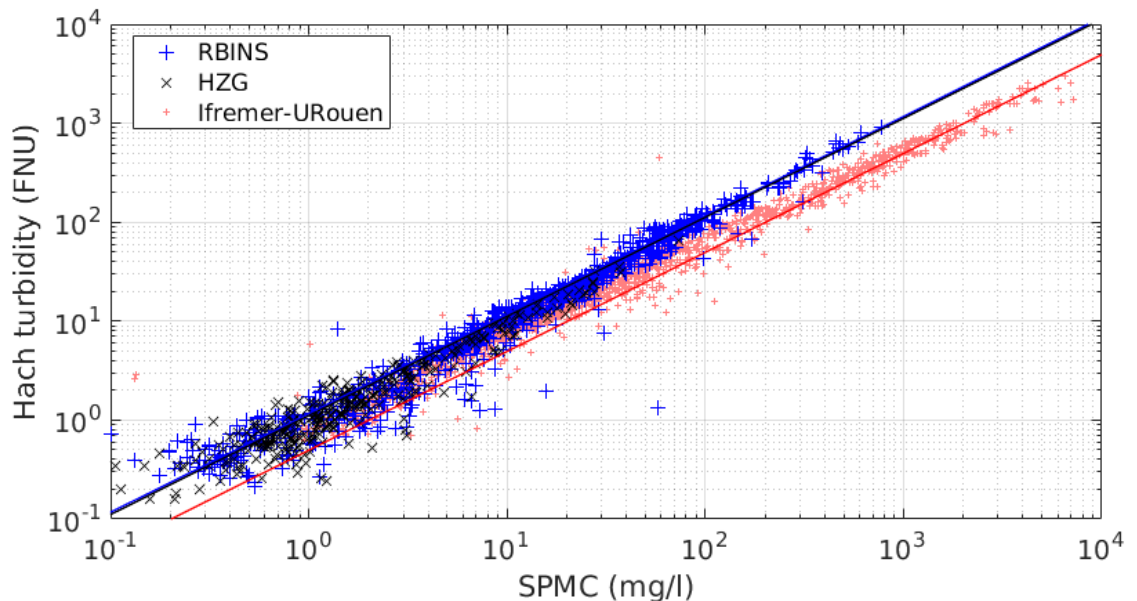


Figure 2.21: Scatterplot of sample SPMC (mg/l) versus turbidity measurements from various waters around the world. The turbidity data from RBINS and HZG have been collected with a Hach 2100S and those from Ifremer and University of Rouen by a Hach 2100N IS. HZG measurements were collected from 2009 to 2013, RBINS data are from 2007 to 2015 and Ifremer and University of Rouen data from 2015-2016. The black line is the 1:1 and the grey lines are the 1:70% and 1:130% lines respectively.

As a simple method to evaluate the quality of the sample SPMC compared with in situ optical measurements we refer to the obviously generally valid close relationship between sample SPMC and Hach turbidity (Figure 2.21). Large inconsistency between the Hach sample turbidity measured on board with a well-defined subsample, in-situ turbidity and sample SPMC would designate this sample as unreliable.

2.3.2.4 *Choice of the linear regression model*

This source of uncertainty has some significance as it is systematic and leads to SPMC that are all either too high or too low. It is quite evident that a calibration data set within an $R^2 > 0.9$ should be achieved to keep uncertainties involved with the choice of a specific regression model well below 10%, independent of the model and the range of the calibration data compared to the complete data set. Please note that this statement refers only to the choice of the regression model and not to any systematic changes in the IOPs or IAPs beyond the sample calibration period. Any random uncertainties created in the former steps of the workflow have therefore to be kept as small as possible. Even then, in waters with highly variable conditions over the sample calibration period, such a high R^2 may not be achievable. In this case we recommend to use either the Eigenvalue regression or averaging between regressions with exchanged dependent and independent variables. Visual inspection indicated that this mean regression follows nicely the linear trend of the data independent of R^2 .

Regressions to \log_{10} -transformed data exhibit a generally higher sensitivity to the model choice for $Turb_{Norm} > 0$ that increase substantially for turbidities above the calibration data. In this respect, regressions with \log_{10} -transformed data bear the risk of substantial biases in the SPMC computed from higher optical turbidity or acoustical backscatter data. For low turbidities, the sensitivity is low as after re-transformation, regression are forced to meet the data origin point.

For acoustical data, $R^2 > 0.9$ is difficult to achieve and model choice sensitivity is even further enhanced as the dB-signal has to be raised to the power of 10. Hence the use of acoustical devices for SPMC-estimation seems to be accompanied with large uncertainties at this step of the workflow.

2.3.2.5 *Variabilities in SPM inherent optical and acoustical properties*

Uncertainties due to undetected changes in inherent optical and acoustical particle properties of the SPM are difficult to quantify or control during long-term SPMC measurements. Most of them can be ascribed to changes in particle size, shape, composition and density. Regular water sampling to compare filter weights (the sample SPMC) with sensor output in parallel post-processing will provide insight into the stability/variability of models used to estimate sensor SPMC over time and/or space. The examples of §2.2.4.3 show that even intra-tidal variations or events of several hours duration lead to systematic uncertainties of 50% to 200% demonstrating the significance of this effect for specific sites and periods. Therefore it is recommended to add further sensor technologies to the observing system that give direct indication for changes in the IOPs and IAPs, e.g. when particle size or composition is expected to change beyond previous uncertainties and systematically at the observation site (Table 2.2).

2.3.3. *Turbidity as a surrogate for SPMC?*

2.3.3.1 *Uncertainty between SPMC and turbidity*

To separate variability due to measurement errors from variability due to natural variations in IOPs protocols that use the same water sample for filtration and for turbidity estimation should be used in parallel to the in-situ procedures. Figure 2.21 shows a collection of sample SPMC versus turbidity measurements of the same water sample recorded with a portable ISO Hach 2100P nephelometer from various waters around the world (North Sea, English Channel, Mediterranean Sea, Rio de la Plata, French Guiana nearshore, Gironde estuary, Scheldt estuary, see Table 2.3), collected by the RBINS (Dogliotti et al., 2015; Knaeps et al., 2015) and HZG (Röttgers et al., 2014). The protocols for sample SPMC

and turbidity measurements are those described in Neukermans et al. (2012a) for RBINS and Röttgers et al. (2014) for HZG. The figure shows that the ratio between sample SPMC and Hach turbidity is quite stable within an uncertainty of 20% throughout the regions. In this collection, 4.1% of couples fail outside of the 95% confidence interval regarding the t-distribution of sample SPMC/turbidity in the logarithmic space. The outlying couples probably reflect the tails of the combined natural variability of particles mass-specific side-scattering coefficient, and sampling and filtration errors. The average ratio of sample SPMC to turbidity from all data is about 1.13 mg/l/FNU (RBINS data), and 1.19 mg/l/FNU (HZG data).

Despite calibration to a formazine reference solution and the use of ISO-normed optical sensors, model calibration may vary considerably in recorded turbidity for a same SPMC solution across different instruments resulting in instrument-specific turbidity-SPMC relations, see Figure 2.22. Although different types of optical sensors have been calibrated against a reference solution, they yield up to 20% differences results in the field. Another example concerns data collected by Ifremer and the University of Rouen at different locations in the Seine estuary (Druine et al., 2018) with a ISO Hach 2100N nephelometer (same constructor, but different type as the above mentioned 2100P) give significant different turbidity values for the same SPMC. We assume, given the stability of the Hach 2100P over a wide range of areas that the deviations are mainly caused by the instrument specificity. The latter was confirmed during intercalibration of both ISO standardized nephelometers with StablCal Formazin and with SPMC solutions.

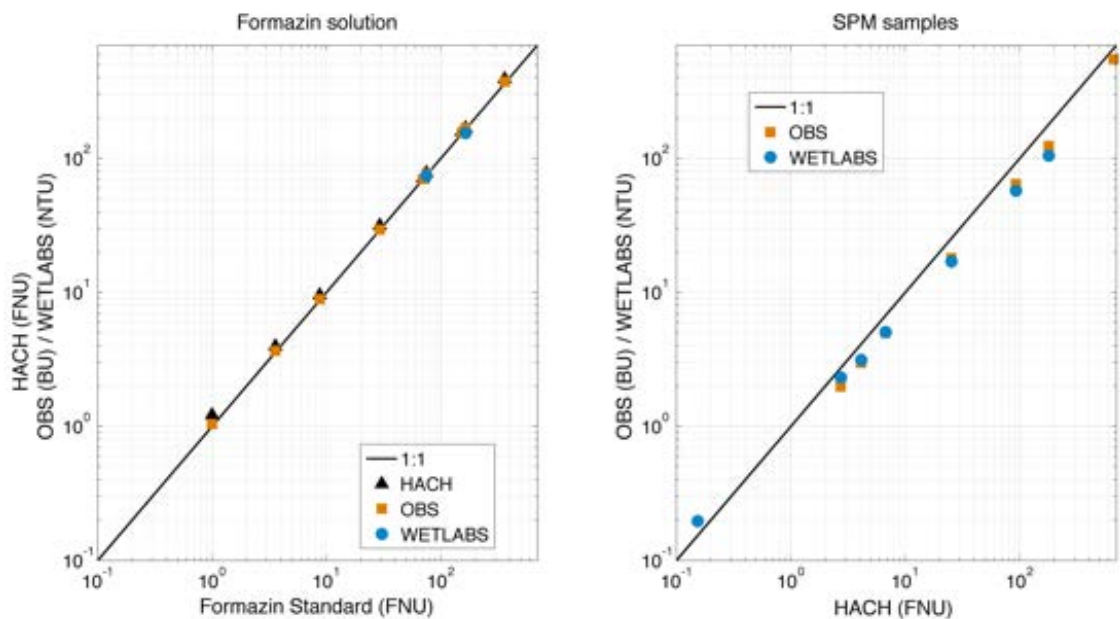


Figure 2.22: The performance of different sensors (side-scattering: Hach; backscattering: OBS3+ and Wetlabs) during sensor calibration with different Formazin solutions (left) and as compared with natural SPM samples.

2.3.3.2 Need for further sample SPMC?

Nevertheless similar outputs against a reference solution, optical sensors have different sensitivities to the inherent properties of the SPM. This prohibits comparing the turbidity values measured by different type of optical sensors. Despite differences in turbidity readings for a given SPMC, well correlated relationships between instrument specific turbidity and sample SPMC can be established during model calibration. The generally high correlation between sensor specific turbidity and sample SPMC show that turbidity as a surrogate of SPMC is reliable, as long as site-specific (model) and instrument-specific (sensor) cali-

brations are carried out. Although differences have been observed in turbidity recordings between different sensors the data in Figure 2.21 show that the relationship between SPMC and turbidity is quite stable throughout different localities for a same sensor type when a similar protocol is followed. This relationship could be used as a first estimate of SPMC from a turbidity values without collecting sample SPMC for model calibration and underlines the importance of a well calibrated reference system. The Figure 2.22 also shows that nephelometers that follow the ISO protocol are not giving the same value; this means that even following the same protocols at the same site and periods turbidity is a vague unit to estimate SPMC. It strengthen further that any turbidity unit should be referred to the instrument used and the protocol applied, hence the many turbidity units (see § 2.1.1).

Considering the stable ratio of Hach-turbidities to sample SPMC over a broad range of coastal regions it may be interesting to address the question whether one could use the scaled Hach turbidities instead of sample filter weights. The former ones introduce a random uncertainty of some 20%, but the advantage are less laboratory effort and therefore more available calibration data. The site specific regressions for sample SPMC versus Hach turbidities vary by only 20% for the RBINS data set shown in Figure 21. Using the global fit at different sites still reproduces the sample SPMC within less than 20% with an average bias of 3%. Especially given the high uncertainties of low sample SPMC due to the filter offsets that can only be controlled by several filters per sample, a 20% random error for Hach-derived SPMC seems to be a suitable and cheap alternative to filter weights.

The sample SPMC and the sensor data should preferably be collected in-situ as it is more reliable than in lab model calibrations (ISO, 2014). In case no in situ samples can be collected or if the range of sample SPMC is too small, in lab model calibration can be applied with representative samples. Bollen et al. (2006) describes a laboratory model calibration using a representative in-situ bed sample taken near the monitoring station. The bed sample was sieved on a 63 μ m sieve, followed by desalination and drying, to finally produce standard solutions with defined SPMC that have other IOP then the sample SPMC. The regression model using in-situ data only has a larger slope compared to the relation derived from the standard SPMC solution and will overestimate the sensor output by about 10%.

2.4. Conclusions and outlook

Optical and acoustical sensors have proved invaluable in the study of SPM dynamics in marine and estuarine environments as they allow collecting easily in-situ, high-frequency SPMC time series over long periods of time. The payback is the availability of large homogenous data set of SPMC from various locations on the globe; the drawback is that the quality or certainty of the data and thus also the inter-comparability depends on factors that are only to a certain level avoidable. The factors that hamper the quality of the data have been described in chapter 3 and grouped according to the functioning of the sensor, the environment, the collection of sample SPMC for calibration, the calibration using linear regression models, the inherent optical and acoustical properties of the SPM and human errors (see Table 2.3). While the first four types of errors are detectable and sometimes correctable, the relation of sensor output to environmental condition is difficult to detect outside the calibration period. The latter affects the inherent properties of the particle and can result in over- or underestimation of the SPMC by up to factor 2 or more. A good understanding of the processes that are causing changes in SPM concentration and particle inherent properties (size, shape, density and composition) is required in order to estimate their importance and to possibly rescale the sensor data to some reference particle properties. Further the use of both acoustic and optical sensors extended by addi-

tional sensors that measure size and composition of the SPM (see Table 2.2) is a measure to identify changes in inherent particle properties. For long-term observations with remote stand-alone systems this presently requires unsurmountable effort. As a consequence, intensive measuring campaigns remain necessary to understand the variability in the relation between sensor output and sample SPMC that can allow a correction of the sensor data.

Acoustical and optical sensors require both the conversion of the sensor output (after sensor calibration) to a mass concentration. This is done by relating the sensor output to a reference SPMC, which is preferably the sample SPMC. The choice of the regression model, the dependent and independent variable and the error associated with the reference SPMC determines the coefficient of determination of the regression. We have build a model that based on the R^2 and the normalized turbidity/dB quantifies the uncertainty of the sensor derived SPMC in the calibration range and outside of it.

Our study confirms that the relation between turbidity sample SPMC is depending on protocols (EPA, ISO), technology (scattering angle) and the manufacturer, and even may differ between sensors of the same type (e.g. Downing, 2006; Rai and Kumar, 2015; Rymaszewicz et al., 2017). The relation between the output of an acoustical sensor and SPMC is even more variable. Nevertheless this uncertainty, turbidity is still often used as a proxy for water clarity or SPMC as is the dB of acoustical sensors. We strongly advice to not use turbidity (or dB) for scientific purposes as it diminishes the comparability of the data. Instead, the sensor output should be transformed into a mass concentration, a unit that is comparable in time and between regions. If this is not possible, then the turbidity data should always be referred to the instrument used and the protocol applied. The problem aggravates when turbidity data that have been collected using different technologies and protocols over a long period of time and are stored in international data bases (e.g. turbidity in EMODnet, see <http://www.emodnet.eu>), are used to derive conclusive trends of the environmental status of marine and estuarine areas. The uncertainty analysis presented here could be the basis for further validation of existing historical data of turbidity and SPMC by estimating the uncertainties related to the measurements and could offer guidelines to obtain intercomparable high quality long-term SPMC time series in the future.

3. Referenties

- Abarzua S, Jakubowski S. 1995. Biotechnological investigation for the prevention of biofouling. I Biological and biochemical principles for the prevention of biofouling. *Marine Ecology Progress Series* 123, 301-312.
- Adriaens R, Zeelmaekers E, Fettweis M, Vanlierde E, Vanlede J, Stassen P, Elsen J, Środoń J, Vandenberghe N. 2018. Quantitative clay mineralogy as provenance indicator for recent muds in the southern North Sea. *Marine Geology* 398, 48-58. doi:10.1016/j.margeo.2017.12.011
- Agrawal YC, Pottsmith HC. 2000. Instruments for particle size and settling velocity observations in sediment transport. *Marine Geology* 168, 89-114.
- Ainslie MA, McColm JG. 1998. A simplified formula for viscous and chemical absorption in sea water. *Journal of the Acoustical Society of America* 103, 1671-1672.
- Anastasiou S, Sylaios GK, Tsihrintzis VA. 2015. Suspended particulate matter estimates using optical and acoustic sensors: application in Nestos River plume (Thracian Sea, North Aegean Sea). *Environmental Monitoring and Assessment* 187, 1-17. doi:10.1007/s10661-015-4599-y
- Babin M, Morel A, Fournier-Sicre V, Fell F, Stramski D. 2003. Light scattering properties of marine particles in coastal and open ocean waters as related to the particle mass concentration. *Limnology and Oceanography* 48, 843-859. doi:10.4319/lo.2003.48.2.0843
- Badewien TH, Zimmer E, Bartholomä A, Reuter R. 2009. Towards continuous long-term measurements of suspended particulate matter (SPM) in turbid coastal waters. *Ocean Dynamics* 59, 227-238. doi:10.1007/s10236-009-0183-8
- Baeye M, Fettweis M. 2015. In situ observations of suspended particulate matter plumes at an offshore wind farm. *Geo-Marine Letters* 35, 247-255. doi:10.1007/s00367-015-0404-8
- Baeye M, Quinn R, Deleu S, Fettweis M. 2016. Detection of shipwrecks in ocean colour satellite imagery. *Journal of Archeological Sciences* 66, 1-6. doi:10.1016/j.jas.2015.11.006
- Baker ET, Lavelle JW. 1984. The effect of particle size on the light attenuation coefficient of natural suspensions. *Journal of Geophysical Research* 89 (C5), 8197-8203.
- Banse K, Falls CP, Hobson LA. 1963. A gravimetric method for determining suspended matter in sea water using Millipore filters. *Deep Sea Research and Oceanographic Abstracts*. 639-642.
- Barillé-Boyer A-L, Barillé L, Massé H, Razet D, Héral M. 2003. Correction for particulate organic matter as estimated by loss on ignition in estuarine ecosystems. *Estuarine, Coastal and Shelf Science* 58, 147-153. doi:10.1016/S0272-7714(03)00069-6
- Barter PJ, Deas T. 2003. Comparison of portable nephelometric turbidimeters on natural waters and effluents. *New Zealand Journal of Marine and Freshwater Research* 37, 485-492.
- Baschek B, Schroeder F, Brix H, Riethmüller R, Badewien TH, Breitbach G, Brügge B, Colijn F, Doerffer R, Eschenbach C, Friedrich J, Fischer P, Garthe S, Horstmann J, Krasemann H, Metfies K, Merckelbach L, Ohle N, Petersen W, Pröfrock D, Röttgers R, Schlüter M, Schulz J, Schulz-Stellenfleth J, Stanev E, Staneva J, Winter C, Wirtz K, Wollschläger J, Zielinski O, Ziemer F. 2017. The Coastal Observing System for Northern and Arctic Seas (COSYNA). *Ocean Sciences* 13, 379-410. doi:10.5194/os-13-379-2017
- Becherer J, Flöser G, Umlauf L, Burchard H. 2016. Estuarine circulation versus tidal pumping: Sediment transport in a well-mixed tidal inlet. *Journal of Geophysical Research* 121, 6251-6270. doi:10.1002/2016JC011640
- Becker M, Schrottke K, Bartholomä A, Ernstsens V, Winter C, Hebbeln D. 2013. Formation

- and entrainment of fluid mud layers in troughs of subtidal dunes in an estuarine turbidity zone. *Journal of Geophysical Research* 118, 2175–2187. doi:10.1002/jgrc.20153.
- Berthon J-F, Shybanov E, Lee ME-G, Zibordi G. 2007. Measurements and modeling of the volume scattering function in the coastal northern Adriatic Sea. *Applied Optics* 46, 5189-5203.
- Binding CE, Bowers DG, Mitchelson-Jacob EG. 2005. Estimating suspended sediment concentrations from ocean colour measurements in moderately turbid waters; the impact of variable particle scattering properties. *Remote sensing of Environment* 94, 373-383. doi:10.1016/j.rse.2004.11.002
- Bolanos R, Amoudry L, Doyle K. 2011. Effects of instrumented bottom tripods on process measurements. *Journal of Atmospheric and Oceanic Technology* 28, 827-837. doi:10.1175/2010JTECHO816.1
- Bollen M, Sas M, Vanlede J, de Mulder T. 2006. Measuring High Concentration Benthic Suspensions (HCBS), using a high resolution SiltProfiler. Proc. 15th International Congress of the International Federation of Hydrographic Societies. Special Publication, 55, 138-140. www.vliz.be/imisdocs/publications/114165.pdf
- Boss E, Pegau WS. 2001. Relationship of light scattering at an angle in the backward direction to the backscattering coefficient. *Applied Optics* 40, 5503–5507.
- Boss E, Pegau WS, Lee M, Twardowski MS, Shybanov E, Korotaev G, Baratange F. 2004. The particulate backscattering ratio at LEO 15 and its use to study particle composition and distribution. *Journal of Geophysical Research* 109(C01014). doi:10.1029/2002JC001514
- Boss E, Taylor L, Gilbert S, Gundersen K, Hawley N, Janzen C, Johengen T, Purcell H, Robertson C, Schar DWH, Smith GJ, Tamburri MN. 2009. Comparison of inherent optical properties as a surrogate for particulate matter concentration in coastal waters. *Limnology & Oceanography Methods* 7, 803–810. doi:10.4319/lom.2009.7.803
- Boss E, Slade W, Hill P. 2009b. Effect of particulate aggregation in aquatic environments on the beam attenuation and its utility as a proxy for particulate mass. *Optic Express* 17, 9408-9420.
- Bowers DG, Binding CE. 2006. The optical properties of mineral suspended particles: a review and synthesis. *Estuarine, Coastal and Shelf Science* 67, 219–23. doi:10.1016/j.ecss.2005.11.010
- Bowers DG, Braithwaite KM, Nimmo-Smith WAM, Grahams GW. 2009. Light scattering by particles suspended in the sea: The role of particle size and density. *Continental Shelf Research* 29 (2009) 1748–1755 doi:10.1016/j.csr.2009.06.004
- Bowers DG, McKee D, Jago CF, Nimmo-Smith WAM. 2017. The area-to-mass ratio and fractal dimension of marine flocs. *Estuarine, Coastal and Shelf Science*, 189, 224-234. doi:10.1016/j.ecss.2017.03.026
- Butman B, Noble M, Folger DW. 1979. Long-term observations of bottom current and bottom sediment movement on the mid-Atlantic continental shelf. *Journal of Geophysical Research* 84(C3), 1187–1205. doi:10.1029/JC084iC03p01187.
- Capuzzo E, Stephens D, Silva T, Barry J, Forster RM. 2015. Decrease in water clarity of the southern and central North Sea during the 20th century. *Global Change Biology* 21, 2206–2214. doi:10.1111/gcb.12854
- Chami M, Marken E, Stamnes JJ, Khomenko G, Korotaev G. 2006. Variability of the relationship between the particulate backscattering coefficient and the volume scattering function measured at fixed angles. *Journal of Geophysical Research* 111(C5), C05013.
- Delauney L, Compère C, Lehaitre M. 2010. Biofouling protection for marine environmental sensors. *Ocean Science* 6, 503–511. doi:10.5194/os-6-503-2010

- Dogliotti A-I, Ruddick K, Nechad B, Doxaran D, Knaeps E. 2015. A single algorithm to retrieve turbidity from remotely-sensed data in all coastal and estuarine waters. *Remote Sensing of Environment* 156, 157–168.
- Dogliotti A, Nechad B, Ruddick K, Gossn JI. 2016. Towards an autonomous turbidimeter network for multi-mission ocean colour satellite validation activities. In: *Proc. Living Planet Symposium* (ed. Ouwehand, L.), ESA-SP Volume 740, ISBN: 978-92-9221-305-3
- Dolphin TJ, Green MO, Radford JDJ, Black KP. 2000. Biofouling of optical backscatter sensors: Prevention and analytical correction of data. *Journal of Coastal Research*, SI34, 334–341.
- Downing A, Thorne PD, Vincent CE. 1994. Backscattering from a suspension in the near field of a piston transducer. *Journal of the Acoustical Society of America* 97 (3), 1614-1620.
- Downing J. 2005. Turbidity Monitoring. In *Environmental Instrumentation and Analysis Handbook* (Eds. Down RD, Lehr JH), John Wiley & Sons Inc. doi:10.1002/0471473332.ch24
- Downing J. 2006. Twenty-five years with OBS sensors: The good, the bad, and the ugly. *Continental Shelf Research* 26, 2299-2318. doi:10.1016/j.csr.2006.07.018
- Doxaran D, Leymarie E, Nechad B, Dogliotti A, Ruddick K, Gernez P, Knaeps E. 2016. Improved correction methods for field measurements of particulate light backscattering in turbid waters. *Optics Express* 24(4), 3615-3637
- Droppo I, Leppard G, Liss S, Milligan T. 2005. *Flocculation in Natural and Engineered Environmental Systems*, CRC Press, Boca Raton, Fla.
- Druine F, Verney R, Deloffre J, Lemoine J-P, Chapalain M, Landemain V, Lafite R. 2018. In situ high frequency long term measurements of suspended sediment concentration in turbid estuarine system (Seine Estuary, France): Optical turbidity sensors response to suspended sediment characteristics. *Marine Geology*, 400, 24-37. doi:10.1016/j.margeo.2018.03.003
- Duan N. 1983. Smearing estimate—A nonparametric retransformation method: *Journal of the American Statistical Association* 78 (383), 605–610.
- Dufois F, Verney R, Le Hir P, Dumas F, Charmasson S. 2014. Impact of winter storms on sediment erosion in the Rhone River prodelta and fate of sediment in the Gulf of Lions (North Western Mediterranean Sea). *Continental Shelf Research* 72, 57–72. doi:10.1016/j.csr.2013.11.004
- Dyer KR, Manning AJ. 1999. Observation of the size, settling velocity and effective density of flocs, and their fractal dimensions. *Journal of Sea Research* 41, 87–95.
- Edwards TK, Glysson GD. 1999. Field methods for measurement of fluvial sediment. U.S. Geological Survey Techniques of Water-Resources Investigations, USGS Survey Book 3, chap. C2, 89 pp.
- Eisma D. 1986. Flocculation and de-flocculation of suspended matter in estuaries. *Netherlands Journal of Sea Research* 20, 183–199.
- EPA. 1993. Method 180.1 - Determination of turbidity by nephelometry (revision 2.0), Environmental Protection Agency, Cincinnati, 10.
- Fettweis M, Sas M, Monbaliu J. 1998. Seasonal, Neap-spring and Tidal Variation of Cohesive Sediment Concentration in the Scheldt Estuary. Belgium. *Estuarine, Coastal and Shelf Science* 47, 21–36.
- Fettweis M, Francken F, Pison V, Van den Eynde D. 2006. Suspended particulate matter dynamics and aggregate sizes in a high turbidity area. *Marine Geology* 235, 63–74.
- Fettweis M. 2008. Uncertainty of excess density and settling velocity of mud flocs derived from in situ measurements. *Estuarine, Coastal and Shelf Science* 78, 426-436.

doi:10.1016/j.ecss.2008.01.007

- Fettweis M, Baeye M, Lee BJ, Chen P, Yu JCR. 2012. Hydro-meteorological influences and multimodal suspended particle size distributions in the Belgian nearshore area (southern North Sea). *Geo-Marine Letters* 32, 123-137. doi:10.1007/s00367-011-0266-7
- Fettweis M, Baeye M. 2015. Seasonal variation in concentration, size and settling velocity of muddy marine flocs in the benthic boundary layer. *Journal of Geophysical Research* 120, 5648–5667. doi:10.1002/2014JC010644
- Fettweis M, Baeye M, Cardoso C, Dujardin A, Lauwaerts B, Van den Eynde D, Van Hoesenberghe T, Vanlede J, Van Poucke L, Velez C, Martens C. 2016. The impact of disposal of fine grained sediments from maintenance dredging works on SPM concentration and fluid mud in and outside the harbor of Zeebrugge. *Ocean Dynamics* 66, 1497-1516. doi:10.1007/s10236-016-0996-1
- Fettweis M, Lee BJ. 2017. Spatial and seasonal variation of biomineral suspended particulate matter properties in high-turbid nearshore and low-turbid offshore zones. *Water* 9, 694. doi:10.3390/w9090694
- Fugate DC, Friedrichs CT. 2002. Determining concentration and fall velocity of estuarine particle populations using ADV, OBS and LISST. *Continental Shelf Research* 22, 1867–1886.
- Ganju NK, Schoellhamer DH. 2006. Annual sediment flux estimates in a tidal strait using surrogate measurements. *Estuarine, Coastal and Shelf Science* 69, 165-178. doi:10.1016/j.ecss.2006.04.008
- Garel E, Ferreira O. 2011. Monitoring estuaries using non-permanent stations: practical aspects and data examples. *Ocean Dynamics* 61, 891–902. doi:10.1007/s10236-011-0417-4
- Gibbs RJ. 1985. Estuarine flocs: Their size, settling velocity and density. *Journal of Geophysical Research* 90 (C2), 3249-3251.
- Gil Y, David CH, Demir I, Essawy BT, Fulweiler RW, Goodall JL, Karlstrom L, Lee H, Mills HJ, Oh J-H, Pierce SA, Pope A, Tzeng MW, Villamizar SR, Yu X. 2016. Toward the geoscience paper of the future: Best practices for documenting and sharing research from data to software to provenance. *Earth and Space Science*, 3, 388–415, doi:10.1002/2015EA000136
- Gilbert RO. 1987. *Statistical Methods for Environmental Pollution Monitoring*. Van Nostrand Reinhold Company Inc. New York, 320pp.
- Gostiaux L, van Haren H. 2010. Extracting meaningful information from uncalibrated backscattered echo intensity data. *Journal of Atmospheric and Oceanic Technology*, 27, 943-949. doi:10.1175/2009JTECHO704.1
- Grabemann I, Krause G. 1989. Transport processes of suspended matter derived from time series in a tidal estuary. *Journal of Geophysical Research* 94(C10), 14373–14379. doi:10.1029/JC094iC10p14373.
- Gray JR, Gartner JW. 2009. Technological advances in suspended-sediment surrogate monitoring, *Water Resources Research*, 45, W00D29. doi:10.1029/2008WR007063
- Grove MK, Bilotta GS. 2014. On the use of loss-on-ignition techniques to quantify fluvial particulate organic carbon. *Earth Surface Processes and Landforms* 39, 1146–1152. doi:10.1002/esp.3509
- Guerrero M, Di Federico V. 2018. Suspended sediment assessment by combining sound attenuation and backscatter measurements – analytical method and experimental validation. *Advances in Water Resources*, 113, 167-179
- Guézennec L, Lafite R, Dupont JP, Meyer R, Boust D. 1999. Hydrodynamics of suspended particulate matter in the tidal freshwater zone of a macrotidal estuary (the Seine Estu-

- ary, France). *Estuaries* 22, 717-727.
- Ha HK, HsuW-Y, Maa JP-Y, ShaoYY, Holland CW. 2009. Using ADV backscatter strength for measuring suspended cohesive sediment concentration. *Continental Shelf Research* 29, 1310–1316.
- Ha HK, Maa JP-Y, Park K, Kim YH. 2011. Estimation of high-resolution sediment concentration profiles in bottom boundary layer using pulse-coherent acoustic Doppler current profilers. *Marine Geology* 279, 199–209. doi:10.1016/j.margeo.2010.11.002
- Hatcher A, Hill P, Grant J, Macpherson P. 2000. Spectral optical backscatter of sand in suspension: effects of particle size, composition and colour. *Marine Geology* 168, 115-128.
- Helsel DR, Hirsch RM. 2002. *Statistical Methods in Water Resources*. Techniques of Water-Resources, Investigations of the US Geological Survey, Book 4, Hydrologic Analysis and Interpretation, 510pp. <https://pubs.usgs.gov/twri/twri4a3/>
- HELCOM. 2015. *Manual for Marine Monitoring in the COMBINE Programme of HELCOM*, 466pp. <http://helcom.fi/action-areas/monitoring-and-assessment/manuals-and-guidelines/combine-manual>
- Henson SA. 2014. Slow science: the value of long ocean biogeochemistry records. *Philosophical Transactions of the Royal Society A* 372, 20130334. doi:10.1098/rsta.2013.0334
- Hoitink AJF, Hoekstra P. 2005. Observations of suspended sediment from ADCP and OBS measurements in a mud-dominated environment. *Coastal Engineering* 52, 103-118. doi: 10.1016/j.coastaleng.2004.09.005
- Holdaway GP, Thorne PD, Flatt D, Jones SE, Prandle D. 1999; Comparison between ADCP and transmissometer measurements of suspended sediment concentration. *Continental Shelf Research* 19(3), 421-441.
- IOCCG. 2011. Bio-optical sensors on ARGO floats. In: Claustre, H. (ed.), reports of the International Ocean-Colour Coordinating Group, No. 11, IOCCG, Dartmouth, Canada. http://www.ioccg.org/reports/IOCCG_Report11.pdf
- ISO. 1997. *Water quality -- Determination of suspended solids by filtration through glass-fibre filters*. ISO Standard 11923:1997, International Organization for Standardization.
- ISO. 1999. *Water quality - determination of turbidity*, ISO Method 7027, International Organization for Standardization.
- ISO. 2008. *Evaluation of measurement data — Guide to the expression of uncertainty in measurement*. ISO/IEC Guide 98-3:2008 (JCGM/WG1/100) International Organization for Standardization, Geneva, Switzerland.
- ISO. 2014. *Hydrometry -- Suspended sediment in streams and canals -- Determination of concentration by surrogate techniques*. International Organization for Standardization, Switzerland, ISO 11657:2014.
- ISO. 2017. *Guidance for the use of repeatability, reproducibility and trueness estimates in measurement uncertainty estimation*, ISO 21748, International Organization for Standardization, Geneva, Switzerland.
- Jafar-Sidik M, Gohin F, Bowers D, Howarth J, Hull T. 2017. The relationship between Suspended Particulate Matter and turbidity at a mooring station in a coastal environment: consequences for satellite-derived products. *Oceanologia* 59, 365—378. doi:10.1016/j.oceano.2017.04.003
- Jalón-Rojas I, Schmidt S, Sottolichio A. 2015. Turbidity in the fluvial Gironde Estuary (southwest France) based on 10-year continuous monitoring: sensitivity to hydrological conditions. *Hydrology and Earth System Science* 19, 2805-2819. doi:10.5194/hess-19-2805-2015

- JAMP. 2012. Eutrophication monitoring guidelines: Chlorophyll a in Water. OSPAR Joint Assessment & Monitoring Programme, Agreement 2012-11.
- Jourdin F, Tessier C, Le Hir P, Verney R, Lunven M, Loyer S, Lusven A, Filipot J-F, Lepesqueur J. 2014. Dual-frequency ADCPs measuring turbidity. *Geo-Marine Letters* 34, 381-397. doi:10.1007/s00367-014-0366-2.
- Kappenberg J, Berendt M, Ohle N, Riethmüller R, Schuster D, Strotmann T. 2018. Variation of hydrodynamics and water constituents in the mouth of the Elbe estuary, Germany. *Civil Engineering Research Journal* 4, 555643. doi:10.19080/CERJ.2018.04.555643
- Kerr A, Cowling MJ, Beveridge CM, Smith MJ, Parr ACS, Head RM, Davenport J, Hodgkiess T. 1998. The early stages of marine biofouling and its effects on two types of optical sensors. *Environment International* 24, 331-343.
- Kineke GC, Sternberg RW. 1992. Measurements of high concentration suspended sediments using the optical backscatterance sensor. *Marine Geology*, 108, 253-258
- Klein H. 2003. Investigating sediment re-mobilisation due to wave action by means of ADCP echo intensity data Field data from the Tromper Wiek, western Baltic Sea. *Estuarine, Coastal and Shelf Science* 58, 467-474. doi:10.1016/S0272-7714(03)00113-6.
- Krivtsov V, Howarth MJ, Jones SE, Souza AJ, Jago CF. 2008. Monitoring and modelling of the Irish Sea and Liverpool Bay: An overview and an SPM case study. *Ecological Modelling* 212, 37-52. doi:10.1016/j.ecolmodel.2007.10.038
- Lane A, Riethmüller R, Herbers D, Rybaczkov P, Günther H, Baumert H. 2000. Observational data sets for model development. *Coastal Engineering* 41, 125-153.
- Lauwaert B, Fettweis M, De Witte B, Devriese L, Van Hoesel G, Timmermans S, Martens C. 2016. Synthesis report on the effects of dredged material disposal on the marine environment (licensing period 2012-2016). RBINS-ILVO-AMT-AMCS-FHR report BL/2016/09, 107pp.
- Lynch TP, Roughan M, McLaughlan D, Hughes D, Cherry D, Critchley G, Allen S, Pender L, Thompson P, Richardson AJ, Coman F, Steinberg C, Terhell D, Seuront L, Mclean C, Brinkman G, Meyers G. 2008. National reference station infrastructure for Australia: Using telemetry and central processing to report multi-disciplinary data streams for monitoring marine ecosystem response to climate change. *OCEANS 2008*, Quebec City, QC, 2008, pp. 1-8. doi:10.1109/OCEANS.2008.5151856
- Maerz J, Hofmeister R, van der Lee EM, Gräwe U, Riethmüller R, Wirtz KW. 2016. Maximum sinking velocities of suspended particulate matter in a coastal transition zone. *Biogeosciences* 13, 4863-4876, doi:10.5194/bg-13-4863-2016
- Manov V, Chang GC, Dickey TD. 2004. Methods for Reducing Biofouling of Moored Optical Sensors. *Journal of Atmospheric and Ocean Technology*, 21, 958-968.
- Many G, Bourrin F, Durrieu de Madron X, Pairaud I, Gangloff A, Doxaran D, Ody A, Verney R, Menniti C, Le Berre D, Jacquet M. 2016. Particle assemblage characterization in the Rhone River ROFI. *Journal of Marine Systems* 157, 39-51. doi: 10.1016/j.jmarsys.2015.12.010
- McAnally WH, Friedrichs C, Hamilton D, Hayter E, Shrestha P, Rodriguez H, Sheremet A, Teeter AM. 2007. Management of fluid mud in estuaries, bays, and lakes. I: Present state of understanding on character and behaviour. *Journal of Hydraulic Engineering* 133, 9-22.
- Medwin H, Clay CS. 1998. *Fundamentals of acoustical oceanography*. Academic Press, New York, 712pp.
- Mishchenko MI, Travis LD, Lacis AA. 2002. *Scattering, absorption, and emission of light by small particles*. Cambridge University Press, Cambridge.
- Moody JA, Butman B, Bothner MH. 1987. Near-bottom suspended matter concentration

- on the continental shelf during storms: estimates based on in-situ observations of light transmission and a particle size dependent transmissometer calibration. *Continental Shelf Research* 7, 609-628.
- Mullison J. 2017. Backscatter estimation using Broadband Acoustic Doppler Current Profilers – updated. ASCE Hydraulic Measurements & Experimental Methods Conference, Durham, NH (USA). July 9-12.
- Muste M, Kim D, Burkhardt A, Brownson Z. 2006. Near-transducer errors in Acoustic Doppler Current Profiler measurements. World Environmental and Water Resources Congress, Omaha (Nebraska, USA), May 21-25, [https://doi.org/10.1061/40856\(200\)164](https://doi.org/10.1061/40856(200)164)
- Nauw JJ, Merckelbach LM, Ridderinkhof H, van Aken HM. 2014. Long-term ferry-based observations of the suspended sediment fluxes through the Marsdiep inlet using acoustic Doppler current profilers. *Journal of Sea Research* 87, 17–29. doi:10.1016/j.seares.2013.11.013
- Nechad B, Ruddick K, Neukermans G. 2009. Calibration and validation of a generic multi-sensor algorithm for mapping of turbidity in coastal waters. *Proceedings SPIE "Remote Sensing of the Ocean, Sea Ice, and Large Water Regions"*, SPIE Vol. 7473, 74730H.
- Nechad B, Dogliotti A, Ruddick K, Doxaran D. 2016. Particulate backscattering retrieval from remotely-sensed turbidity in various coastal and riverine turbid waters. In: *Proc. Living Planet Symposium* (ed. Ouwehand L), ESA-SP Volume 740, ISBN: 978-92-9221-305-3
- Neukermans G, Ruddick K, Loisel H, Roose P. 2012a. Optimization and quality control of suspended particulate matter concentration measurement using turbidity measurements. *Limnology and Oceanography Methods* 10, 1011-1023.
- Neukermans G, Loisel H, Mériaux X, Astoreca R, McKee D. 2012b. In situ variability of mass-specific beam attenuation and backscattering of marine particles with respect to particle size, density, and composition. *Limnology and Oceanography* 57, 124-144. doi:10.4319/lo.2011.57.1.0124 1
- Ocean Optics Web Book, 2018. A collaborative web-based book on optical oceanography <http://www.oceanopticsbook.info/>
- Pait AS, Galdo Jr FR, Hartwell SI, Mason AL, Apeti DA, Jeffrey CFG, Hoffman AM, Pittman SJ. 2015. An assessment of nutrients, sedimentation, and total suspended solids (TSS) in the St. Thomas East End Reserves (STEER). NOAA Technical Memorandum NOS/NCCOS 184. Silver Spring, MD. 66pp
- Palinkas CM, Ogston AS, Nittrouer CA. 2010. Observations of event-scale sedimentary dynamics with an instrumented bottom boundary-layer tripod. *Marine Geology* 274, 151-164. doi:10.1016/j.margeo.2010.03.012
- Pearlman SR, Costa HS, Jung RA, McKeown JJ, Pearson HE. 1995. Solids (section 2540). In: Eaton AD, Clesceri LS, Greenberg AE (Eds.), *Standard Methods for the Examination of Water and Wastewater*. American Public Health Association, Washington DC, USA, pp. 2-53–2-64.
- Press WH, Flannery BP, Teukolsky SA, Vetterling WT. 1989. *Numerical recipes*. Cambridge University Press, 702pp.
- Puleo JA, Johnson RV, Butt T, Kooney TN, Holland KT. 2006. The effect of air bubbles on optical backscatter sensors. *Marine Geology*, 230, 87-97. doi:10.1016/j.margeo.2006.04.008
- Rai AK, Kumar A. 2015. Continuous measurement of suspended sediment concentration: Technological advancement and future outlook. *Measurements* 76, 209–227. doi:10.1016/j.measurement.2015.08.013

- Ramsey MH, Ellison SLR (Eds.). 2007. Measurement uncertainty arising from sampling: A guide to methods and approaches. Eurachem/EUROLAB/ CITAC/Nordtest/AMC Guide.
- Randolph K, Dierssen HM, Twardowski M, Cifuentes-Lorenzen A, Zappa CJ. 2014. Optical measurements of small deeply penetrating bubble populations generated by breaking waves in the Southern Ocean. *Journal of Geophysical Research Oceans* 119, 757–776. doi:10.1002/2013JC009227
- Rasmussen PP, Gray JR, Glysson GD, Ziegler AC. 2009. Guidelines and procedures for computing time-series suspended-sediment concentrations and loads from in-stream turbidity-sensor and streamflow data: U.S. Geological Survey Techniques and Methods Book 3, chap. C4, 53pp.
- Ridd P, Larcombe P. 1994. Biofouling control for optical backscatter suspended sediment sensors. *Marine Geology*, 116, 255-258.
- Ross MA, Mehta AJ. 1989. On the mechanics of lutoclines and fluid mud. *Journal of Coastal Research* S15, 51-61.
- Röttgers R, Heymann K, Krasemann H. 2014. Suspended matter concentrations in coastal waters: Methodological improvements to quantify individual measurement uncertainty. *Estuarine, Coastal and Shelf Science* 151, 148-155. doi:10.1016/j.ecss.2014.10.010
- Rouhnia M, Keyvani A, Strom K. 2014. Do changes in the size of mud flocs affect the acoustic backscatter values recorded by a Vector ADV? *Continental Shelf Research* 84, 84-92. doi: 10.1016/j.csr.2014.05.015
- Rymaszewicz A, O'Sullivan JJ, Bruen M, Turner JN, Lawler DM, Conroy E, Kelly-Quinn M. 2017. Measurement differences between turbidity instruments, and their implications for suspended sediment concentration and load calculations: A sensor inter-comparison study. *Journal of Environmental Management* 199, 99-108. doi:10.1016/j.jenvman.2017.05.017
- Sadar M. 1999. Turbidimeter instrument comparison: Low-level sample measurements technical information series. Hach Company, report D90.5, 55pp.
- Sahin C, Verney R, Sheremet A, Voulgaris G. 2017. Acoustic backscatter by suspended cohesive sediments: field observations, Seine Estuary, France . *Continental Shelf Research* 134, 39-51. doi:10.1016/j.csr.2017.01.003
- Salehi M, Strom K. 2011. Using velocimeter signal to noise ratio as a surrogate measure of suspended mud concentration. *Continental Shelf Research* 31, 1020-1032
- Schmechtig C, Thierry V, the Bio Argo Team. 2015. Argo quality control manual for biogeochemical data. doi:10.13155/40879
- Schwarz C, Cox TJS, Van Engeland T, Van Oevelen D, Van Belzen, J, van de Koppel J, Soetaert K, Bouma TJ, Meire P, Temmerman S. 2017. Field estimates of floc dynamics and settling velocities in a tidal creek with significant along-channel gradients in velocity and SPM. *Estuarine, Coastal and Shelf Science* 197, 221-235. doi: 10.1016/j.ecss.2017.08.041
- Schwendeman M, Thomson J. 2015. Observations of whitecap coverage and the relation to wind stress, wave slope, and turbulent dissipation, *Journal of Geophysical Research Oceans* 120, 8346–8363. doi:10.1002/2015JC011196.
- Sheng J, Hay AE. 1988 An examination of the spherical scatterer approximation in aqueous suspensions of sand. *Journal of the Acoustical Society of America* 83, 598–610.
- Shreve EA, Downs AC. 2005. Quality-assurance plan for the analysis of fluvial sediment. U.S. Geological Survey Kentucky Water Science Center Sediment Laboratory, USGS Open-File Report 2005-1230, 28pp.
- Slade WH, Agrawal YC, Mikkelsen O.A. 2013. Comparison of measured and theoretical scattering and polarization properties of narrow size range irregular sediment parti-

- cles. Presented at Oceans, San Diego, 23–7.
- Sottolichio A, Hurther D, Gratiot N, Bretel P. 2011. Acoustic turbulence measurements of near-bed suspended sediment dynamics in highly turbid waters of a macrotidal estuary. *Continental Shelf Research*, 31, S36–S49.
- Spinrad RW, Yentsch CM, Brown J, Dortch Q, Haugen E, Revelante N, Shapiro L. 1989. The response of beam attenuation to heterotrophic growth in a natural population of plankton. *Limnology and Oceanography* 34, 1601-1605.
- Stanton TK. 1989. Simple approximate formulas for backscattering of sound by spherical and elongated objects. *Journal of the Acoustical Society of America* 86, 1499–1510.
- Stavn RH, Rick HJ, Falster AV. 2009. Correcting the errors from variable sea salt retention and water of hydration in loss on ignition analysis: Implications for studies of estuarine and coastal waters. *Estuarine Coastal and Shelf Science* 81, 575–582. doi:10.1016/j.ecss.2008.12.017
- Strickland JDH, Parsons TR. 1968. A practical handbook of seawater analysis. Bulletin 167. Fisheries Research Board of Canada, Ottawa, Canada, 181–184.
- Sutherland TF, Lane PM, Amos CL, Downing J. 2000. The calibration of optical backscatter sensors for suspended sediment of varying darkness levels. *Marine Geology*, 162, 587-597.
- Tessier C. 2006. Caractérisation et dynamique des turbidités en zone côtière: l'exemple de la région marine Bretagne Sud. PhD thesis Université de Bordeaux, France, 400pp.
- Tessier C, Le Hir P, Lurton X, Castaing P. 2008. Estimation de la matière en suspension à partir de l'intensité acoustique rétrodiffusée des courantomètres acoustiques à effet Doppler (ADCP). *Comptes Rendus Geoscience* 340, 57–67.
- Thorne PD, Vincent CE, Hardcastle PJ, Rehman S, Pearson N. 1991. Measuring suspended sediment concentrations using acoustic backscatter devices. *Marine Geology*, 98, 7-16.
- Thorne PD, Hardcastle PJ, Holdaway GP, Born AJ. 1994. Analysis of results obtained from a triple frequency acoustic backscatter system for measuring suspended sediments, Proceedings of the 6th International Conference on Electronic Engineering in Oceanography, 394, 83-89.
- Thorne PD, Hanes DM. 2002. A review of acoustic measurement of small-scale sediment processes. *Continental Shelf Research* 22, 603–632.
- Thorne PD, MacDonald IT, Vincent CE. 2014. Modelling acoustic scattering by suspended flocculating sediments. *Continental Shelf Research* 88, 81-91.
- TMAP. 2009. Monitoring Handbook: Eutrophication – Nutrients (version 16.09.2009, TMAG 09-2). <http://www.waddensea-secretariat.org/monitoring-tmap/manual-guidelines>
- Topping DJ, Wright SA. 2016, Long-term continuous acoustical suspended-sediment measurements in rivers—Theory, application, bias, and error. U.S. Geological Survey, USGS Professional Paper 1823, 98 pp. <http://dx.doi.org/10.3133/pp1823>.
- Tzeng MW, Dzwonkowski B, Park K. 2016. Data processing for a small-scale long-term coastal ocean observing system near Mobile Bay, Alabama. *Earth and Space Science* 3, 510–522. doi:10.1002/2016EA000188.
- van der Hout CM, Gerkema T, Nauw JJ, Ridderinkhof H. 2015. Observations of a narrow zone of high suspended particulate matter (SPM) concentrations along the Dutch coast. *Continental Shelf Research* 95, 27–38. doi:10.1016/j.csr.2015.01.002
- van Maren DS, Oost AP, Wang ZB, Vos PC. 2016. The effect of land reclamations and sediment extraction on the suspended sediment concentration in the Ems Estuary. *Marine Geology* 376, 147–157. doi:10.1016/j.margeo.2016.03.007
- Wagner RJ, Boulger Jr RW, Oblinger CJ, Smith BA. 2006. Guidelines and standard procedu-

- res for continuous water-quality monitors—Station operation, record computation, and data reporting. U.S. Geological Survey, USGS Techniques and Methods 1–D3, 51 pp. <http://pubs.water.usgs.gov/tm1d3>
- Waldmann C, Tamburri M, Prien RD, Fietzek P. 2010. Assessment of sensor performance. *Ocean Science* 6, 235–245.
- Wang DW, Wijesekera HW, Teague WJ, Rogers WE, Jarosz E. 2011. Bubble cloud depth under a hurricane. *Geophysical Research Letters* 38, L14604. doi:10.1029/2011GL047966
- Wang DW, Wijesekera HW, Jarosz E, Teague WJ. 2016. Turbulent diffusivity under high winds from acoustic measurements of bubbles. *Journal of Physical Oceanography* 46, 1593–1613. doi:10.1175/JPO-D-15-0164.1
- Whelan A, Regan F. 2006. Antifouling strategies for marine and riverine sensors. *Journal of Environmental Monitoring* 8, 880–886. doi: 10.1039/b603289c
- Wilcox RR. 2001, *Fundamentals of modern statistical methods substantially improving power and accuracy*. Springer-Verlag, 249pp.
- Winterwerp JC, van Kesteren WGM. 2004. Introduction to the physics of cohesive sediment in the marine environment. *Developments in Sedimentology* 56, Elsevier, 466pp.
- Yeats PA, Brüggmann L. 1990. Suspended particulate matter: collection methods for gravimetric and trace metal analysis. *ICES Techniques in Marine Environmental Sciences* 7, 9pp.
- Yentsch CS. 1962. Measurement of visible light absorption by particulate matter in the ocean. *Limnology and Oceanography* 7, 207-217.
- Zhang X, Stavn RH, Falster AU, Gray D, Gould Jr RW. 2014. New insight into particulate mineral and organic matter in coastal ocean waters through optical inversion. *Estuarine, Coastal and Shelf Science* 149, 1-12. doi:10.1016/j.ecss.2014.06.003
- Ziegler AC. 2003. Breakout session 1 – Definition of optical methods for turbidity and data reporting. In: *Proceedings of the Federal Interagency Workshop on Turbidity and Other Sediment Surrogates* (Gray JR, Glysson GD, Eds.), U.S. Geological Survey, USGS Circular 1250, 9 – 13. <http://water.usgs.gov/pubs/circ/2003/circ1250/>

COLOPHON

Dit rapport werd voorbereid door de BMM in juli 2018

Zijn referentiecode is MOMO/8/MF/201808/NL/AR/3

De scheepstijd met de RV Belgica werd voorzien door BELSPO en KBIN-OD Natuur

Indien u vragen hebt of bijkomende copies van dit document wenst te verkrijgen, gelieve een e-mail te zenden naar mfettweis@naturalsciences.be, met vermelding van de referentie, of te schrijven naar:

Koninklijk Belgisch Instituut voor Natuurwetenschappen

OD Natuur – BMM

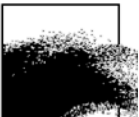
t.a.v. Michael Fettweis

Gulledelle 100

B-1200 Brussel

België

Tel: +32 2 773 2132



APPENDIX 1

Bijdrage 50th Liège Colloquium on Ocean Dynamics, 18 May – 1 June, Liège (Belgium)

Uncertainties associated with long-term observations of suspended particulate matter concentration using optical and acoustic sensors

Michael Fettweis¹, Rolf Riethmüller², Romaric Verney³, Marius Becker⁴

¹ Royal Belgian Institute of Natural Sciences, OD Nature, Gulledele 100, 1200 Brussels, Belgium
E-mail: mfettweis@naturalsciences.be

² Helmholtz-Zentrum Geesthacht, Institute for Coastal Research, Max-Planck-Str. 1, 21502 Geesthacht, Germany

³ IFREMER, Hydrodynamics and Sediment Dynamics Laboratory (DYNECO/PHYSED), BP 70, 29280 Plouzané, France

⁴ MARUM, Centre for Marine Environmental Sciences, University of Bremen, Leobener Str. 8, 28359 Bremen, Germany

Water clarity or turbidity is an important parameter to understand the marine ecosystem and is mainly controlled by suspended particulate matter concentration (SPMC). Environmental data on water clarity collected during the last century in coastal seas and estuaries indicate significant local and global environmental changes due to human activities and climate change (Capuzzo et al., 2015; van Maren et al., 2016). The conclusions from these studies are, however, hampered by the often limited and undocumented quality of the historical data and the very low temporal resolution of measurements with regard to the high dynamic nature of the systems in which the data have been collected. In view of documenting current and future trends, high quality measurements of SPMC spanning long temporal and large spatial scales have therefore become a matter of growing importance in the last decades. Worldwide observation platforms were installed to capture the temporal and spatial SPMC variability on scales ranging from turbulent fluctuations to decadal changes over large areas. The infrastructure on which the sensors are attached is as diverse as the time scale of the processes studied, and includes fixed and moving platforms or a combination of both. The same holds for SPMC itself. In addition, measurements are affected by SPMC composition, i.e., the clastic or organic content, controlling the specific non-cohesive or cohesive properties.

The estimation of SPMC by optical and acoustical sensors generally results from the combination of a number of technically independent calibration measurements with regression or inverse models. Long-term in-situ measurements of SPMC involve in general one or several optical and acoustical sensors of similar or different technical specifications and, as the best ground truth reference, gravimetric measurements of filtered water samples. The SPMC obtained during these long-term measurements is thus a surrogate of the real SPMC. It is well-known that a variety of parameters, particle (floc) size and composition have an impact on the optical and acoustical inherent properties of the SPM and thus on the sensor output. Variations in the state of the studied system change the inherent particle properties which may require repeated field surveys for water sampling. Electronic drift, mechanical threats or growing coverage of sensor transmitter/receiver windows by living (biofouling) or non-living matter (fouling) requires regular maintenance and sensor cleansing with sensor monitoring against well-defined references.

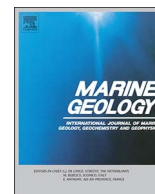
Direct or indirect measurements of SPMC are thus inherently associated with a number of uncertainties along the whole operational chain from planning over laboratory work, i.e. technical difficulties during mostly unsupervised deployment, and the conversion of observed continuous proxy values (the optical and acoustical signals) to SPMC. The aim of the study therefore is to present and discuss potentials and limitations related to the use of optical and acoustical backscatter sensors, describing challenges and yet unsolved problems with long-term observations of SPMC, to present degrees of uncertainties involved in the analysis steps of the operation chain, and to formulate recommendations as a basis to acquire quality-controlled SPMC data sets. On the basis of examples the main sources of errors as well as means to quantify and reduce the uncertainties associated with SPMC measurements are illustrated.

References

- Capuzzo E, Stephens D, Silva, T, Barry J, Forster RM. 2015. Decrease in water clarity of the southern and central North Sea during the 20th century. *Global Change Biology* 21, 2206–2214.
- van Maren DS, Oost AP, Wang ZB, Vos PC. 2016. The effect of land reclamations and sediment extraction on the suspended sediment concentration in the Ems Estuary. *Marine Geology* 376, 147–157.

APPENDIX 2

Adriaens R, Zeelmaekers E, Fettweis M, Vanlierde E, Vanlede J, Stassen P, Elsen J, Środoń J, Vandenberghe N. 2018. Quantitative clay mineralogy as provenance indicator for recent muds in the southern North Sea. *Marine Geology*, 398, 48-58



Quantitative clay mineralogy as provenance indicator for recent muds in the southern North Sea

R. Adriaens^{a,b,*}, E. Zeelmaekers^{a,1}, M. Fettweis^c, E. Vanlierde^d, J. Vanlede^d, P. Stassen^{a,e}, J. Elsen^a, J. Środoń^f, N. Vandenberghe^a

^a Department of Earth and Environmental Sciences, KU Leuven, Celestijnenlaan 200E, 3001, Leuven, Belgium

^b Qmineral Analysis & Consulting, Gaston Geenslaan 1, 3001 Leuven, Belgium

^c Royal Belgian Institute of Natural Sciences, OD Natural Environment, Guldelle 100, B-1200 Brussels, Belgium

^d Flanders Hydraulics Research, Berchemlei 115, 2140 Borgerhout, Belgium

^e Royal Belgian Institute of Natural Sciences, OD Earth and History of Life, Vautierstraat 29, B-1000 Brussels, Belgium

^f Institute of Geological Sciences, Polish Academy of Sciences, Research Centre in Kraków, ul. Senacka 1, PL-31002 Kraków, Poland

ARTICLE INFO

Editor: G.J. de Lange

Keywords:

North Sea
Clay minerals
Shelf processes
Estuaries
Scheldt river

ABSTRACT

The origin of recent mud deposits as well as the coastal turbidity maximum in the French-Belgian-Dutch nearshore area of the southern North Sea is still under debate in the literature. Some models favor the erosion of the Cretaceous chalk cliffs along the English Channel and subsequent NE ward directed transport, other models focus on the erosion of Eocene to earliest Oligocene, and Pleistocene to Holocene clays outcropping on the seafloor off the Belgian coast. In order to validate these hypotheses, the detailed qualitative and quantitative clay mineral composition of these sediments was used as a provenance indicator. By comparing the clay mineral composition of the mud deposits and the associated suspended particulate matter (SPM) with the composition of potential nearby and more remote sources such as the present day marine environment, estuaries and rivers, coastal erosion areas and the geological substratum, the origin of the mud deposits and the SPM could be traced. Results showed that only the clay composition of the Scheldt estuary coincides with those of the mud deposits and the coastal turbidity maximum and that all other potential sources could be excluded. Our data suggest that the clay mineral composition of the mud deposits has a similar composition since at least about 100,000 years, indicating that these deposits originate from a paleo-Scheldt river rather than from the recent river system, as the present-day Scheldt estuary is not source of fine-grained sediments. The present-day SPM in the Belgian-Dutch nearshore area originates mainly from the erosion and resuspension of the existing mud deposits situated in the Belgian nearshore. This study demonstrates the value and suitability of quantitative bulk and clay mineralogy techniques in sediment provenance studies and highlights the importance of incorporating the recent geological history in hydrodynamic studies of sedimentary basins.

1. Introduction

Sediment fluxes and budgets are required to assess the state of a marine environment and to predict changes induced by natural variability, human activities or climate change. The flux includes the transport of fine-grained suspended particulate matter (SPM) from an erosional source to a depositional sink often over long distances. Regional fine-grained sediment dynamics can be complicated by the multitude of local and remote sources, transport routes and sink. This starts with the erosion of a varying geological substratum, complex river patterns, coastal erosion and accretion, and the consecutive and

temporal deposition, storage and resuspension of sediments in inter- or subtidal areas. The fine-grained sediment dynamics in the French-Belgian-Dutch nearshore area of the southern North Sea is an example of such a complicated system where the origin of a coastal turbidity maximum and of a cohesive mud deposit are still under debate as shown by the following summary of mud provenance paths suggested in literature (Fig. 1).

Fine-grained SPM entering the North Sea through the Dover Strait is suggested based on in situ and remote sensing measurements of SPM concentration, hydrodynamics and numerical models (Prandle et al., 1996; Velegrakis et al., 1999; Lafite et al., 2000; Fettweis et al., 2007a).

* Corresponding author at: Department of Earth and Environmental Sciences, KU Leuven, Celestijnenlaan 200E, 3001 Leuven, Belgium.

E-mail address: rieko.adriaens@kuleuven.be (R. Adriaens).

¹ Currently at Shell Exploration & Production Company, Houston, TX, USA.

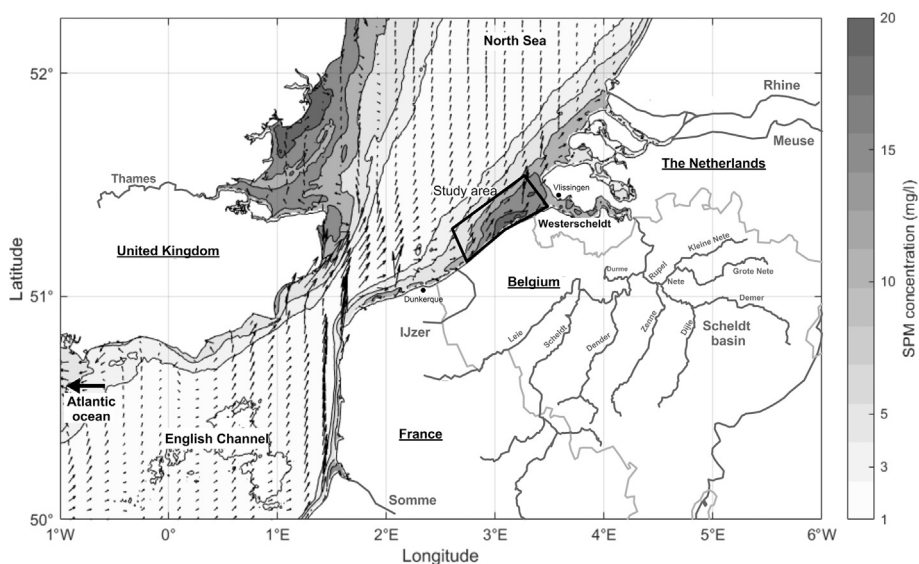


Fig. 1. Geographical overview of the southern North Sea basin showing the mud plate (black polygon) in the Belgian-Dutch nearshore area and the averaged surface SPM concentration derived from MODIS satellite and the coastal turbidity maxima of the Belgian-Dutch nearshore area indicated as greyscale variations. Arrows indicate the residual water transport in the southern North Sea and English Channel, showing a dominantly SW-NE direction (after Fettweis et al., 2007a, 2007b). The different possible source areas, English Channel, Atlantic Ocean, Scheldt river basin, Rhine & Meuse rivers are all indicated. Paleogene clays outcropping on the North Sea seafloor occur in the north to northeastern part of the mud plate.

Erosion of the Cretaceous chalk cliffs along the English Channel and the Dover Strait and the subsequent NE ward directed transport is suggested as a predominant source of fine-grained sediments in the southern Bight of the North Sea. This is based on the ruling tidal regime and wind patterns, sediment transport modeling, qualitative clay mineralogy and microfossil analysis (Eisma, 1981; Irion and Zöllmer, 1999; Gerritsen et al., 2001; Fontaine, 2004; Fettweis et al., 2007a). Fettweis and Van den Eynde (2003) suggested that the accumulation of fine-grained material in the coastal turbidity maximum results from a decrease of the residual NE ward directed SPM transport originating from the Strait of Dover. Other studies however emphasize that local erosion of Holocene to Pleistocene mud layers is most likely the main source of the cohesive mud deposits and the SPM in the turbidity maximum area (Baeteman, 1999; Beets and van der Spek, 2000; Mathys, 2009). Bastin (1974) and Le Bot et al. (2005) have suggested erosion of outcropping Eocene to earliest Oligocene clays as possible sources. Fontaine (2004) reported the presence of earliest Oligocene nanoplankton microfossils in the cohesive mud deposit implying at least a partial provenance contribution from either outcropping deposits in the southern North Sea or from their erosion in the Scheldt estuary. The contribution of the Scheldt, the Rhine-Meuse river system and the Seine is an additional potential source as these rivers had a major impact on the sediment distribution in the North Sea during the recent geological history and also presently play their role (Lacroix et al., 2004; Busschers et al., 2005; Peeters et al., 2015). The large maintenance dredging and disposal operations in the area could have an influence on the sediment dynamics as these operations relocate locally fine-grained sediments by local relocation of sediments although their regional extent remains unknown (Fettweis et al., 2009). These different mud provenance hypotheses are mainly based on an understanding of residual flow patterns in the Dover Strait and the southern North Sea and on regional geological and general sedimentological considerations. However, no systematic sediment composition analyses were carried out in support of the mud provenance.

Several studies applied qualitative and semi-quantitative clay mineral analysis as a tracer of fine-grained sediment pathways in marine, tidal and fluvial environments (Irion and Zöllmer, 1999; Sandler and Herut, 2000; Zuther et al., 2000; Kessarkar et al., 2003; Ramaswamy et al., 2007; Liu et al., 2008, 2010; Pache et al., 2008; Dou et al., 2010; Howell et al., 2014; Li et al., 2014; Schroeder et al., 2015). However, conclusions of these studies were hampered by the low resolution and limited accuracy of the applied methods. Recent methodological developments however allow for a fully quantitative and accurate analysis of clay minerals which makes them also applicable for provenance

studies in fine-grained deposits (Hillier, 1999; Sakharov et al., 1999; Środoń et al., 2001; Omotoso et al., 2006; Aplin et al., 2006; Ufer et al., 2008; Hubert et al., 2009; Zeelmaekers et al., 2015; Raven and Self, 2017). The aim of the present study therefore is to apply these advanced quantitative clay mineral analysis to compare the turbidity maximum and the cohesive bottom mud sediments of the French-Belgian-Dutch nearshore area with the suggested provenance areas.

2. Background and methodology

2.1. Study area

The study area is located between the English Channel and the central North Sea (Fig. 1). The area is bounded by the Strait of Dover to the southwest and the Western Scheldt estuary to the northeast and can be considered as a link between the Atlantic Ocean and the North Sea in terms of exchanges of water, sediment and other substances. The area is a macrotidal environment, with tidal ranges up to 6 m at Dunkerque and 4.5 m at Vlissingen during spring tide. The tides are semidiurnal and tidal currents are strong, ranging between 0.5 and 1.5 m s⁻¹. The Belgian Continental Shelf (BCS) is a high-energy sedimentary environment consisting dominantly of fine- to medium-sized sand deposits structured in elongated ridges and mud to muddy sand deposits (Trentesaux et al., 1999; Le Bot et al., 2005; Verfaillie et al., 2006). The occurrence of a high turbidity zone located between about Ostend and the Western Scheldt estuary is of special interest (Fig. 1), see e.g. Fettweis and Van den Eynde (2003). The cohesive sediments on the BCS, further referred to as BCS mud plate, consist of three types with variable thicknesses (Fettweis et al., 2009, 2010): 1) fluid mud, forming the uppermost layer (cm- to dm-range) of the mud plate with a density of 1100–1200 kg/m³, 2) weakly-consolidated, soft butter-like muds (decimeters to meters thick) with a bulk density of 1300–1500 kg/m³ and, 3) medium-consolidated, stiffer muds sometimes intercalated with more sandy layers (0.5 m to a few meters thick) with a bulk density of 1500–1800 kg/m³. These more consolidated muds often underlain the more weakly-consolidated and fluid muds and together form the mud plate.

2.2. Clay mineral analysis method

In the present study proven robust quantitative clay mineral analyses are used following the approach outlined by Drits et al. (1997); Sakharov et al. (1999); Środoń et al. (2001); Zeelmaekers et al. (2015). All collected samples were subjected to a systematic preparation

procedure in order to characterize both bulk mineral composition and clay mineral composition < 2 μm using X-ray diffraction analysis.

Approximately 100 g of each sample was dried at 60 °C and subsequently gently powdered and homogenized in a mortar. For clay mineral analysis, 15 g of powdered sample was subjected to a chemical preparation (modified after Jackson, 1975) during which carbonate cements, organic matter and free Fe-(hydr)oxides were removed using respectively acetic acid/Na-acetate buffer solution, 30% H₂O₂ solution and Na-dithionite in a Na-citrate-bicarbonate environment respectively. Subsequently, clay material < 2 μm was extracted using a Thermo-Scientific SL-40R centrifuge and Ca-saturated using CaCl₂. Clay slides were prepared by sedimenting 160 mg of clay material < 2 μm on a glass slide. Both bulk powders and clay slides were measured using a Philips PW1050/37 goniometer connected to a PW1830 generator equipped with Cu-K α radiation and PW3011/00 proportional detector in Bragg-Brentano θ –2 θ setup. Clay slides were measured in air-dry conditions and saturated with ethylene glycol, each time from 2 to 47° 2 θ with steps of 0.02° lasting 2 s per step. Clay slides were also exposed to 550 °C heating during 1 h and measured from 2 to 15° 2 θ . Diffraction patterns of oriented slides were analyzed and quantified using the Sybilla clay modeling software (© Chevron ETC) (Zeelmaekers, 2011; Adriaens et al., 2014; Zeelmaekers et al., 2015; Adriaens, 2015.)

For bulk mineralogy, a representative portion of each sample was mixed with a 10% internal standard (ZnO) and 4 ml of ethanol. This mixture was milled for 5 min. using a McCrone micronizing mill and afterwards recuperated in porcelain cups (Środoń et al., 2001). The material was passed through a 250 μm sieve, side-loaded into alumina diffractometer holders to optimize the random orientation of crystallites. Bulk powders were measured by X-ray diffraction from 5 to 65° 2 θ with steps of 0.02° lasting 2 s per step. Bulk powder diffraction patterns were analyzed and quantified using the Quanta software (© Chevron ETC) which combines summation of pure reference standards and the use of a ZnO internal standard.

2.3. Sampling

Different sampling campaigns were organized between 2004 and 2016 to characterize the clay mineral composition of the BCS mud plate, the SPM in the English Channel and southern North Sea, and all the potential source areas as reviewed above. These comprise recent bottom mud and suspension samples representing present-day transported mud, outcrop material subject to erosion and also older strata considered as potential mud sources sampled from borehole core material. Surface mud samples were collected by a Van Veen grab or box corer and suspension samples using an ALFA Laval MMB 304S flow-through centrifuge, either in stationary positions or in tracks. In total 43 BCS samples and 241 potential source area samples were collected and analyzed. For each potential source area, the clay mineral composition of the < 2 μm fraction, referred to as the clay fraction, was quantified and compared with the BCS clay fraction composition. As the bulk mineralogical composition of these deposits mainly delivers information regarding the clayey (clays) or sandy (quartz) nature of the sample, this analysis has a low provenance potential but has its value in mass balance calculations. Results of the bulk analysis are therefore only provided for the BCS mud plate itself (see Supplementary Table 2) whereas the bulk composition of other samples is not discussed in detail. All sample information can be retrieved in Supplementary Tables 1 to 9.

3. Clay mineral analysis results

3.1. Belgian Continental Shelf mud plate and SPM

3.1.1. Samples

A set of 34 surface mud samples and 8 suspension samples were collected by the RV Belgica (Fig. 2). The lithology of the surface mud

samples ranges from fluid to weakly-consolidated and medium-consolidated mud and locally also muddy sand of recent and Holocene age. Additional mud plate samples were collected from cored boreholes on top of the Stroombank and Wenduinebank sandbanks and the swale Grote Rede (Geological Survey of Belgium repository) (Fig. 2).

3.1.2. Results

The bulk mineralogical composition of the mud plate samples consists of mainly quartz, carbonates and clays (Fig. 3 and Supplementary Table 2). The 3–10% amorphous material is authigenic organic matter and amorphous silica from diatoms. Pyrite, halite, gypsum and anatase are typical accessory minerals and occur in low quantities (< 2%). Quartz and clay mineral contents are inversely correlated and depend on the relative dominance of sandy or muddy lithologies. However, these minerals are transported together as 30–100 μm SPM flocs (Eisma, 1986; Agrawal and Pottsmith, 2000; Lee et al., 2012) which consist of mainly clay and silt and small amounts of fine sand. This SPM furthermore has the same grain-size range and a very similar mineralogical composition as the bottom mud sediments on the BCS. The slight difference between SPM composition and bottom mud composition is due to carbonates (Fig. 3). Whereas clay minerals, quartz and feldspars are detrital, carbonates are for the largest part autochthonic biogenic minerals and therefore not provenance indicators. The dominantly autochthonic biogenic origin of the carbonates is confirmed by microscopic observation of non-transported 32–125 μm -sized calcareous skeleton fragments and carbon isotopic data of the Scheldt estuary and coastal SPM and their erratic distribution in the bottom sediments (Salomons and Mook, 1987). This demonstrates that the use of clay mineral instead of the bulk composition is a reasonable approach and that given their abundance in these sediments, clay minerals are suitable provenance indicators.

The clay mineralogical composition of weakly- and medium consolidated mud from the BCS mud plate and of SPM collected above the mud plate (Table 1 and Supplementary Table 3) is similar and all analyses show low variability. The composition consists of smectite (34–42%), randomly interstratified (R0) and highly-illitic interstratified illite-smectite (18–30%), illite (16–22%), kaolinite (12–15%) and 4–6% chlorite (Fig. 5). The illite content in the interstratified illite-smectite (I/S) varies between 67% and 79%.

The quantitative clay composition of the BCS fluid and weakly consolidated mud, the medium consolidated mud and suspension samples are plotted in a ternary compositional diagram (Fig. 6). This plot shows the distinctive uniformity in clay composition, both laterally over the mud plate and in depth, and therefore allows for further comparison with the different potential sources. In the ternary diagram, “smectite”, “illitic minerals” and “kaolinite + chlorite” form the end-member compositions. For the end member “illitic minerals”, highly illitic (65–75% illite) interstratified illite-smectite is summed together with discrete illite into one group “illitic minerals” (see also Table 1). This simplifies the comparison between samples and sample groups by plotting the two dominant groups of clay minerals, “illitic minerals” versus “smectite”. In addition, the sum of these illitic phases is judged to be more precise than the separate phases as they are considered for a few % interchangeable during quantification.

3.2. English Channel

3.2.1. Samples

Coastal cliffs or beach sediments along the French or English coasts were collected to characterize all muds that can reach the southern North Sea through the English Channel. To understand the composition of the SPM in the prevailing residual water transport from the Atlantic Ocean to the southern North Sea, suspension water samples were collected by the RV Belgica along tracks in several parts of the English Channel at varying distance from the French coast. In addition two long suspension tracks were collected in the English Channel and one at the

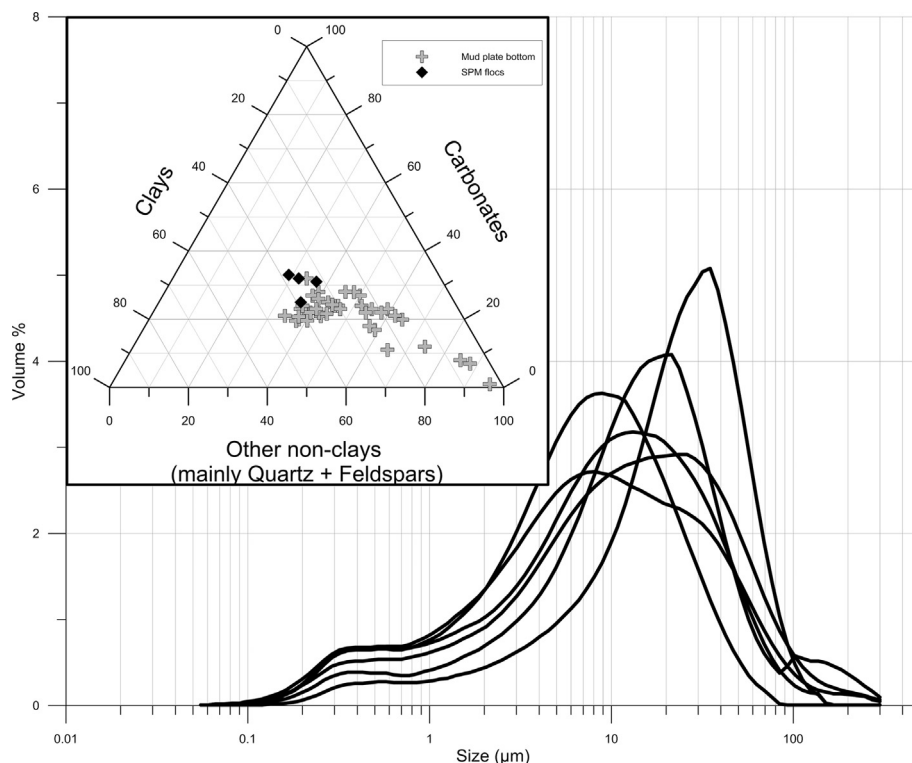


Fig. 2. Particle size frequency distribution of flocculated SPM measured in situ on the Belgian Continental Shelf by laser diffraction (Malvern Mastersizer-S) illustrating that clay-sized fraction coexist with silt-sized and fine sand-sized particles or floccs. Upper left: Ternary diagram illustrating the bulk mineralogical composition of the three main mineral components, namely Carbonates, Quartz + Feldspars + “both non-clays” and Clays, of BCS bottom mud (grey crosses) and SPM occurring mainly as floccs (black squares). For data see Supplementary Table 2.

transition of the Atlantic Ocean and the English Channel, considered to be representative for the Atlantic Ocean waters entering the English Channel (Fig. 4). No sampling campaign was set up for the Thames river system as the hydrodynamics and sediment transport is directed in northeastern direction and not southward (Fettweis et al., 2007a, 2007b).

3.2.2. Results

The clay mineral composition of the various bottom and suspension samples are all significantly different from the BCS mud plate composition (Table 1 and Supplementary Table 4). English Channel sources generally contain 10–30% less smectite and form an independent clay compositional domain outside the BCS mud clay domain (Figs. 7 and 8). Although English beach samples are characterized by more variable clay mineralogy, the smectite and interstratified illite-smectite minerals in all English Channel samples have different structural characteristics

compared to the smectite and interstratified illite-smectite of the BCS mud plate samples.

It is therefore highly unlikely that any of the English Channel sources can be accounted as the main clay supplier of the BCS mud plate.

3.3. Paleogene sea floor

3.3.1. Samples

The Paleogene seafloor of the BCS underneath the thin Quaternary cover consists mainly of Eocene (Priabonian) strata to earliest Oligocene (Rupelian), stratigraphically getting younger from west to east (Le Bot et al., 2005; Fettweis et al., 2007b). Areas where the Quaternary cover is < 2.5 m extend over approximately 20% of the BCS, 6% of the French North Sea area and 3% of the Dutch studied area, and these areas could act as a source of the SPM and the fine-grained

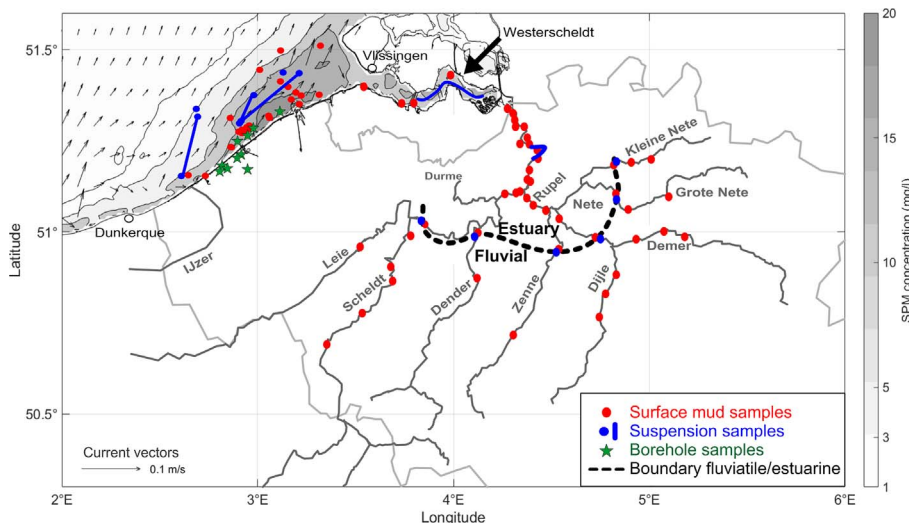


Fig. 3. Sampling of the BCS mud plate, the Scheldt estuary and river basin. Bottom mud samples (red dots) and suspension samples (blue lines) and sample tracks (blue lines) were collected on the BCS and in the Scheldt river basin. Borehole samples (green stars) of the BCS mud plate and Early-Holocene clay were collected from the Stroombank (SB1, SB2), Grote Rede (Gr1) and Wenduinebank (SBW) boreholes. Late-Pleistocene (Saalian-Eemian-Weichselian) deposits were sampled near Nieuwpoort (NP1, NP2, NP3), Middelkerke (Mdk2) and Westende (We4) and at Leeuwenhof borehole (LWH). The fluvial-estuary boundary in the Scheldt river basin is indicated with a dotted line. For coordinates and data see Supplementary Tables 1 to 9. (For interpretation of the references to color in this figure legend, the reader is referred to the web version of this article.)

Table 1

Averages and standard deviations of the clay mineralogical compositions < 2 μm of the BCS mud plate and SPM and comparison with the different potential sediment sources. For the present day sources, only the Scheldt estuary and river system have a similar clay composition. In the studied coastal plain deposits of Holocene and Pleistocene age, it appears that Early-Holocene and Weichselian tidal flats have a similar composition than the BCS. For Eemian to Saalian deposits, tidal flats are very different and resemble the composition of the Paleogene sea floor. Eemian to Saalian fluvial channel deposits however again correspond to the typical BCS mudplate composition. For all data see Supplementary Tables 1 to 9.

	Illite		Interstratified illite/smectite		Total illitic		Smectite		Kaolinitic		Chloritic	
	Average	Stdev	Average	Stdev	Average	Stdev	Average	Stdev	Average	Stdev	Average	Stdev
BCS bottom	18	3	25	3	43	4	39	5	13	1	5	1
BCS suspension	18	6	23	3	41	4	42	6	12	1	5	2
English Channel sources	20	4	35	7	56	5	24	5	17	5	3	2
Paleogene sea floor	4	2	23	3	27	2	71	3	3	2	0	0
Dutch coastal SPM	16	2	24	2	40	2	42	4	15	3	4	1
Rhine river (Holocene–present)	30	13	30	12	61	3	24	8	10	2	6	5
Meuse river (Pleistocene–present)	32	13	34	20	65	11	16	8	14	2	4	3
Westerschelde	19	3	25	3	44	3	38	3	13	1	4	1
Upper Scheldt estuary	15	2	23	4	38	5	46	6	13	2	3	1
Scheldt river system (1992–2009 calc.)	14	0.1	33	0.4	47	0.6	40	0.4	9	0.2	3	0.1
Early Holocene coastal plain	24	4	26	3	50	5	33	5	11	3	7	2
Weichselian tidal flat	16	1	27	3	44	2	42	3	11	1	4	0
Eemian to Saalian tidal flat	8	4	14	2	22	5	74	7	4	1	0.3	1
Eemian to Saalian fluvial channel	18	6	25	0	43	6	38	11	11	3	9	2

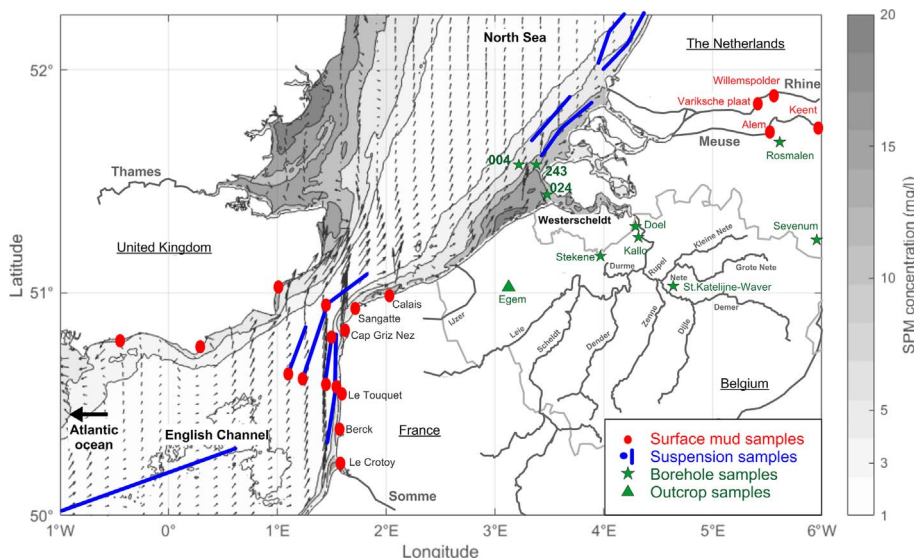


Fig. 4. Sampling of potential sources of the BCS mud plate: present-day Rhine (Variksche Plaat and Willemspolder), Holocene Rhine at Sevenum, present-day Meuse (Keent and Alem), Mid-Pleistocene Meuse at Rosmalen, English Channel and coasts (suspension samples as blue lines, bottom mud or beach coast samples as red dots), Dutch nearshore (blue lines as suspension samples), Paleogene sea floor (TNO boreholes codes BS07004 “004”, BS110024 “024” and BS070243 “243”) and Paleogene Ieper Group clays on-shore (borehole cores at Doel, Kallio, Sint-Katelijne-Waver and Stekene and from the Egem outcrop). See Supplementary Table 5 for coordinates and data. (For interpretation of the references to color in this figure legend, the reader is referred to the web version of this article.)

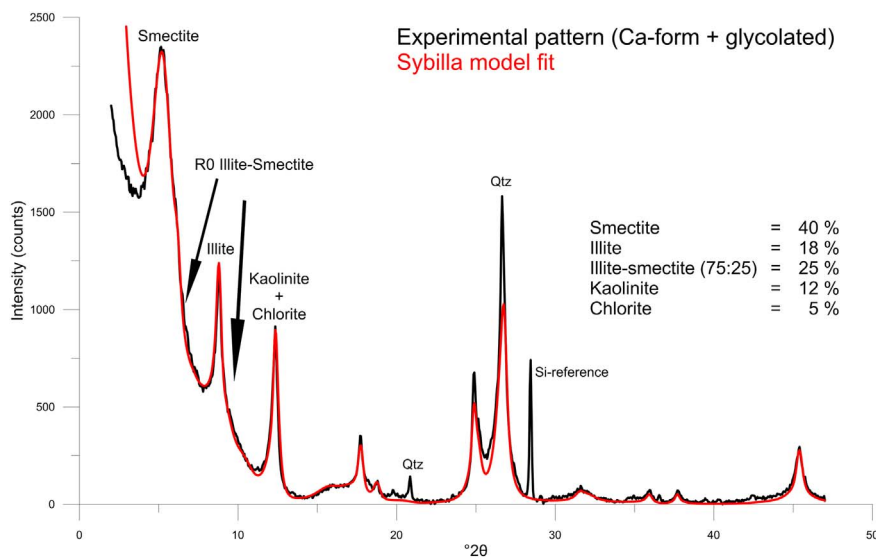


Fig. 5. Quantitative clay model of a BCS mud plate sample (sample KFT9 – see Supplementary Table 1) showing a dominance of smectite, illite and interstratified illite-smectite minerals. Silicon was added to the sample as a peak position reference, quartz occurs naturally in the < 2 μm size fraction.

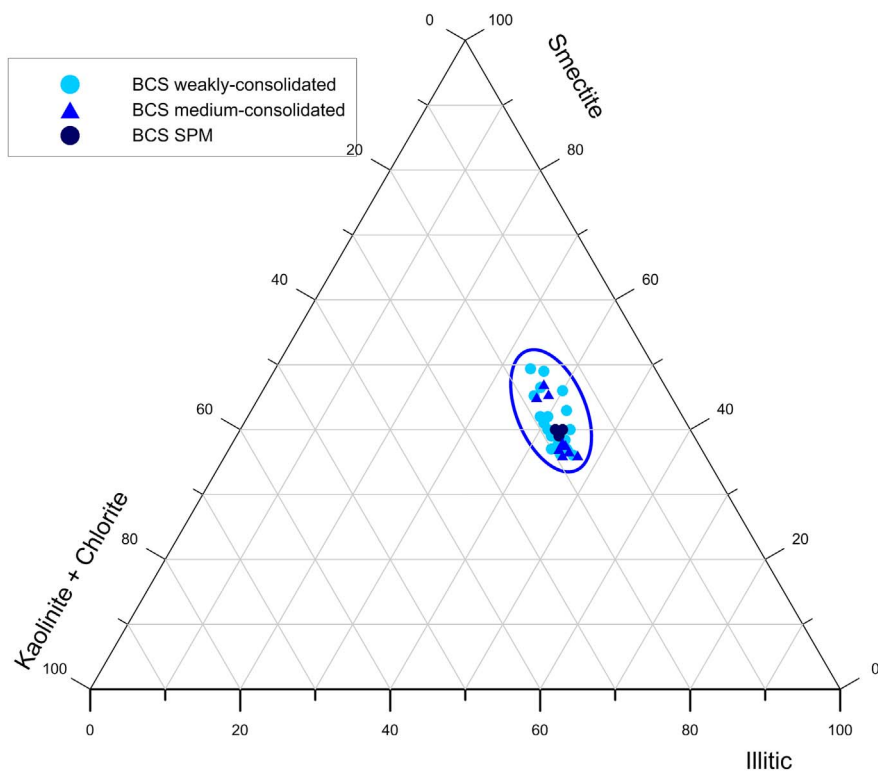


Fig. 6. Ternary diagram of the quantitative clay composition < 2µm with smectite, illitic minerals (illite + interstratified illite-smectite) and kaolinite + chlorite as end-member compositions. The weakly-, medium-consolidated and SPM samples from the BCS mud plate all plot within a limited compositional field. For coordinates and data see Supplementary Tables 1 to 3.

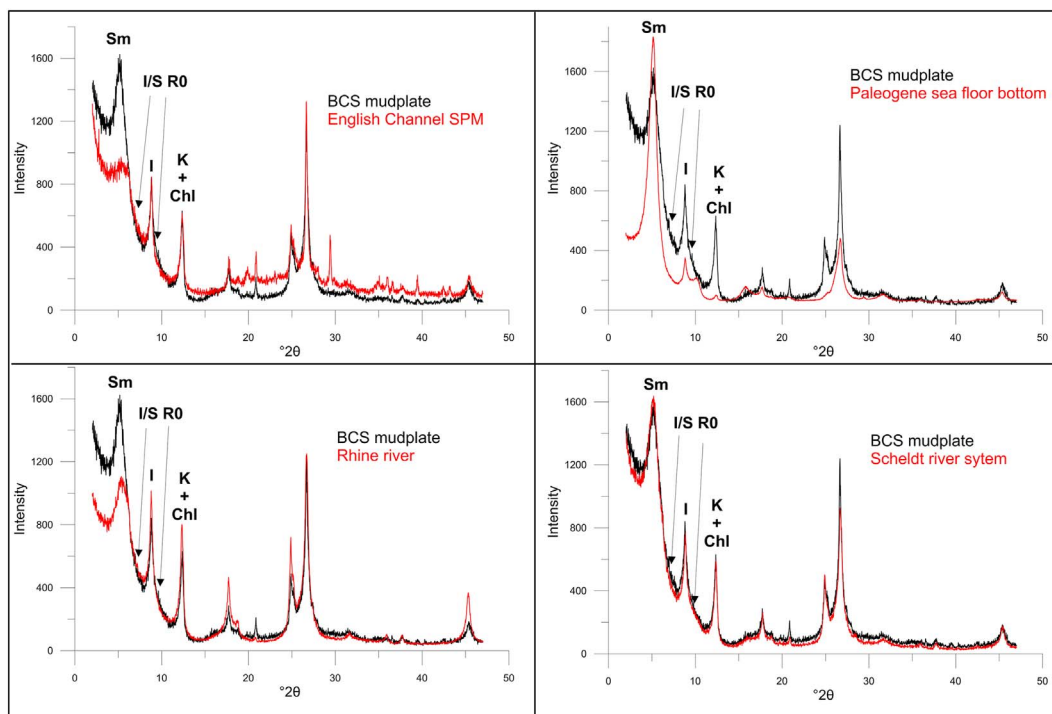


Fig. 7. Examples of diffraction patterns of ethylene glycolated clay fractions < 2µm representative for the English Channel, Paleogene, Rhine and Scheldt potential sources as compared with the diffraction pattern of the BCS mud plate, illustrating that the Scheldt river system is the only source with a matching diffraction pattern. Sm: smectite; I/S R0: randomly interstratified illite-smectite; I: illite; K: kaolinite; Chl: chlorite.

sediments of the mud plate. [Zeelmaekers \(2011\)](#) reported the clay mineralogy of this entire Eocene-Oligocene succession from several boreholes on land in Belgium (Geological Survey of Belgium repository) ([Fig. 4](#)). The geological map shows the lateral continuity of this succession into the Belgian shelf area and it is known that the clay mineralogy is also laterally maintained ([Vandenberghé et al., 1998](#)). Clay

samples from the Paleogene sea floor on the Dutch Continental shelf, presumably Bartonian or earliest Priabonian in age, were selected from three boreholes positioned very near to the BCS mud plate (TNO repository) ([Fig. 4](#)).

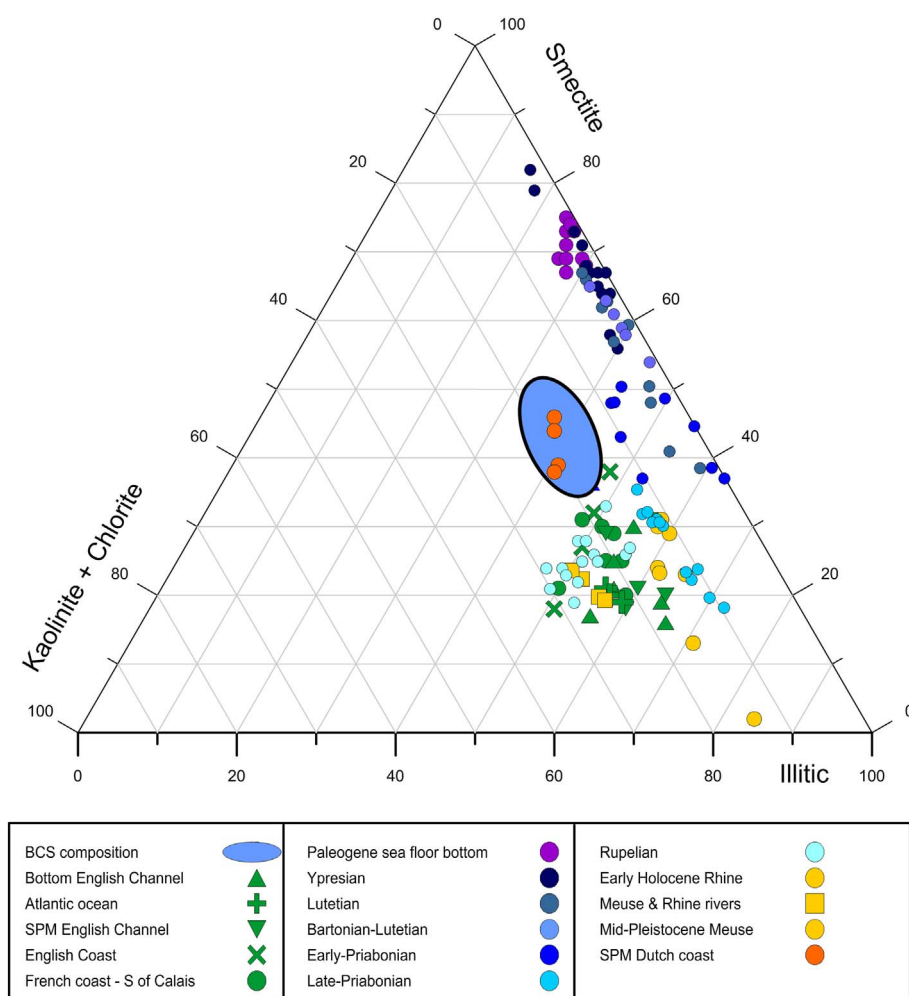


Fig. 8. Ternary diagram of the quantitative clay composition $< 2\mu\text{m}$ of the samples from the English Channel (green symbols), the Paleogene clay samples offshore (purple symbols) and onshore (blue symbols) and the present-day and Pleistocene Meuse-Rhine (yellow symbols). They all plot outside the BCS mud plate compositional domain taken from Fig. 6. SPM samples from the Dutch nearshore and the Early-Holocene subsurface of the BCS mud plate plot entirely inside the BCS mud plate compositional domain. For coordinates and data see Supplementary Table 5. (For interpretation of the references to color in this figure legend, the reader is referred to the web version of this article.)

3.3.2. Results

The clay mineral composition of the Paleogene sea floor samples (Table 1 and Supplementary Table 5) is typically characterized by $> 70\%$ smectite, much higher than the content of the BCS muds (Fig. 7). Furthermore, kaolinite occurs mainly as interstratified kaolinite-smectite. Such a smectite-rich composition is well-known from the Eocene marine clays in the subsurface of Belgium and this composition remains stable up to the Bartonian-Priabonian boundary, above which the smectite content rapidly diminishes to evolve towards the Oligocene Rupelian (e.g. Boom clay) composition (Zeelmaekers et al., 2015). Hence, the clay compositional domain of these Eocene deposits, offshore and onshore, is distinctly different from the BCS mud plate (Fig. 8). The Paleogene offshore clays are mainly situated outside the turbidity maximum area in a zone with low SPM concentrations ($< 5\text{ mg/l}$); therefore the dissimilar clay mineral composition indicates a very low erosion rate of these clays.

3.4. Rhine-Meuse river system and southern Dutch nearshore

3.4.1. Samples

Bottom mud samples were collected from the Rhine-Meuse river system at various locations: the Willemspolder, the Variksche plaat, Keent and Alem (Fig. 4). Subsurface samples of Holocene Rhine and Mid-Pleistocene Meuse deposits were collected from the B45BO290 Rosmalen borehole and the B52DO143 Sevenum borehole from the TNO core repository. Additionally, suspension water samples were collected off the southern Dutch coast (Fig. 4).

3.5. Results

Present-day Rhine-Meuse, Holocene Rhine and Mid-Pleistocene Meuse sediments have a very similar quantitative clay mineral composition, however, containing significantly less smectite than the BCS mud plate (Table 1, Supplementary Table 5 and Fig. 7). The composition of the SPM from the southern Dutch nearshore on the other hand is significantly different from the above river sediments and the clay mineralogy resembles the BCS mud plate composition (Fig. 8). Hence, the clay composition of the recent Rhine-Meuse river system, does not directly correspond to the composition of the southern Dutch nearshore SPM and the BCS mud plate.

3.6. The Scheldt river and estuary system

3.6.1. Samples

A sampling program was designed to understand the relationship between the mineralogical composition of the fluvial and the estuarine parts of the Scheldt. Bottom mud and suspension samples in the lower and middle part of the Scheldt estuary were collected between 2004 and 2006 by the RV Belgica. Upstream fluvial bottom samples of the major tributary river (i.e. Demer, Kleine Nete, Grote Nete, Dijle, Zenne, Dender, Scheldt and Leie) were collected between 2010 and 2012. Suspension material of each tributary was collected at the boundary between the fluvial and estuarine regime of the river system (Fig. 2).

3.6.2. Results

The clay mineralogical composition of the Scheldt estuary and

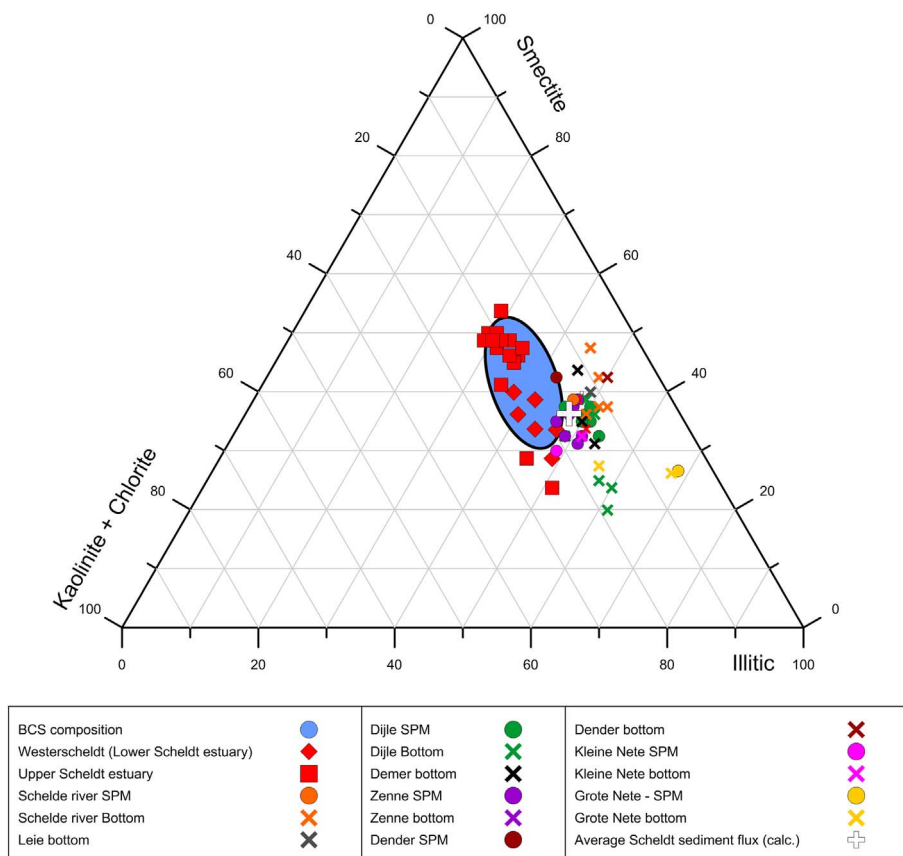


Fig. 9. Ternary diagram of the quantitative < 2 μm clay composition of samples from the Scheldt river system, the Western Scheldt estuary (lower estuary), the upper estuary and the brackish to fresh intertidal flats as compared with the compositional domain of the BCS mud plate. The average sediment flux discharged by the combination of all tributary rivers is indicated with a white cross. Interstratified glauconite-smectite is part of the group “Illitic” as glauconite is the Fe-rich equivalent of illite.

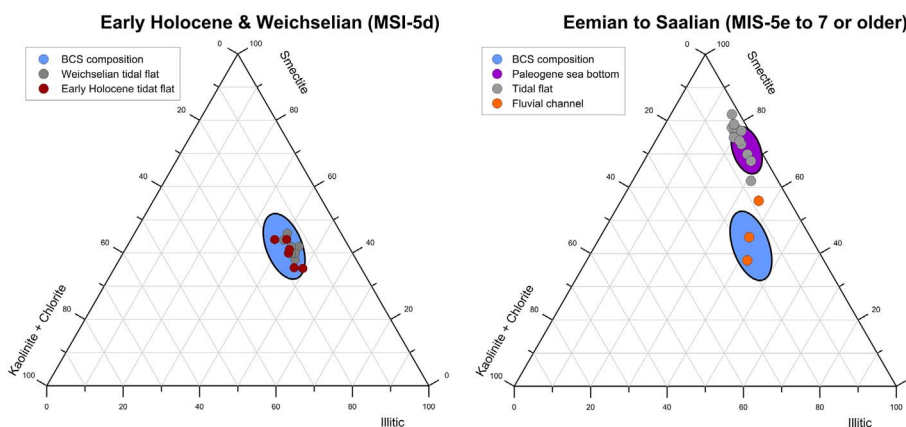


Fig. 10. Ternary diagram of the quantitative < 2 μm clay composition of the Early Holocene and Weichselian tidal flat samples (left) and the Eemian to Saalian tidal flat and fluvial channel samples of the Belgian coastal plain (right) and comparison with the compositional domain of the BCS mud plate. Whereas marine samples from MIS 7-5E age systematically have a smectite-rich composition, which resembles that of the Paleogene sea bottom, the clay composition gradually evolves towards the BCS mud plate composition during a facies change from marine towards a fluvial depositional environment. From the Weichselian onwards, also the clay composition of tidal flats remains highly similar to the BCS mud plate composition.

tributary river samples is shown in Table 1 and Supplementary Tables 6 and 7.

The suspension samples from the estuary and the tributary rivers are most valuable for detecting a potential relationship between the BCS mud plate and the Scheldt river system as they represent the eventual dynamic spatial link with the fluvial part of the river basin. The < 2 μm clay mineral composition of the Scheldt estuary samples is very similar to that of the BCS mud plate, as illustrated by their near identical diffraction patterns (Fig. 7). Individual clay mineral quantities are very similar and the mineral composition plots almost entirely within the BCS mud plate compositional domain, although the spread on the data is slightly larger (Fig. 9). Size-dependent differential settling of clay minerals, sometimes invoked in estuaries and coastal waters (e.g. Irlon and Zöllmer, 1999) is not observed.

The clay composition of the bottom sediment along river trajectories remains stable or only changes slightly. Also the SPM clay compositions collected at the fresh-brackish water interface display very low seasonal

and annual variability and thus remain stable through time (Supplementary Table 8).

The SPM and bottom samples of the tributary rivers Dijle, Zenne, Dender, Scheldt and Leie all have a similar quantitative clay composition, comparable to the lower estuary and the BCS mud plate compositions. Other rivers, such as the Demer, the Kleine Nete and Grote Nete contain interstratified glauconite-smectite in the clay fraction which is derived from the glauconite-rich Neogene deposits in the drainage area (Adriaens, 2015).

To investigate the mixture of clay minerals from the rivers entering the Scheldt estuary, sediment fluxes were calculated at the fresh-brackish water interface (Fig. 2). Daily discharge data and weekly SPM concentration data were measured for 17 consecutive years during the 1992–2009 and were recalculated to annual sediment fluxes allowing the relative sediment flux for each tributary river in the Scheldt river basin to be estimated (Supplementary Table 8). These annual sediment fluxes were then converted to the annual clay mineral fluxes of each

tributary and subsequently to the total discharged clay mineral content of the Scheldt river basin into the estuary. This calculated clay composition is considered representative for the present total discharged clay composition of the Scheldt river basin. The results indicate that the Scheldt, Leie, the Dijle, the Zenne and the Dender discharge the largest sediment fluxes towards the estuary (Supplementary Table 8). Although the interstratified glauconite-smectite is a very distinctive mineral in the upstream Kleine Nete and Grote Nete rivers, it cannot be detected anymore in the estuarine sediments because of the heavy dilution downstream in the estuary. The total clay mineral flux of the Scheldt river basin to the estuary plots closer to the BCS mud plate composition than any other potential source (Fig. 9) and is furthermore prone to little variation over the 17 analyzed years (Table 1 and Supplementary Table 8).

3.7. Holocene and Pleistocene mud deposits in the Belgian coastal plain

3.7.1. Samples

For comparison with the clay mineral composition of the BCS mud plate, clay minerals were also investigated from slightly older deposits in the coastal area using core material from the Geological Survey of Belgium. Early-Holocene tidal muds of the Vlaanderen Fm (NCS, 2017), mapped as the seismostratigraphic unit U4 by Mathys (2009) and underlying the BCS mud plate deposits (unit U6 in Mathys, 2009), were collected from cored boreholes Stroombank, Grote Rede and a location between the shore and the Wenduine bank (Fig. 2 and Supplementary Table 9). Core samples from Weichselian (Marine Isotope Stage MIS-5d), Eemian (MIS-5e) and Saalian (MIS-7 or older) deposits in the Belgian Coastal Plain were collected from several boreholes Nieuwpoort, Middelkerke and Westende and Leeuwenhof borehole (Baeteman and De Gans, 1993) (Fig. 2 and Supplementary Table 9).

3.7.2. Results

The Holocene mud from seismic unit “U4” (Mathys, 2009) and the overlying BCS mud plate (seismic unit “U6” in Mathys, 2009) have a nearly identical clay mineral composition (Fig. 10). The clay mineral analysis of the Pleistocene muds is more variable (Fig. 10). Marine tidal flat sediments during MIS-5d (Weichselian) also show a composition similar to the BCS mud plate. Earlier on during the MIS-7 (Saalian) and MIS-5e (Eemian), marine tidal flats show a highly smectitic composition, far away from the BCS composition. However, sediments identified as fluvial channels clearly have with a more illitic clay mineral composition during the MIS-7 to 5e (Saalian to Eemian). The Nieuwpoort NP1 borehole record shows a gradual change from a smectite-dominated Paleogene-derived composition to the BCS mud plate composition already in a MIS-7 fluvial channel (Supplementary Table 8 and Fig. 10).

4. Discussion

4.1. Potential source areas

The BCS mud plate clay composition is identical to that of the overlying SPM of the coastal turbidity maximum. The clay mineral compositional fields (Figs. 8 to 10) demonstrate that the English Channel, Paleogene strata outcropping on the sea floor and Rhine-Meuse SPM and deposits can be excluded as the main sources of the BCS mud plate and SPM. The estuary of the Scheldt river system is the only present-day source with a clay mineral composition of bottom and suspended sediments analogous to the BCS mud plate and the coastal turbidity maximum. It is therefore clear that the Scheldt river system is the predominant sediment source of the BCS mud plate. The mixing of other provenance areas would result in a much more variable clay composition of the BCS mud plate in depth-time and space. Still, minor sediment contributions from the other hypothesized source areas are not excluded as evidenced by the rare occurrence of Cretaceous

nannoplankton in the top meters of the muds (Fontaine, 2004).

4.2. Scheldt sediment export and present tidal regime: a contradiction

The observation that the large majority of mud sediment in the BCS mud plate was originally discharged from the Scheldt estuary contradicts with the currently observed marine-dominated tidal regime with only negligible amounts of fluvial mud being discharged into the North Sea (Verlaan, 2000; Van Kessel et al., 2015; Elias et al., 2017). This apparent contradiction can be explained if the major mud export phase from the Scheldt river occurred in the past, well before modern hydrodynamic and sediment flux measurements (Baeteman et al., 1992; Houziaux et al., 2011) in the estuary started. The compositional similarity between the Scheldt tributaries and of the estuary indicates that the SPM clay minerals in the estuary are primarily delivered by the tributaries. The import of similar clay minerals from the sea into the estuary therefore reflects a recirculation of particles originally delivered by the river system to the estuary and the nearshore mud plate. The understanding of SPM transport based on present data is thus only a snapshot in the geological history of the Scheldt estuary.

4.2.1. The SPM and the coastal turbidity maximum

This observation also implies that the currently existing coastal turbidity maximum above the BCS mud plate is not fed by the Scheldt estuary. However the similarity of the clay mineral composition of the BCS mud plate and the SPM, implies a close relationship between both. Consequently the coastal turbidity maximum in the Belgian coastal waters is formed mainly by ongoing erosion of the BCS muds and local hydrodynamic conditions constrains SPM in this area for an extended time (Fettweis and Van den Eynde, 2003). The latter is confirmed by the presence fluffy, unconsolidated mud deposits in the area, thus of present age (Fettweis et al., 2009). Eventually, parts of the SPM above the BCS are transported further towards the northeast as is demonstrated by the similar clay mineral composition in the southern Dutch nearshore area. This result also implies that, although large water masses are being transported from the English Channel towards the North Sea and the net sediment transport is in the same direction (Prandle et al., 1996; Velegrakis et al., 1999; Lafite et al., 2000; Fettweis et al., 2007a, 2007b), the English Channel is not a major contributor to the SPM and the freshly deposited muds found in the southern North Sea (Belgian-Dutch) nearshore area. Because the SPM concentrations in the English channel are about an order of magnitude lower compared to BCS waters (Fig. 1), the dominant source of SPM along the Belgian-Dutch side of the southern North Sea is the erosion of the BCS mud plate. This is confirmed by the clear zonation in clay mineral composition of the SPM found in the English Channel, ranging from a smectite-poor (< 30%) province south-west of the Dover Strait to a smectite-enriched (ca. 40%) province north-east of the Dover Strait.

Ongoing erosion of the mud plate is in line with the observed erosion of medium consolidated BCS mud near the port of Zeebrugge during storm conditions (Fettweis et al., 2010) and naturally formed narrow belts of about 30 cm thick fresh to softly consolidated mud aligned parallel to the coastline already in the beginning of the 20th century (Fettweis et al., 2009).

4.3. On anthropogenic and natural changes in the Scheldt

The observation that the present-day mud plate and the SPM are no longer actively fed by the Scheldt sediment supply triggers the question why this sediment export regime stopped. Anthropogenic influence is a reasonable candidate to explain the flow direction reversal with marine waters and sediment flowing into the Scheldt estuary. Salden (2000) and Chen et al. (2005) have estimated that the inflow of marine waters in the estuary has doubled as a result of deepening of the navigation channels and construction works in the Scheldt estuary, related to the expansion of the port of Antwerp. Fettweis et al. (2009) have pointed

out that also in the coastal area more early-Holocene mud was brought into circulation since the beginning of the 20th century as a consequence of its exposure by the construction and extension of the Zeebrugge port and the related deepening of the navigation channel. Also the slightly more smectitic composition of the estuary sediments compared to the present measured suspended sediment in the individual tributaries (Fig. 9), could be an indication of anthropogenic influence. It is suspected that modern canalization of the rivers and also more intense land use has modified the river sediment composition favoring at present more superficial erosion of illitic Quaternary eolian cover sediments compared to earlier erosion mainly from more smectite-rich Eocene clay (see Fig. 8), especially by incisions during lowered sea-level in glacial times.

While the strongest anthropogenic changes on the natural estuarine system were imposed during the last 50 years, significant interaction of human occupation and landscape development in the Scheldt estuary dates back almost 2 millennia, inevitably changing the sediment dynamics in the area (Baeteman et al., 2002). In that time also the lower Scheldt evolved from a main course along and to the northwest of the Brabantse Wal, into the Eastern Scheldt and finally the Western Scheldt (Kiden, 2006; Heyse and Demoulin, 2018). All major erosive episodes documented since the Middle Ages along the North Sea coast are related to storm events (Houthuys et al., 1993) and Mathys (2009) has associated the origin of the mud plate to the storm erosion of the Wulpen island in the Western Scheldt.

4.4. The start of the BCS mud type export from the Scheldt

Although the sample resolution is too limited for a comprehensive investigation when and why the Scheldt started to export sediments with a BCS clay mineral composition, the analyses of the coastal plain boreholes (Fig. 10) suggest a relatively recent geological age. In this area marine tidal-flat muds, deposited during the Saalian and Eemian, still consist of locally reworked Eocene clays while fluvial muds are already gradually resemble a mineralogical composition more similar to the BCS mud plate. Around 110 ka (MIS 5d), the fluvial output to the sea had become sufficiently large to completely transform the tidal flat composition into the composition of the BCS mud plate.

This preliminary model needs further analysis but this late Middle Pleistocene (MIS 7) arrival of a clay mineral composition typical for the presently observed composition of the Scheldt estuary, and for the BCS mud plate, makes sense paleogeographically. The present Scheldt river system pattern started with the incision of the Flemish Valley, when the major north-south oriented tributaries were captured and the westward drainage of the Scheldt started discharging a mixture of clay minerals from the same basin area as today. The incision of the Flemish Valley (Mathys, 2009; Heyse and Demoulin, 2018) was a consequence of massive proglacial lake breakthroughs in the southern North Sea at the end of major glaciations, around 450 ka and 160 ka, which resulted in the erosion of the Dover Strait and the installation of a southwards drainage system to the Atlantic Ocean (Gibbard, 2007). Therefore this major paleogeographical change in the drainage system could have resulted in the start of the westward discharge of muds with the BCS mud composition by the newly configured Scheldt river system.

Deciphering the provenance, transport and depositional history of clay mineral in a coastal area over a few 100 kyr is therefore beneficial for understanding the reasons for the present situation.

5. Conclusions

It has been demonstrated that detailed quantitative clay mineralogy has strong potential as a provenance indicator in fine-grained sediments. Most provenance areas proposed in the literature for the muds found in the Belgian-Dutch nearshore area (BCS mud plate) do not clay mineralogically match with the BCS mud plate composition whereas the Scheldt river and estuary system clay minerals are highly similar.

The apparent contradiction with the present inflow of SPM from the North Sea into the estuary implies that the present situation was preceded by a prolonged time of mud export from the estuary into the sea. Present-day hydrodynamics of the Scheldt estuary and the nearshore area result from multiple natural and anthropogenic morphological changes. The clay mineral mixture now characterizing the Scheldt estuary could have developed when all tributaries became connected into a westward draining Scheldt river and preliminary data show that the coastal tidal flat composition became similar to the present BCS mud already about 100 ka ago. As the Scheldt river system is currently not exporting significant amounts of mud to the sea, it can also be concluded that the present-day SPM in the southern North Sea originates from the erosion and resuspension of material of the BCS mud plate. As the SPM concentration of English Channel waters is very low, only re-suspension of the local BCS muds can be responsible for the observed coastal turbidity maxima and the further distribution of suspended sediment towards the northeastern part of the North Sea. This paper demonstrates that provenance studies can greatly benefit from a proper understanding of the paleogeographic and paleohydrodynamic regime history around the basin.

Supplementary data to this article can be found online at <https://doi.org/10.1016/j.margeo.2017.12.011>.

Acknowledgments

The authors wish to acknowledge the late Wim Westerhoff (TNO) and Hans Middelkoop (Utrecht University) and Frieda Bogemans and Cecile Baeteman (Royal Belgian Institute of Natural Sciences) for their help and comments during the study. Ship time of RV Belgica was provided by BELSPO and the RBINS–Operational Directorate Natural Environment. The results of this study have been obtained in the doctoral theses of E. Zeelmaekers and R. Adriaens under the supervision of N. Vandenberghe, J. Śródoń and J. Elsen. Laboratory work was carried out at the KU Leuven by Ria Brepoels, Nancy Weyns and Wathab Mohammad. The authors are grateful to Chevron Energy Technology Company, which allowed using the Quanta© and Sybilla© software for academic purposes. This study was funded partly by the Belgian Science Policy projects MOCHA (EV35), and supported by the Maritime Access Division of the Flemish Ministry of Mobility and PublicWorks (MOMO project). The PhD grant of E. Zeelmaekers was funded by the Flemish Agency of Innovation by Science and Technology (IWT). The reviewers and the editor are thanked for their comments improving the original manuscript.

References

- Adriaens, R., 2015. Neogene and Quaternary Clay Minerals in the Southern North Sea. PhD dissertation. KU Leuven 280p.
- Adriaens, R., Vandenberghe, N., Elsen, J., 2014. Natural clay-sized glauconite in the Neogene deposits of the Campine basin (Belgium). *Clay Clay Miner.* 62, 35–52.
- Agrawal, Y.C., Pottsmith, H.C., 2000. Instruments for particle size and settling velocity observations in sediment transport. *Mar. Geol.* 168, 89–114.
- Amman, L., Bergaya, F., Lagaly, G., 2005. Determination of the cation exchange capacity of clays with copper complexes revisited. *Clay Miner.* 40, 441–453.
- Aplin, A.C., Matenaar, I.F., McCarty, D.K., van der Pluijm, B.A., 2006. Influence of mechanical compaction and clay mineral diagenesis on the microfabric and pore scale properties of deep-water Gulf of Mexico mudstones. *Clay Clay Miner.* 54, 500–514.
- Baeteman, C., 1999. The Holocene depositional history of the IJzer paleo-valley (Western Belgian coastal plain) with reference to the factors controlling the formation of intercalated peat beds. *Geol. Belg.* 2, 39–72.
- Baeteman, C., De Gans, W., 1993. INQUA Fieldmeeting 1993. Quaternary Shorelines in Belgium and The Netherlands, September 18–25: Excursion Guide. International Union for Quaternary Research (INQUA), Brussel 108 pp.
- Baeteman, C., de Lannoy, W., Paepe, R., van Cauwenberghe, C., 1992. Vulnerability of the Belgian coastal lowlands to future sea-level rise. In: Jelgersma, S. (Ed.), Tooley M. Impact of Sea-level Rise on European Coastal Lowlands, Blackwell Publications, pp. 56–71.
- Baeteman, C., Scott, D.B., Van Strydonck, M., 2002. Changes in coastal zone processes at a high sea-level stand: a late-Holocene example from Belgium. *J. Quat. Sci.* 17, 547–559.
- Bastin, A., 1974. Regionale sedimentologie en morfologie van de zuidelijke Noordzee en

- het Schelde estuarium. PhD Thesis. Geography-Geology Department, Catholic University of Leuven, Belgium.
- Beets, D.J., van der Spek, A.J.F., 2000. The Holocene evolution of the barrier and the back-barrier basins of Belgium and the Netherlands as a function of late Weichselian morphology, relative sea-level rise and sediment supply. *Neth. J. Geosci.* 79, 3–16.
- Busschers, F.S., Weerts, H.J.T., Wallinga, J., Kasse, C., Cleveringa, P., de Wolf, H., Cohen, K.M., 2005. Sedimentary architecture and optical dating of Middle and Late Pleistocene Rhine-Meuse deposits - fluvial response to climate change, sea-level fluctuation and glaciation. *Neth. J. Geosci. - Geologie en Mijnbouw* 84, 25–41.
- Chen, M.S., Wartel, S., Van Eck, B.T.M., van Maldegem, D., 2005. Suspended matter in the Scheldt estuary. *Hydrobiologia* 540, 79–104.
- Dou, Y., Yang, S., Liu, Z., Clift, P.D., Yu, H., Berne, S., Shi, X., 2010. Clay mineral evolution in the central Okinawa Trough since 28 ka: implications for sediment provenance and paleoenvironmental change. *Palaeogeogr. Palaeoclimatol. Palaeoecol.* 288, 108–117.
- Drits, V.A., Lindgreen, H., Sakharov, B.A., Salyn, A.L., 1997. Sequential structure transformation of illite-smectite-vermiculite during diagenesis of Upper Jurassic shales, North Sea. *Clay Miner.* 33, 351–371.
- Eisma, D., 1981. Supply and deposition of suspended matter in the North Sea. In: Nio, S.-D., Shüttenhelm, R.T.E., Van Weering, T.C.E. (Eds.), *Holocene Marine Sedimentation in the North Sea Basin*. Blackwell Publishing Ltd., Oxford, UK.
- Eisma, D., 1986. Flocculation and de-flocculation of suspended matter in estuaries. *Neth. J. Sea Res.* 20, 183–199.
- Elias, E.P.L., Van der Spek, A.J.F., Lazar, M., 2017. The “Voordelta”, the contiguous ebb-tidal deltas in the SW Netherlands: large-scale morphological changes and sediment budget 1963–2013; impacts of large-scale engineering. *Neth. J. Geosci.* 96, 223–259.
- Fettweis, M., Van den Eynde, D., 2003. The mud deposits and the high turbidity in the Belgian-Dutch coastal zone, Southern Bight of the North Sea. *Cont. Shelf Res.* 23, 669–691.
- Fettweis, M., Nechad, B., Van den Eynde, D., 2007a. An estimate of the suspended particulate matter (SPM) transport in the southern North Sea using SeaWiFS images, in-situ measurements and numerical model results. *Cont. Shelf Res.* 27, 1568–1583.
- Fettweis, M., Du Four, I., Zeelmaekers, E., Baeteman, C., Francken, F., Houziaux, J.-S., Mathys, M., Nechad, B., Pison, V., Vandenberghe, N., Van den Eynde, D., Van Lancker, V., Wartel, S., 2007b. Mud Origin, Characterisation and Human Activities (MOCHA). Final Scientific Report. Belgian Science Policy Office 59pp.
- Fettweis, M., Houziaux, J.-S., Du Four, I., Van Lancker, V., Baeteman, C., Mathys, M., Van den Eynde, D., Francken, F., Wartel, S., 2009. Long-term influence of maritime access works on the distribution of cohesive sediment: analysis of historical and recent data from the Belgian nearshore area (southern North Sea). *Geo-Mar. Lett.* 29, 321–330.
- Fettweis, M., Francken, F., Van den Eynde, D., Verwaest, T., Janssens, J., Van Lancker, V., 2010. Storm influence on SPM concentrations in a coastal turbidity maximum area with high anthropogenic impact (southern North Sea). *Cont. Shelf Res.* 30, 1417–1427.
- Fontaine, K., 2004. Waar komt het slib voor de Belgische kust vandaan? Een kleimineralogische benadering. Masters thesis. KU Leuven, Belgium 118pp.
- Gerritsen, H., Boon, J.G., van der Kaaij, T., Vos, R.J., 2001. Integrated modelling of suspended matter in the North Sea. *Estuar. Coast. Shelf Sci.* 53, 581–594.
- Gibbard, P.L., 2007. Europe cut adrift. *Nature* 448, 259–260.
- Heyse, L., Demoulin, A., 2018. The Flemish Valley: Response of the Scheldt Drainage System to Climatic and Glacio-Eustatic Oscillations. In: Demoulin (Ed.), *Landscapes and Landforms of Belgium and Luxembourg*. Springer International Publishing.
- Hillier, S., 1999. Use of an air brush to spray dry samples for X-ray powder diffraction. *Clay Miner.* 34, 127–135.
- Houthuys, R., De Moor, G., Sommé, J., 1993. The shaping of the French-Belgian sea coast throughout recent geology and history. In: Hillen, R., Verhagen, H.J. (Eds.), *Coastlines of the Southern North Sea*. American Society of Civil Engineers, New York, pp. 27–40.
- Houziaux, J.-S., Fettweis, M., Francken, F., van Lancker, V., 2011. Historic (1900) sea-floor composition in the Belgian-Dutch part of the North Sea: a reconstruction based on calibrated visual sediment descriptions. *Cont. Shelf Res.* 31, 1043–1056.
- Howell, A.L., Bentley Sr., S.J., Xu, K., Ferrell, R.E., Muhammad, S., Septama, E., 2014. Fine sediment mineralogy as a tracer of latest Quaternary sediment delivery to a dynamic continental margin: Pandora Through, Gulf of Papua, Papua New Guinea. *Mar. Geol.* 357, 108–122.
- Hubert, F., Caner, L., Meunier, A., Lanson, B., 2009. Advances in characterization of the soil clay mineralogy using X-ray diffraction: from decomposition to profile fitting. *Eur. J. Soil Sci.* 60, 1093–1105.
- Irion, G., Zöllmer, V., 1999. Clay mineral associations in fine-grained surface sediments of the North Sea. *J. Sea Res.* 41, 119–128.
- Jackson, M.L., 1975. *Soil Chemical Analysis – Advanced Course*, 2nd Edition, Published by the Author, Madison, Wisconsin. 895 p.
- Kessarkar, P.M., Rao, V.P., Ahmad, S.M., Badu, B.A., 2003. Clay minerals and Sr–Nd isotopes of the sediments along the western margin of India and their implication for sediment provenance. *Mar. Geol.* 202, 55–69.
- Kiden, P., 2006. De evolutie van de Beneden-Schelde in België en Zuidwest-Nederland na de laatste ijstijd. *Belgeo* 3, 279–294.
- Lacroix, G., Ruddick, K., Ozer, J., Lancelot, C., 2004. Modelling the impact of the Scheldt and Rhine-Meuse plumes on the salinity distribution in Belgian waters (southern North Sea). *J. Sea Res.* 52 (3), 149–163.
- Lafite, R., Shimwell, S., Grochowski, N., Dupont, J.-P., Nash, L., Salomon, J.-C., Cabioch, L., Collins, M., Gao, S., 2000. Suspended particulate matter fluxes through the Strait of Dover, English Channel: observations and modelling. *Oceanol. Acta* 23, 687–700.
- Le Bot, S., Van Lancker, V., Deleu, S., De Batist, M., Henriët, J.P., Haegemans, W., 2005. Geological characteristics and geotechnical properties of Eocene and Quaternary deposits on the Belgian continental shelf: synthesis in the context of offshore wind farming. *Neth. J. Geosci.* 84, 147–160.
- Lee, B.J., Fettweis, M., Toorman, E., Molz, F.J., 2012. Multimodality of a particle size distribution of cohesive suspended particulate matters in a coastal zone. *J. Geophys. Res.* 117, 1–17.
- Li, J., Hu, B., Wei, H., Zhao, J., Zou, L., Bai, F., Dou, Y., Wang, L., Fang, X., 2014. Provenance variations in the Holocene deposits from the southern Yellow Sea: clay mineralogy evidence. *Cont. Shelf Res.* 90, 41–51.
- Liu, Z., Tuo, S., Colin, C., Liu, J.T., Huang, C.-Y., Selvaraj, K., Chen, C.-T.A., Zhao, Y., Siringan, F.P., Boulay, S., Chen, Z., 2008. Detrital fine-grained sediment contribution from Taiwan to the northern South China Sea and its relation to regional ocean circulation. *Mar. Geol.* 255, 149–155.
- Liu, Z., Colin, C., Li, X., Zha, Y., Tuo, S., Chen, Z., Siringan, F.P., Liu, J.T., Huang, C.-Y., You, C.-F., Huang, K.-F., 2010. Clay mineral distribution in surface sediments of the northeastern South China Sea and surrounding fluvial drainage basins: source and transport. *Mar. Geol.* 277, 48–60.
- Mathys, M., 2009. *The Quaternary Geological Evolution of the Belgian Continental Shelf, Southern North Sea*. Doctoral dissertation. University of Ghent 382pp.
- National Commission on Stratigraphy Belgium, 2017, March 1st. Vlaanderen Formation, retrieved from www.ncs.naturalsciences.be.**
- Omotoso, O., McCarthy, D.K., Hillier, S., Kleberg, R., 2006. Some successful approaches to quantitative mineral analysis as revealed by the 3th Reynolds Cup contest. *Clay Clay Miner.* 54, 748–760.
- Pache, T., Brockamp, O., Clauer, N., 2008. Varied pathways of river-borne clay minerals in a near-shore marine region: a case study of sediments from the Elbe- and Weser rivers, and the SE North Sea. *Estuar. Coast. Shelf Sci.* 78 (3), 563–575.
- Peeters, J., Busschers, F.S., Stouthamer, E., 2015. Fluvial evolution of the Rhine during the last interglacial-glacial cycle in the southern North Sea basin: a review and look forward. *Quat. Int.* 357, 176–188.
- Prandle, D., Ballard, G., Flatt, D., Harrison, A.J., Jones, S.E., Knight, P.J., Loch, S.G., McManus, J.P., Player, R., Tappin, A., 1996. Combining modelling and monitoring to determine fluxes of water, dissolved and particulate metals through the Dover Strait. *Cont. Shelf Res.* 16 (2), 237–257.
- Ramaswamy, V., Nagender, N.B., Vethamony, P., Illangovan, D., 2007. Source and dispersal of suspended sediment in macro-tidal Gulf of Kachchh. *Mar. Pollut. Bull.* 54, 708–719.
- Raven, M., Self, P., 2017. Outcomes of 12 years of the Reynolds Cup quantitative mineral analysis round robin. *Clay Clay Miner.* 65, 122–134.
- Sakharov, B.A., Lindgreen, H., Salyn, A.L., Drits, V.A., 1999. Determination of illite-smectite structures using multispecimen X-ray diffraction profile fitting. *Clay Clay Miner.* 47, 555–566.
- Salden, R.M., 2000. Effecten van systeemgrepen op de water- en bodemkwaliteit van de Westerschelde. In: *Rapport RIKZ/2000.006*, 41 pp.
- Salomons, W., Mook, W.G., 1987. Natural tracers for sediment transport studies. *Cont. Shelf Res.* 11, 1333–1343.
- Sandler, A., Herut, B., 2000. Composition of clays along the continental shelf off Israel: contribution of the Nile versus local sources. *Mar. Geol.* 167, 339–354.
- Schroeder, A., Wiesner, M.G., Liu, Z., 2015. Fluxes of clay minerals in the South China sea. *Earth Planet. Sci. Lett.* 430, 30–42.
- Środoń, J., Drits, V.A., McCarty, D.K., Hsieh, J.C.C., Eberl, D.D., 2001. Quantitative XRD analysis of clay-rich rocks from random preparations. *Clay Clay Miner.* 49, 514–528.
- Trentesaux, A., Stolk, A., Berné, S., 1999. Sedimentology and stratigraphy of a tidal sand bank in the southern North Sea. *Mar. Geol.* 159, 253–272.
- Ufer, K., Stanjek, H., Roth, G., Dohrmann, R., Kleberg, R., Kaufhold, S., 2008. Quantitative phase analysis of bentonites by the Rietveld method. *Clay Clay Miner.* 56 (2), 272–282.
- Van Kessel, T., Vanlede, J., Van Holland, G., 2015. Human vs. natural mud fluxes in the Scheldt estuary: are they significant and if so, how can they best be optimised? In: *E-proceedings of the 36th IAHR World Congress, The Hague, The Netherlands*.
- Vandenberghe, N., Laga, P., Steurbaut, E., Hardenbol, J., Vail, P.R., 1998. Tertiary sequence stratigraphy at the southern border of the North Sea basin in Belgium. In: (Eds): de Graciansky, P.C., Hardenbol, J., Jacquin, Th. & Vail, P.R. *Mesozoic and Cenozoic sequence stratigraphy of European Basins*. SEPM Spec. Publ. 60, 119–154.
- Velegrakis, A.F., Michel, D., Collins, M.B., Lafite, R., Oikonomou, E.K., Dupont, J.P., Huault, M.F., Lecouturier, M., Salomon, J.C., Bishop, C., 1999. Sources, sinks and resuspension of suspended particulate matter in the eastern English Channel. *Cont. Shelf Res.* 19, 1933–1957.
- Verfaillie, E., Van Lancker, V., Van Meirvenne, M., 2006. Multivariate geostatistics for the predictive modelling of the surficial sand distribution in shelf seas. *Cont. Shelf Res.* 26, 2454–2468.
- Verlaan, P.A.J., 2000. Marine vs fluvial bottom mud in the Scheldt Estuary. *Estuar. Coast. Shelf Sci.* 50, 627–638.
- Zeelmaekers, E., 2011. *Computerized Qualitative and Quantitative Clay Mineralogy: INTRODUCTION and Application to Known Geological Cases*. PhD thesis. KU Leuven, Belgium.
- Zeelmaekers, E., Honty, M., Derkowski, A., Środoń, J., De Craen, M., Vandenberghe, N., Adriaens, R., Ufer, K., Wouters, L., 2015. Qualitative and quantitative mineralogical composition of the Rupelian Boom clay in Belgium. *Clay Miner.* 50, 249–272.
- Zuther, M., Brockamp, O., Clauer, N., 2000. Composition and origin of clay minerals in Holocene sediments from the south-eastern North Sea. *Sedimentology* 47, 119–134.